東北大学機関リポジトリ
TOUR
Tohoku University Repository

Seasonal Variations in the Heat and Water Balances for Non-Vegetated Surfaces

著者	徐　健青
学位授与機関	Tohoku University
URL	http://hdl.handle.net/10097/54551

博士論文

Seasonal Variations in the Heat and Water Balances for Non-Vegetated Surfaces

(裸地面の熱収支・水収支の季節変化)

JIANQING XU

徐　健青

平成8年

Seasonal Variations in the Heat and Water Balances for Non-Vegetated Surfaces

(裸地面の熱収支・水収支の季節変化)

JIANQING XU

徐　健青

1996

Contents

1 Introduction 3

2 Method of calculation 5

2.1 Soil model 5

2.2 Boundary and initial conditions 8

2.3 Data set 10

2.3.1 Air temperature 10

2.3.2 Solar radiation 11

2.3.3 Longwave radiation 14

2.3.4 Precipitation 15

3 Parameters 18

3.1 Soil-water potential Ψ 18

3.2 Evaporation efficiency β^* 19

3.3 Albedo 21

3.4 Physical thermal coefficients 26

3.5 Exchange speed $C_H U$ 27

3.6 Snow melting process 28

4 Verification of the method of calculation 29

5 Seasonal variations **32**

5.1 Lanzhou 32

5.2 Turpan 36

5.3 Altay 38

6 Climatological relationship **44**

6.1 Heat balance 44

6.2 Water balance 46

6.3 Soil-water content 48

7 Index of climatological wetness **51**

7.1 Radiation 51

7.2 Potential evaporation 58

7.3 Application 61

8 Summary and conclusion **65**

Acknowledgments **67**

Appendix A. Tables of monthly heat and water balances **68**

Appendix B. Notation **99**

References **103**

Chapter 1

Introduction

The process of evaporation from a land surface is one of the main mechanisms in the heat and water balances over the surface of the earth. The amount of precipitation over arid and semi-arid regions is small and extremely variable in time and space, resulting in a large spatial variability of soil-water, as well as in the sensible-heat flux and water-vapor flux from the surface. Evaporation from the liquid water takes place not only at the soil surface, but also in the underlying soil. According to Kondo et al. (1992), Kondo (1993a), and Kondo and Saigusa (1994), the evaporation rate strongly depends on wind velocity, solar radiation, air temperature and specific humidity in moist regions where the soil surface contains plentiful amount of water. When the soil surfaces become dry enough, however, the evaporation rate depends mainly on the specific humidity of the air and the soil-water content, while being weakly related to the wind velocity, air, and ground temperatures.

Namely, the evaporation rate is difficult to be correctly estimated without considering the soil conditions in arid and semi-arid regions. In dry soil, an equilibrium state exists in small soil pores where vaporization or condensation occurs constantly, and is not formed in large pores exposed to the atmosphere (Kondo *et al.* 1990; Kondo and Saigusa 1994). Philip (1957) had previously pointed out that, when local equilibrium exists between the liquid and vapor phases within the soil pores, the relative humidity h in the pore can be expressed as

$$h = \exp\left(\frac{g\Psi}{R_w T_G}\right) . \tag{1.1}$$

Here Ψ is the soil-water potential, T_G the soil temperature, g the acceleration of gravity, and R_w the specific gas constant for a unit mass of water vapor. It should be

noted that Ψ is a function of the soil-water content and dependent on the soil type (see section 3.1). The soil-water potential is a measure of how much work will be conducted in moving water from a soil pore or soil particle.

In the present study, by employing a soil model that makes use of daily routine meteorological data, the daily and seasonal variation of heat and water balances in different climatic regions are simulated. The following themes are investigated:

1) The variations in the heat balance and the soil-water content under different climatic conditions, such as in moist, semi-arid, and arid regions

2) The relationship between soil type and water balance

3) The effect of snow cover on the heat and water balances.

The model is introduced in chapter 2. In chapter 3, the parameterizations for the soil and land surfaces are described. Vertifications of the model used for calculations of the surface fluxes using real data sets are discussed in chapter 4. The calculated results for arid, semi-arid, and snow covered regions are given in chapter 5. Climatological results from 30 weather stations in China are presented in chapter 6. As an application of the interrelation between heat and water balances, a wetness index of the climatology is presented for delimiting the climatic zonality in chapter 7. Notations used in the present paper are listed in the Appendix.

Chapter 2

Method of calculation

2.1 Soil model

The multi-layer soil model has been proposed by Kondo and Saigusa (1994). Kondo et al. 1995, Kondo and Xu 1996a) have put the model to practical use after simplifications in the calculation scheme. In present study the simplified model is used. Water transportation within the soil is divided into the vapor and liquid phases. The respective heat and water transports within the soil can be expressed as

$$\frac{\partial \theta}{\partial t} = -\frac{1}{\rho_w}\frac{\partial}{\partial z}(Q_{\rm liq} + Q_{\rm vap}) \,, \tag{2.1}$$

and

$$c_g \rho_g \frac{\partial T_{\rm G}}{\partial t} = -\frac{\partial Q_h}{\partial z} - \iota E_{\rm soil} \,, \tag{2.2}$$

where

$$Q_h = -\lambda_g \frac{\partial T_{\rm G}}{\partial z}. \tag{2.3}$$

Here t is the time, z the soil depth and positive in the downward direction Q_h the heat flux, $E_{\rm soil}$ the evaporation rate in the soil, and ι the latent heat of vaporization. Compared with $\partial Q_h/\partial z$, the value of $\iota E_{\rm soil}$ within the soil ($z \geq 0.02\,{\rm m}$) is very small and neglected in the calculation at depths deeper than 0.02m. The variables $Q_{\rm liq}$ and $Q_{\rm vap}$ are the liquid and vapor phase water fluxes, respectively, which are positive in the upward direction. $T_{\rm G}$ is the ground temperature at the depth z, while c_g, ρ_g, and λ_g are the specific heat, density, and thermal conductivity of the given soil, respectively, which change with soil-water content (see section 3.4).

The liquid phase of the water flux $Q_{\rm liq}$ can be written as

$$Q_{\rm liq} = -\rho_w K(\frac{\partial \Psi}{\partial z} + 1) \ , \tag{2.4}$$

where

$$K = k_f K_{\rm SAT}(\frac{\theta}{\theta_{\rm SAT}})^c \ , \tag{2.5}$$

and

$$k_f = 1 - \frac{\Delta_K}{1 + \exp(\frac{1}{\epsilon_K})(\frac{\theta}{\theta_K} - 1)} \ . \tag{2.6}$$

In the above, K is the hydraulic conductivity, $K_{\rm SAT}$ and $\theta_{\rm SAT}$ are the hydraulic conductivity and volumetric soil-water content at saturation, respectively. The constants $K_{\rm SAT}$, $\theta_{\rm SAT}$, c, Δ_K, ϵ_K, and θ_K depend on the soil type and were determined by experiments and from observations (Kondo and Xu 1996a). The values of those constants for the various soil types are listed in Table 3.1.

The soil-water potential Ψ is given as

$$\Psi = \Psi_{01} \exp(-a\theta) + \frac{\Psi_{02}}{1 + \frac{\Psi_{02}}{X}}, \qquad \theta < \theta_{\rm SAT} \ , \tag{2.7}$$

$$\Psi = 0 \ , \qquad \theta \geq \theta_{\rm SAT} \ , \tag{2.8}$$

and

$$\Psi_{01} = -4 \times 10^4 \, {\rm m} \ , \qquad \Psi_{02} = -10^2 \, {\rm m} \ , \tag{2.9}$$

where

$$X = \Psi_{\rm SAT}(\frac{\theta}{\theta_{\rm SAT}})^{-b} \ . \tag{2.10}$$

Here, $\Psi_{\rm SAT}$ is the soil-water potential at saturation, a and b are soil parameters that change with the soil type (Table. 3.1).

For a special case, the soil-water content is so small that the water transport within the soil occurs mainly in the vapor phase (h <100%), the second term in Eq.(2.7) on the right-hand side can be ignored, resulting in

$$\Psi = \Psi_{01} \exp(-a\theta) \ , \qquad \theta \to 0 \ . \tag{2.11}$$

It can be assumed that local equilibrium condition exists between the liquid and vapor phases of water below depths of 0.02m in the soil. Then $Q_{\rm vap}$ at depths below 0.02m can be expressed as

$$Q_{\rm vap} = \frac{\rho D}{F_n}\left(\frac{dq^*}{dz}\right) , \qquad z \geq 0.02\,{\rm m} , \tag{2.12}$$

$$F_n = \frac{1.5\Delta z}{\theta_{\rm SAT} - \theta} , \qquad \theta < \theta_{\rm SAT} , \tag{2.13}$$

$$F_n = \infty , \qquad \theta \geq \theta_{\rm SAT} , \tag{2.14}$$

and

$$q^* = hq_{\rm SAT}(T_{\rm G}) , \tag{2.15}$$

where ρ is the air density, D the coefficient of molecular diffusion of water vapor, and h is given by Eq.(1.1). The parameter F_n describes the transport route of water vapor in the soil. When the volumetric soil-water content is unsaturated, the route is 1.5 times of the layer depth Δz (Eq.2.13), and the constant 1.5 is the porosity and tortuosity factor of the route (Jackson *et al.* 1974). The specific humidity in soil pore is represented by q^*, and $q_{\rm SAT}(T_{\rm G})$ the saturated specific humidity at the temperature $T_{\rm G}$.

For water vapor transport within the top soil layer ($0 - 0.02\,{\rm m}$), an equilibrium state does not exist between the liquid and vapor phases (Kondo *et al.* 1990 ; Kondo 1993a ; Kondo and Saigusa 1994). In this layer, $Q_{\rm vap}$ can be expressed as

$$Q_{\rm vap} \equiv E , \qquad 0 \leq z < 0.02\,{\rm m} , \tag{2.16}$$

where

$$E = \rho C_H U \beta^* (hq_{\rm SAT}(T_{\rm S}) - q) , \tag{2.17}$$

$$\beta^* = \frac{1}{1 + C_H U (F/D)} , \tag{2.18}$$

and

$$F = f_A \exp(-f_B \theta^3) + f_C[\cos(\frac{\pi}{2}\frac{\theta}{\theta_{\rm SAT}})]^{-0.5} , \qquad 0 \le \theta < \theta_{\rm SAT} . \tag{2.19}$$

In the above equations, E is the rate of evaporation from the ground-surface. Equation (2.17) is termed the $h\beta^*$-method, with the surface evaporation efficiency β^* being defined by this formula. Equations (2.17) and (2.18) describe two evaporation processes that occur in the soil surface layer. The first is the water vapor transport by molecular diffusion from the water surface in the soil pore to the ground-surface. The second is the water vapor transport from the ground-surface to the atmosphere by turbulent airflow (Kondo et al. 1990 ; Kondo and Saigusa 1994). In Eqs. (2.17) and (2.18), $C_H U$ is the exchange speed (see section 3.5), q the specific humidity of the air, F the resistance to vaporization and vapor transport in the top soil layer, and f_A, f_B, and f_C are the soil constants and determined by the experiments. (see section 3.2).

2.2 Boundary and initial conditions

In the model, the ground soil is divided into 10 layers, the thickness of each layer is 0.02, 0.04, 0.08, 0.08 m, 0.08, ... until reaching a depth of 0.7 m. Boundary conditions of the ground-surface are

$$Q_{\rm liq}(z = 0) = 0 , \tag{2.20}$$

and

$$Q_{\rm vap}(z = 0) = E . \tag{2.21}$$

The equations for the energy balance at the soil surface are given by

$$\mathrm{Rn} - G = H + \iota E , \tag{2.22}$$

$$\mathrm{Rn} = (1 - ref)S^{\downarrow} - \epsilon(\sigma T_S^4 - L^{\downarrow}). \tag{2.23}$$

$$H = c_p \rho C_H U (T_S - T_A) \,, \tag{2.24}$$

and

$$G = -(\lambda_g \frac{\partial T_S}{\partial z})_{z=0} \,, \tag{2.25}$$

where Rn is the net radiation, G the heat flux into ground, H the sensible heat flux, $S^{\downarrow}$ the downward shortwave radiation (Eq. 2.52), and $L^{\downarrow}$ the downward longwave radiation (Eq. 2.53). In addition, ref the surface albedo which change with season and soil-water content of the top soil layer (section 3.3), σ the Stefan-Boltzman constant, c_p the specific heat of air, T_A the air temperature (see Eq. 2.28). The surface emissivity ϵ is assumed as 1 in the present study.

The boundary conditions at the bottom of the model are

$$Q_{liq}(z_B) = 0.1 \rho K(z_B) \,, \tag{2.26}$$

and

$$Q_{vap}(z_B) = 0 \,, \tag{2.27}$$

where z_B is the depth of the bottom ($z_B = 0.7\,\mathrm{m}$), $K(z_B)$ the hydraulic conductivity at the bottom which changes with the variation in the soil-water content of the bottom layer (Eq. 2.5).

The next problem is the deciding of the initial conditions of volumetric soil-water content θ for each layer. Assumed values of θ are first substituted in the model, and the model calculations are repeated for a time scale of several years or more under the same pattern of weather conditions until the pattern for annual changes of θ in each layer approaches a steady values. These results are then assumed as the initial conditions of θ. It is easy to obtain initial values of θ over a short time scale for moist regions. It could take calculation on time scales of more than a hundred years, however, to obtain values of θ for arid regions such as Turpan, because vapor transport is much slower than liquid water transport within the soil layers.

2.3 Data set

The data used in the present study were taken from routine meteorological data as described in the following:

- daily mean air temperature T_{AM} (K or °C)
- the difference between daily maximum and minimum air temperatures $T_{\mathrm{A,MAX}} - T_{\mathrm{A,MIN}}$ (K or °C)
- sunshine duration N (hour)
- daily amount of precipitation $\mathrm{Pr}_{\mathrm{OBS}}$ (mm)
- daily mean wind speed U_{OBS} (ms^{-1})
- daily mean vapor pressure e (hPa)
- surface pressure p_s (hPa)

2.3.1 Air temperature

From T_{AM} and $T_{\mathrm{A,MAX}} - T_{\mathrm{A,MIN}}$, the daily variation of air temperature T_{A} can be expressed as a trigonometric function having two temporal harmonics, i. e.,

$$T_{\mathrm{A}} = T_{\mathrm{AM}} + \sum_{n=1}^{2} B_n \cos(n\omega t - \frac{\pi}{4}) \,, \tag{2.28}$$

where ω is the angular velocity of the diurnal cycle. The amplitude of T_{A} at the harmonic n denoted by B_n, is given as

$$B_1 = -(T_{\mathrm{A,MAX}} - T_{\mathrm{A,MIN}})/2.09 \,, \tag{2.29}$$

and

$$B_2 = -0.2B_1 \,. \tag{2.30}$$

2.3.2 Solar radiation

The daily mean solar radiation flux $S^{\downarrow}_{\mathrm{M}}$ is obtained from N, with use of the next empirical formulas presented by Kondo *et al.* 1996 .

$$\frac{S^{\downarrow}_{\mathrm{M}}}{S^{\downarrow}_{0}} = a_s + b_s \frac{N}{N_0} \ , \quad 0 < \frac{N}{N_0} \leq 1, \tag{2.31}$$

and

$$\frac{S^{\downarrow}_{\mathrm{M}}}{S^{\downarrow}_{0}} = c_s \ , \qquad \frac{N}{N_0} = 0 \ , \tag{2.32}$$

where

$$a_s = 0.179 + 0.32(1 - \frac{p_s}{1000}) \ , \tag{2.33}$$

$$b_s = 0.55 \ , \tag{2.34}$$

$$c_s = 0.114 + 0.32(1 - \frac{p_s}{1000}) \ . \tag{2.35}$$

Here, N_0 is the duration of possible sunshine, and $S^{\downarrow}_{0}$ the daily mean downward solar radiation at the top of the atmosphere, given by

$$N_0 = 2\zeta \frac{24}{2\pi} = \frac{2\zeta}{0.2618} \ , \tag{2.36}$$

where

$$\zeta = \cos^{-1}(\frac{\sin\alpha - \sin\phi \sin\delta}{\cos\phi \cos\delta}), \tag{2.37}$$

and

$$S^{\downarrow}_{0} = \frac{S_{00}}{\pi} d(\zeta \sin\phi \sin\delta + \cos\phi \cos\delta \sin\zeta) \ , \tag{2.38}$$

where

$$\begin{aligned} d = {} & 1.00011 + 0.034221 \cos\eta + 0.00128 \sin\eta \\ & + 0.000719 \cos 2\eta + 0.000077 \sin 2\eta \ , \end{aligned} \tag{2.39}$$

$$\delta = \sin^{-1}(0.398 \times \sin(4.871 + \eta + 0.033 \sin \eta)) \,, \tag{2.40}$$

and

$$\eta = \frac{2\pi}{365} Day \,. \tag{2.41}$$

In the above equations, S_{00} is the solar constant, ζ the half-day angle, ϕ the latitude, δ the solar declination, and Day the total number of days from 1 January to the day of observation.

It can be expected that N_0 is influenced by the topography around observatories in mountainous regions. For this case, several corrections to N_0 are carried out (Kondo *et al.* 1996).

The daily mean downward solar radiation under clear sky conditions $S^{\downarrow}_{\mathrm{Mf}}$ is expressed as (Kondo 1994)

$$\frac{S^{\downarrow}_{\mathrm{Mf}}}{S^{\downarrow}_{0}} = (C_1 + 0.7 \times 10^{-m_d F_1})(1 - i_3)(1 + j_1) \,, \tag{2.42}$$

where

$$i_3 = 0.014(k_3 m_{\mathrm{noon}} + 7 + 2 \log_{10} w) \log_{10} w \,, \tag{2.43}$$

$$m_{\mathrm{noon}} = (p_s/p_0) \sec(\phi - \delta) \,, \qquad \phi - \delta < \pi/2 \,, \tag{2.44}$$

$$m_{\mathrm{noon}} = \infty \,, \qquad \phi - \delta \geq \pi/2 \,, \tag{2.45}$$

$$\begin{aligned} k_3 = {} & 1.042 - 0.06 \log_{10}(\beta_{\mathrm{DUST}} + 0.02) \\ & -0.1(\sec(\phi - \delta) - 0.091)^{1/2} \,, \end{aligned} \tag{2.46}$$

$$C_1 = 0.21 - 0.2\beta_{\mathrm{DUST}} , \qquad \beta_{\mathrm{DUST}} < 0.3 , \tag{2.47}$$

$$C_1 = 0.15 , \qquad \beta_{\mathrm{DUST}} \geq 0.3 , \tag{2.48}$$

$$F_1 = 0.056 + 0.16(\beta_{\mathrm{DUST}})^{1/2} , \tag{2.49}$$

and

$$j_1 = [0.066 + 0.34(\beta_{\mathrm{DUST}})^{1/2}](ref - 0.15) . \tag{2.50}$$

Here p_0 (= 1013 hPa) is the surface pressure of standard atmosphere, β_{DUST} the atmospheric turbidity defined by Robinson(1966), and w the precipitable water (units of cm) estimated as

$$\log_{10} w \approx \log_{10} w^* + 0.10 . \tag{2.51}$$

The effective precipitable water w^* is expressed by Eqs.(2.58 −− 2.63).

The daily variation of $S^{\downarrow}$ can then be described as the sum of trigonometric functions having four harmonics (Kondo and Xu 1996a), i. e.,

$$S^{\downarrow} = S^{\downarrow}_{\mathrm{M}}[1 + \sum_{n=1}^{4} A_n \cos(n\omega t)] , \tag{2.52}$$

with,

$$A_1 = -1.503, \;\; A_2 = 0.584, \;\; A_3 = -0.058, \;\; and \;\; A_4 = -0.023.$$

The coefficients A_n will change with latitute and season if daily variations are emphasized, but they will have no influence on daily mean calculations.

2.3.3 Longwave radiation

The downward longwave radiation at the ground-surface is obtained from the following (Kondo 1994)

$$L^{\downarrow} = \sigma T_{\rm AM}^4 [1 - (1 - \frac{L_{\rm f}^{\downarrow}}{\sigma T_{\rm AM}^4})C] \,, \tag{2.53}$$

and

$$C = 0.826(\frac{N}{N_0})^3 - 1.234(\frac{N}{N_0})^2 + 1.135(\frac{N}{N_0}) + 0.298 \,, \qquad 0 < \frac{N}{N_0} \leq 1 \,, \tag{2.54}$$

$$C = 0.2235 \,, \qquad \frac{N}{N_0} = 0 \,. \tag{2.55}$$

$$L_f^{\downarrow} = (0.74 + 0.19x + 0.07x^2)\sigma T_{\rm AM}^4 \,, \tag{2.56}$$

$$x \equiv \log_{10} w^* \,, \tag{2.57}$$

and

$$w^* = \frac{1}{g}\int_0^{p_s} q \frac{p}{p_0} dp \,. \tag{2.58}$$

In the present paper, the following empirical formulas are used (Kondo and Xu 1996c)

$$x = 0.027 T_{\rm DEW} - 0.15 - x_0 \,, \qquad T_{\rm DEW} < -5 \ ^{\circ}{\rm C} \,, \tag{2.59}$$

$$x = 0.031 T_{\rm DEW} - 0.13 - x_0 \,, \quad -5^{\circ}C \leq T_{\rm DEW} < 23 \ ^{\circ}{\rm C} \,, \tag{2.60}$$

$$x = 0.015 T_{\rm DEW} - 0.238 - x_0 \,, \quad 23^{\circ}C \leq T_{\rm DEW} < 30 \ ^{\circ}{\rm C} \,, \tag{2.61}$$

with

$$x_0 = 1 - (\frac{p_s}{p_0})^{1/2} , \tag{2.62}$$

and

$$T_{\mathrm{DEW}} = \frac{237.3 \times \log_{10}(e/6.1078)}{7.5 - \log_{10}(e/6.1078)} . \tag{2.63}$$

The values of T_{DEW} and e are the daily mean dew-point temperature and water vapor pressure, respectively.

2.3.4 Precipitation

Rainfall data from the observatories are given as total daily amounts. According to Kondo (1993b), the temporal variation of precipitation intensity γ ($\mathrm{kg\,m^{-2}\,s^{-1}} = \mathrm{mm\,s^{-1}}$) can be expressed as

$$\gamma = \gamma_{\max} \sin(\frac{\pi t}{\tau}) , \qquad 0 \leq t \leq \tau , \tag{2.64}$$

$$\gamma = 0 , \qquad \tau < t , \tag{2.65}$$

with

$$\tau = C \times \mathrm{Pr}_{\mathrm{OBS}}^{1/2} , \tag{2.66}$$

$$C = 6 \times 10^3 , \tag{2.67}$$

and

$$\gamma_{\max} = \frac{\pi}{2C} \times \mathrm{Pr}_{\mathrm{OBS}}^{1/2} . \tag{2.68}$$

Here $\gamma_{\max}$ is the maximum γ, and τ the duration time of the rainfall. Equation (2.66) was statistically obtained.

If the air temperature is low enough, rainfall changes to snow. Snow and rain are distinguished by the criterion temperature T_c given by Kondo (1994)

$$T_c = 11.01 - 1.5e , \tag{2.69}$$

$$T_{\mathrm{AM}} > T_c \ : \qquad RAIN \ , \tag{2.70}$$

$$T_{\mathrm{AM}} \leq T_c \ : \qquad SNOW \ . \tag{2.71}$$

The 'capture rate' of a rain gauge *cor* was used to correct the value of $\mathrm{Pr}_{\mathrm{OBS}}$ when the precipitation falls as snow (Kondo and Xu 1996d), given by

$$cor = 0.5 \exp(-0.26sU) + 0.5 \exp(-0.16sU) \ , \tag{2.72}$$

where

$$U = 0.7U_{\mathrm{OBS}} \ , \tag{2.73}$$

and

$$s = 1 - \frac{1}{1 + \exp(T_c - T_{\mathrm{AM}})} \ . \tag{2.74}$$

The corrected value of precipitation Pr is written as

$$\mathrm{Pr} = \frac{\mathrm{Pr}_{\mathrm{OBS}}}{cor} \ . \tag{2.75}$$

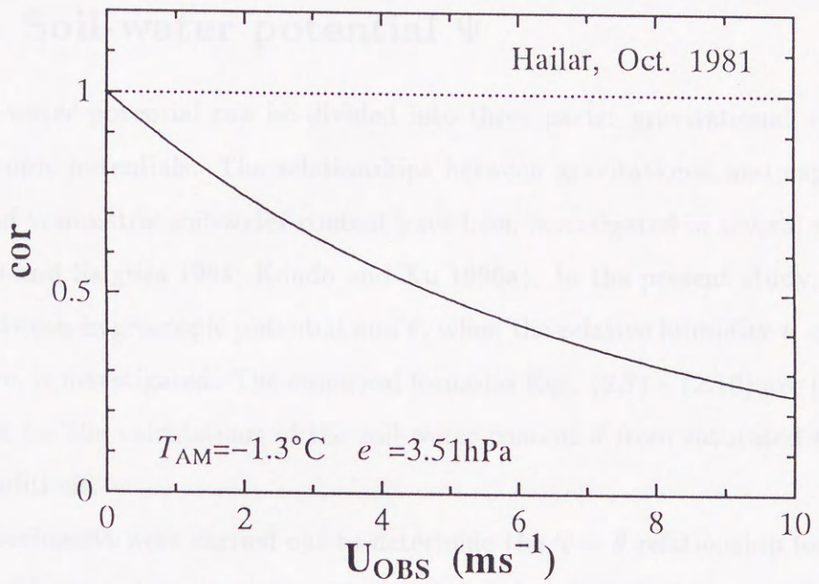

Fig. 2.1: The relationship between the observed daily mean wind speed U_{OBS} and the capture rate *cor* of rain gauge. The corresponding formulas are Eqs.(2.72)–(2.74) and Eq.(2.69), e.g., when T_{AM} is -1.3°C and e equals 3.51hPa, in Hailar, Oct. 1981.

Chapter 3

Parameters

3.1 Soil-water potential Ψ

Soil-water potential can be divided into three parts: gravitational, capillary, and hygroscopic potentials. The relationships between gravitational and capillary potentials and volumetric soil-water content have been investigated in several recent studies (Kondo and Saigusa 1994; Kondo and Xu 1996a). In the present study, the relationship between hygroscopic potential and θ, when the relative humidity $h < 100\%$ in the soil pore, is investigated. The empirical formulas Eqs. (2.7) – (2.10) are presented and adapted for the calculations of the soil-water content θ from saturated to sufficiently dry conditions.

Experiments were carried out to determine the $\Psi - \theta$ relationship for hygroscopic ranges. The sample soils used are the volcanic ash soil (Soil 1), clay loam (Soil 2), silty sand (Soil 3), and sand (Soil 4),The sampling locations for these soil types are Tsukuba (Japan), Lanzhou (China), Chiba (Japan), and Tottori (Japan), respectively. In the laboratory, small pans 0.02m high and 0.145m in diameter were filled with soil samples from each location. The evaporation rate and volumetric soil-water content for each sample were obtained through the weight changes of the pans. An electronic balance (Chyo MP-3000) having a precision of 0.01-grams was used to weigh the pans. Water vapor pressure e in the laboratory was measured every hour by a Vaisala psychrometer (RH and T probe HMP 13), and soil temperature T_G was simultaneously measured by a thermocouple. The temperature and the humidity of the laboratory room were maintained in a manner to force the evaporation from the soil to zero. On this state, it is considered that a local equilibrium existed between the liquid phase of water in

the soil particles and the vapor phase of water in the air. The $\Psi - \theta$ relationship for the hygroscopic range was then obtained from the following formula

$$h = \frac{e}{e_{SAT(T_G)}} = \exp[\frac{g\Psi(\theta)}{R_w T_G}] , \tag{3.1}$$

where $e_{SAT}(T_G)$ is the saturated vapor pressure at temperature T_G.

Note that the volumetric soil-water content in an equilibrium state θ_{EQ} can be obtained From Eqs. (2.11) and (3.1) as

$$\theta_{EQ} = -\frac{1}{a} \ln \frac{g\Psi(\theta_{EQ})}{\Psi_{01}} . \tag{3.2}$$

The potential $\Psi(\theta_{EQ})$ can be estimated from Eq.(3.1) when h in the equilibrium state is known.

Figure 3.1 shows the experimental results of the $\Psi - \theta$ relationships for the 4 types of soil. The solid line represents the volcanic ash soil (Soil 1), the dash-dotted line the clay loam (Soil 2), the dashed line the silty sand (Soil 3), and the dotted line the sand (Soil 4). Regions a, b and c represent the hygroscopic, capillary, and gravitational potential ranges, respectively. Figure 3.1 demonstrates that the removal of the water (water moving or evaporation) from Soil 1 is the most difficult and Soil 4 the easiest. When the liquid phase of water dominates in the soil, water movement in sand is easier than in volcanic ash soil. When the vapor phase dominates in the soil, the sand surface is the easiest type of soil to achieve to an equilibrium state with the atmosphere.

3.2 Evaporation efficiency β^*

There are several methods to parameterize the processes of evaporation from the soil surface. The $h\beta^*$-method (Eq. 2.17) is used in the present paper.

Experiments for estimating F for very small value of θ have been carried out in the laboratory. The instruments and framework are similar to those mentioned above (section 3.1). In this case, however, there is no need to obtain an equilibrium state between the atmosphere and the samples. The exchange speed $C_H U$ for the small pan

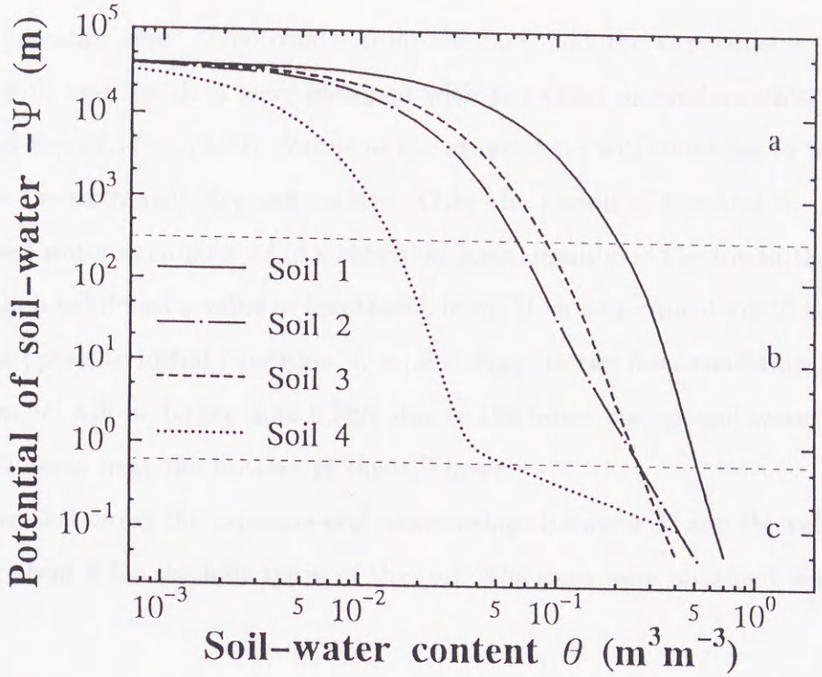

Fig. 3.1: The relationships between volumetric soil-water content θ and soil-water potential Ψ for the four types of soil. The solid line represents Soil 1 (volcanic ash soil), dash-dotted line Soil 2 (clay loam), dashed line Soil 3 (silty sand), dotted line Soil 4 (sand). The three regions of soil-water potential are shown by a) hygroscopic potential, b) capillary potential, and c) gravitational potential. The corresponding formula is Eq.(2.7).

was also determined by keeping another soil sample saturated by the hourly addition of water, maintaining the weight of the sample. It was assumed that the surface evaporation efficiency β^* would maintain a value of 1. A value of $C_H U$ =0.001ms^{-1} was adopted for each soil sample in this experiment.

Figure 3.2 shows the relationship between the volumetric soil-water content θ and the resistance F in the top soil layer (0.02m). The open squares denote observed data obtained from field observations (Kondo and Saigusa 1994; Kondo et al. 1995). The open circles represent the experimental results carried out in the laboratory. The solid lines were determined from the data and the use of Eq.(2.19). Parameters of f_A, f_B, f_C, and θ_{SAT} for each soil type are listed in Table 3.1.

In Fig. 3.2, a decreasing trend in the experimental data (open circles) can be seen

as θ approaches zero. This results from the fact that the experiments were started with $\theta = 0$, and the data were obtained with the value of condensation (negitive E) by use of Eqs.(2.17) – (2.19). Vapor in the atmosphere will condense to water when it contacts the extremely dry soil surface. Over the period of the first 0 – 2 hours, the condensed water accumulated in a very thin layer, mainly on the top of the soil surface and F then exhibited a value of less than 0.02m. If an experiment could be carried out from the opposite initial condition, i. e., $\theta = \theta_{\rm SAT}$, to the final condition in which θ is near zero, F will be larger than 0.02m due to the latest step of soil-water evaporation that will occur near the bottom of the soil layer.

Figure 3.3 shows the experimental relationships between β^* and the volumetric soil-water content θ for the four types of the soil. The lines were obtained with Eq.(2.18).

3.3 Albedo

The albedo calculations are carried out for both the bare soil and snow surfaces. The albedo of the surfaces differ from each other, and in addition change seasonally.

For the bare soil surface, it is assumed that the albedo changes with the soil-water content in the surface layer (0–0.02m). The surface albedo ref is given by

$$ref = ref_{\rm DRY}[1 - (1 - \frac{ref_{\rm WET}}{ref_{\rm DRY}} \times \frac{1}{B_{ref}})] \,, \tag{3.3}$$

where

$$ref_{\rm DRY} = ref_0\{6 - 5\cos[0.3(\phi - \delta)]\} \,, \tag{3.4}$$

with

$$B_{ref} = 1 + \exp[\frac{1}{\delta_{ref}}(\theta_{ref} - \theta)] \,. \tag{3.5}$$

In the above ref_0 is the albedo as the soil-water content approaches zero and the solar zenith angle is zero, $ref_{\rm WET}$ the albedo when the soil is wet, and ref_0, $ref_{\rm WET}$, δ_{ref}, and θ_{ref} are constants for each type of soil, being determined by experiments and observations (Table 3.1).

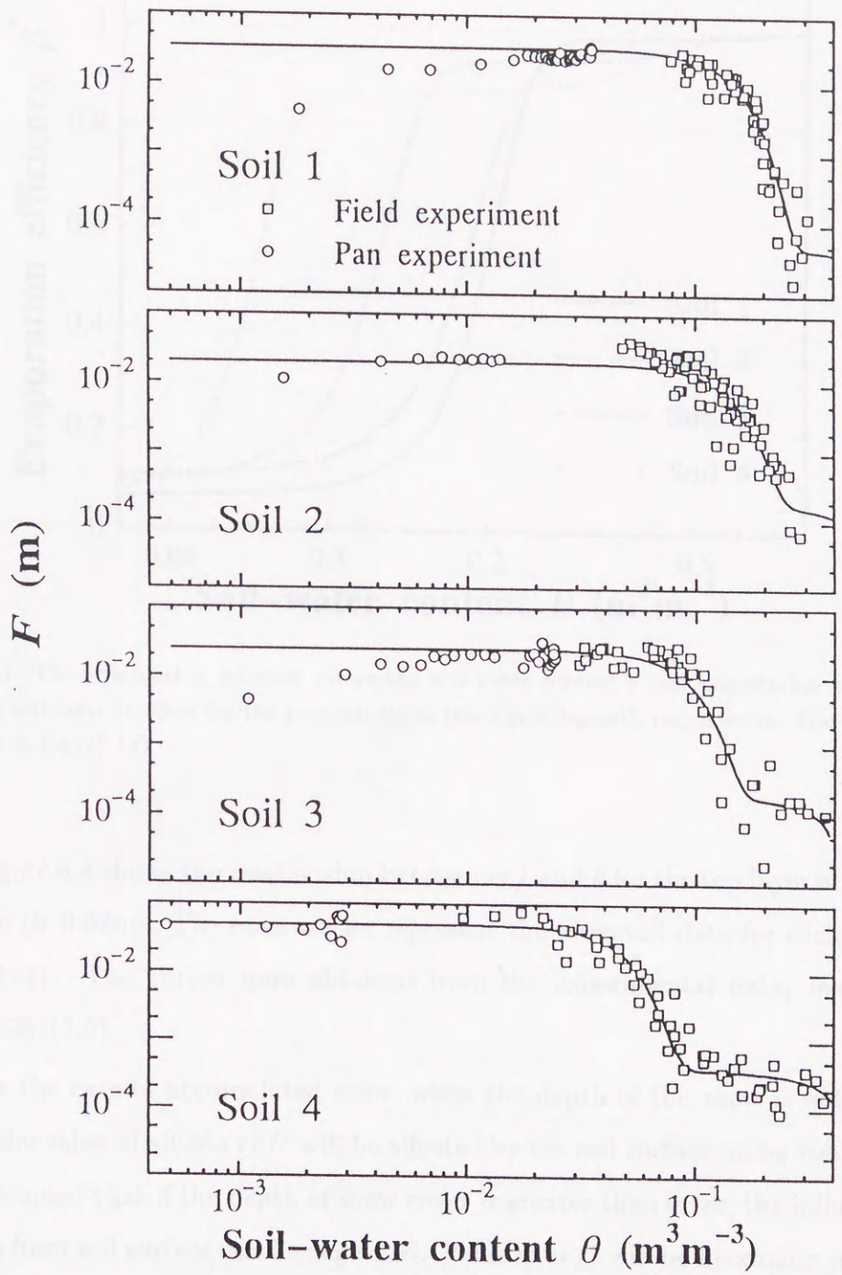

Fig. 3.2: The relationship between volumetric soil-water content θ and resistance F in the top soil layer (0.02m). From the top panel to the bottom panel, the plotted points are the observed data (squares) and experiments (circles) for Soil 1 to 4. Solid lines are results from Eq.(2.19).

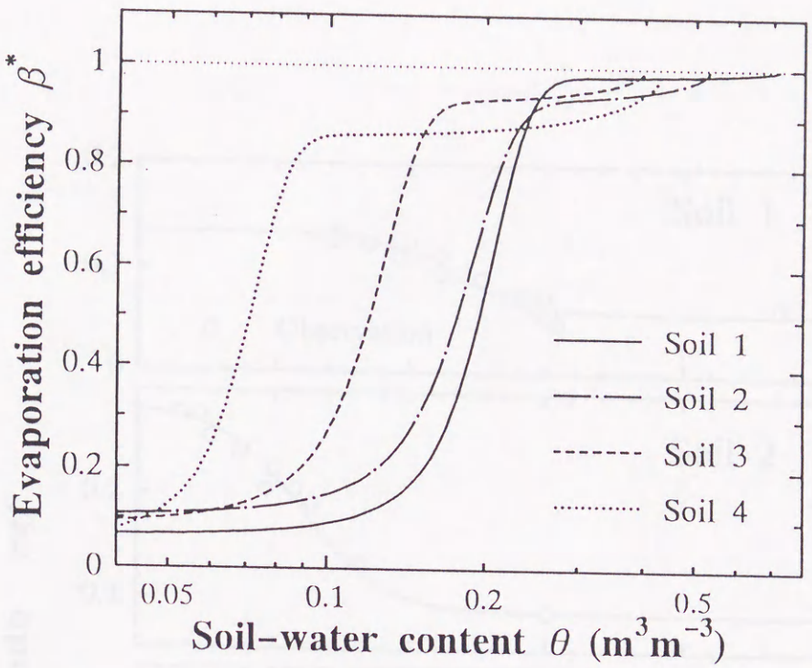

Fig. 3.3: The relationship between volumetric soil-water content θ and evaporation efficiency β^* in the top soil layer (0.02m) for the four soil types (see figure legend), respectively. The corresponding formula is Eq. (2.18).

Figure 3.4 shows the relationship between ref and θ for the top layer of the ground-surface (0–0.02m). The open circles represent the observed data for each soil surface (Soil 1–4). The curves were obtained from the experimental data, making use of Eqs.(3.3)–(3.5).

For the case of accumulated snow, when the depth of the snow is not sufficiently deep, the value of albedo ref^* will be affected by the soil surface under the snow cover. It is assumed that if the depth of snow cover is greater than 0.1m, the influence on the albedo from soil surface can be neglected. Value of ref^* will be maximum just after the snowfall occurrence, and reduced until another snow event. When the precipitation is determined to be snow according to Eqs.(2.69)–(2.71), and $\mathrm{Pr} > 3\,\mathrm{mm\,d^{-1}}$, the day is defined as a 'new snow day' ($m = 0$). The albedo of a 'new snow day' is $ref_{m=0}$, and

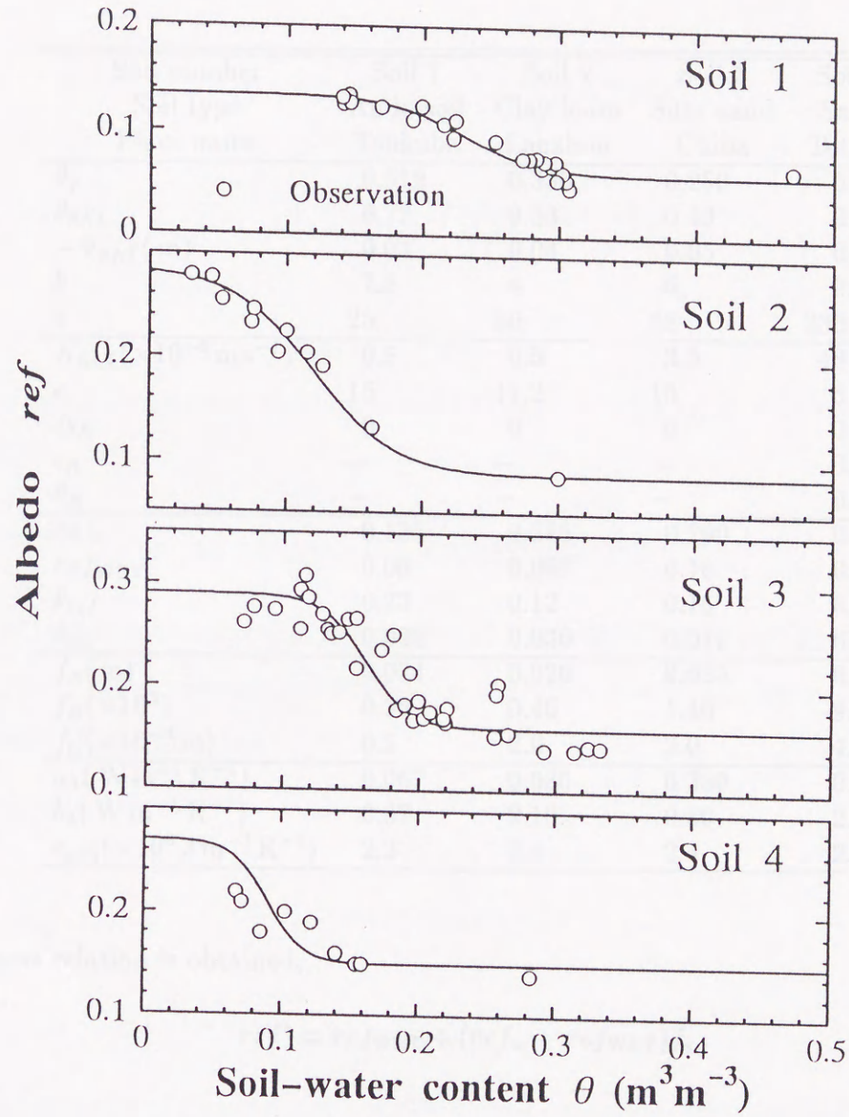

Fig. 3.4: Soil surface albedo (ref) versus volumetric soil-water content (θ) in the top soil layer (0.02m). From the top panel to the bottom panel, the plotted points are the observed data for Soil 1 to 4, respectively. The solid lines are calculated values by Eqs.(3.3) – (3.5).

Table 3.1: Soil parameters used in the present study.

Soil number	Soil 1	Soil 2	Soil 3	Soil 4
Soil type	Ando-soil	Clay loam	Silty sand	Sand
Place name	Tsukuba	Lanzhou	Chiba	Tottori
θ_f	0.512	0.336	0.250	0.086
$\theta_{\rm SAT}$	0.72	0.53	0.40	0.43
$-\Psi_{\rm SAT}(\,{\rm m})$	0.04	0.04	0.05	0.1
b	7.8	4	6	0.9
a	25	80	58	330
$K_{\rm SAT}(\times 10^{-5}\,{\rm m\,s^{-1}})$	0.5	0.5	3.5	48
c	15	11.2	15	6
Δ_K	0	0	0	0.9
ϵ_K	–	–	–	0.05
θ_K	–	–	–	0.07
ref_0	0.135	0.285	0.290	0.270
$ref_{\rm WET}$	0.06	0.087	0.16	0.15
θ_{ref}	0.23	0.12	0.16	0.09
δ_{ref}	0.028	0.030	0.016	0.013
$f_A(\,{\rm m})$	0.034	0.020	0.025	0.050
$f_B(\times 10^3)$	0.36	0.40	1.40	9.00
$f_C(\times 10^{-4}\,{\rm m})$	0.5	2.0	2.0	4.0
$a_\lambda(\,{\rm W\,m^{-1}\,K^{-1}})$	0.067	0.080	0.380	0.300
$b_\lambda(\,{\rm W\,m^{-1}\,K^{-1}})$	0.67	2.10	0.80	2.00
$c_s\rho_s(\times 10^6\,{\rm J\,m^{-3}\,K^{-1}})$	2.2	2.4	2.4	2.4

the next relation is obtained,

$$ref^* = ref_{\rm WET} + (ref_m - ref_{\rm WET})f_s\,. \tag{3.6}$$

Here,

$$f_s = 1 - \exp(-0.2W_{\rm snow})\,, \qquad ref_{m=0} = ref_{\rm MAX}\,, \tag{3.7}$$

$$ref_{\rm MAX} = 0.76 - 0.12T_{\rm AM}\,, \qquad (T_{\rm AM} \geq -1\ ^\circ{\rm C})\,, \tag{3.8}$$

$$ref_{\rm MAX} = 0.88\,, \qquad (T_{\rm AM} < -1\ ^\circ{\rm C})\,, \tag{3.9}$$

$$ref_m = (ref_{m-1} - 0.4)\exp(-1/k) + 0.4 \,, \tag{3.10}$$

$$k = 5.5 - 3T_{\mathrm{AM}} \,, \qquad (T_{\mathrm{AM}} < 0.5\ ^{\circ}\mathrm{C}) \,, \tag{3.11}$$

$$k = 0.4 \,, \qquad (T_{\mathrm{AM}} \geq 0.5\ ^{\circ}\mathrm{C}) \,, \tag{3.12}$$

and

$$ref_m \geq 0.4 \,, \tag{3.13}$$

where W_{snow} is the snow-water equivalent ($1\,\mathrm{kg\,m^{-2}} = 1\,\mathrm{mm}$), k is attenuation coefficient.

3.4 Physical thermal coefficients

For bare soil, the thermal conductivity λ_g, specific heat c_g, and soil density ρ_g of the ground are considered to be functions of the volumetric soil-water content in the 2nd layer (0.02–0.06m) as

$$\lambda_g = a_\lambda + b_\lambda \theta \,, \tag{3.14}$$

$$c_g \rho_g = (1 - \theta_{\mathrm{SAT}}) c_s \rho_s + \theta c_w \rho_w \,, \tag{3.15}$$

and

$$c_w \rho_w = 4.2 \times 10^6\,\mathrm{J\,m^{-3}\,K^{-1}} \,. \tag{3.16}$$

The parameters a_λ, b_λ, and $c_s\rho_s$ are determined experimentally (see Table 3.1).

The following formulas are substituted for a snow surface (Kondo and Xu 1996a),

$$\lambda_g^* = \lambda_g + (\lambda_{\mathrm{snow}} - \lambda_g) f_s \,, \tag{3.17}$$

$$c_g \rho_g^* = c_g \rho_g + (c\rho_{\mathrm{snow}} - c_g \rho_g) f_s \,, \tag{3.18}$$

where

$$\lambda_{\rm snow} = 0.2\,{\rm W\,m^{-1}\,K^{-1}}\ , \tag{3.19}$$

$$c\rho_{\rm snow} = 0.4 \times 10^6\,{\rm J\,m^{-3}\,K^{-1}}\ . \tag{3.20}$$

The constants $\lambda_{\rm snow}$ and $c\rho_{\rm snow}$ are the thermal conductivity and the thermal capacity of snow, respectively, and f_s is defined by Eq. (3.7).

3.5 Exchange speed C_HU

For bare soil surface, C_HU is given by

$$C_HU = 0.0027 + 0.0031 \times 0.7U_{\rm OBS}\ . \tag{3.21}$$

According to Kondo and Ishida (1997), the exchange speed under very unstable atmospheric conditions can be expressed as

$$C_HU = 0.0036(T_{\rm S} - T_{\rm A})^{1/3}\ . \tag{3.22}$$

Here $T_{\rm S}$ is the calculated value of the surface temperature. The larger value between Eq.(3.21) and Eq.(3.22) is used in the present calculations.

For a snow surface, C_HU is expressed as

$$C_HU = 0.001 + 0.002 \times 0.7U_{\rm OBS}\ . \tag{3.23}$$

When the atmosphere is very unstable ($T_{\rm A} \ll T_{\rm S}$) over a snow surface, C_HU can be written as

$$C_HU = 0.0012(T_{\rm S} - T_{\rm A})^{1/3}\ . \tag{3.24}$$

As in the snow surface case, the larger value between Eq. (3.23) and Eq. (3.24) is substituted in the model calculations.

3.6 Snow melting process

Snow over a ground-surface melts in the daytime if it is warm enough, and freezes during the night. This processes was simulated by the heat budget method used in the research of Kondo and Yamazaki (1990). Several simplifications were then carried out by Kondo and Xu (1996a).

Chapter 4

Verification of the method of calculation

The verification of the calculated results will be accomplished with observed data from the volcanic ash soil (Soil 1) surface in Tsukuba, and from the Tottori sand (Soil 4) dune field (details can be found in Kondo and Xu 1995).

Figure 4.1 shows the calculated and observed results for the Soil 1 surface in Tsukuba, during the year 1983. The top panel in Fig.4.1 exhibits the solar radiation (solid line) and the downward longwave radiation (open circles), the 2nd panel the input data of observed daily precipitation. The solid line in the 3rd panel is the calculated result of volumetric soil-water content on 0900JST at the depth of 0.1m every day, while the circles indicate the observed data on 0900JST (Okuyama 1988). The calculated values are in good agreement with those observed. The 4th panel in Fig.4.1 shows the calculated temperature (solid line) on 0900JST at the depth of 0.05m and the observed temperature (circles) at the depth of 0.04m every day. There is a good agreement between observed and calculated results of ground temperature. The bottom panel in Fig.4.1 shows the calculated result of daily evaporation. The value of total evaporation from the Soil 1 surface was 774mm in 1983.

The calculations were also carried out for the Tottori sand dune field from 21 June to 28 July 1983. The value of total evaporation during this period was 56.6mm. There was a 33.5mm rainfall event on 23 July. Figure 4.2 shows the hourly time series of calculated and observed results for the five days from 24 (the day after the rain event) to 28 July 1983 (the bottom abscissa is labelled in hours after Jan. 1st and the top abscissa is in day). The top panel of Fig.4.2 shows the solar radiation. The

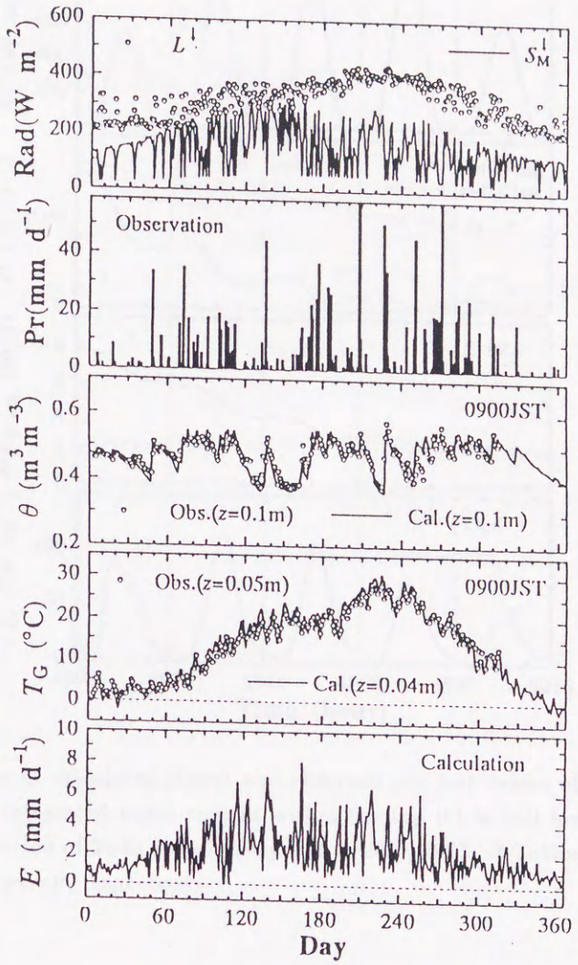

Fig. 4.1: Seasonal variations of the calculated and observed values for the volcanic ash soil field at Tsukuba in 1983. The top panel shows calculated daily means of the solar radiation $S^{\downarrow}_{M}$ (line) and the daily mean downward longwave radiation $L^{\downarrow}$ (circles), the 2nd panel the observed daily amount of precipitation, the 3rd panel the calculated (line) and observed (circles) soil-water content at the depth of $z = 0.1$m on 0900JST, the 4th panel the calculated (line) and observed (circles) ground temperature at the depth of $z = 0.04$m (calculation) or $z = 0.05$m (observation) on 0900JST, and the bottom panel the calculated daily evaporation.

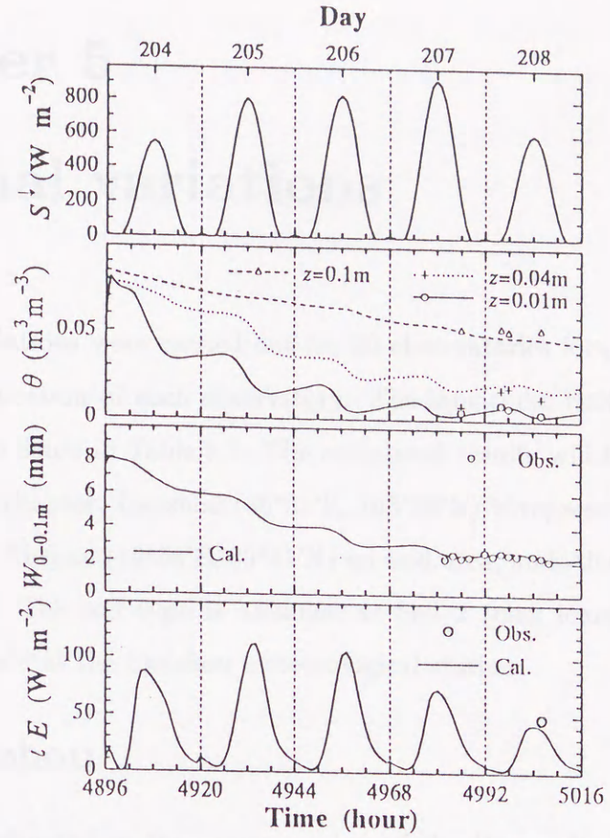

Fig. 4.2: Time series of calculated (lines) and observed (circles) values of the solar radiation $S^{\downarrow}$, soil-water content θ, integrated water content within the top 0.1 m soil layer $W_{0-0.1\,\mathrm{m}}$, and latent heat flux ιE for the period of 24 to 28 July (day 204 to 208), 1983, at Tottori sand dune field, shown in the top to bottom panels, respectively.

curves in the 2nd panel represent the volumetric soil-water content at the depths of 0.1m (dashed line), 0.04m (dotted), and 0.01m (solid), while the plotted points are the observed data (Kobayashi *et al.* 1991) corresponding to the three depths (see the figure legend). Integral values of volumetric soil-water content from the soil surface to the depth of 0.1m (solid line) are shown in the 3nd panel of Fig. 4.2. Observed values (plotted points) agree very well with the calculated values. The 4th panel is the hourly time series of the latent-heat flux.

Chapter 5

Seasonal variations

Model calculations were carried out for 30 observatories located in China. Figure 6.1 shows the location of each observatory. The longitude, latitude and elevation of each station are listed in Table.6.1. The calculated results will be discussed for three stations in this chapter. Lanzhou (36°03'E, 103°53'N) is representative of a semi-arid climatic region, Turpan (42°56'E, 89°31'N) an arid area, and Altay (47°44'E, 88°05'N) a snow region. The soil type is assumed as Soil 2 (clay loam) collected from the observational field at the Lanzhou meteorological station.

5.1 Lanzhou

Lanzhou is situated in the upper reaches of the Huang He (Yellow River), with the Tibetan Plateau located to the southwest. Figure 5.1 shows the calculated results for the year 1981 at Lanzhou. Figure 5.1a displays the seasonal variation of the daily mean net radiation Rn (Eq.2.23). The curve is generally sinusoidal during the year, but displays a decrease in the value of Rn during the dry season (day 113–169) due to the low surface soil-water content and increased albedo. After rainfall events (Fig.5.1e), such as during days 83, 104, 110, 195, and 232, the values of Rn obviously increased, due to smaller surface albedo for these days, with more shortwave radiation being absorbed by the humid ground surface. Figs.5.1b and 5.1c display the seasonal variations of the daily mean sensible and latent heat fluxes, respectively. Values of H generally exhibit a sinusoidal throughout the year, except for the decrease in H from day 231–254 due to abundant soil-water content (see Fig. 5.1d). Over this period, the evaporation process dominated the heat energy balance. Values of ιE were small,

and then increased during or after a rainfall event. Figure 5.1d shows the daily mean values of the soil-water content at the depths of 0.01m (the mean value for 0–0.02m, solid line), 0.04m (mean value for 0.02–0.06m, dotted line), 0.1m (mean value for 0.06–0.14m, dashed line), and 0.66m (mean value for 0.62–0.70m, dash-dotted line). If no rainfall occurred, the profile of the soil-water content tends to an increase from the surface layer ($\theta \approx 0.05 \mathrm{m^3 m^{-3}}$) to the bottom layer ($\theta \approx 0.28 \mathrm{m^3 m^{-3}}$). When a rainfall event occurs, the soil-water content will increase. The values of θ in the surface layer (solid line) are very sensitive to rainfall, but at deeper depths, θ will increase later than those in the surface layer. Figure 5.1e is the distribution of corrected precipitation values (Eqs. 2.64– 2.75) for Lanzhou. The total annual precipitation was 202mm during 1981. Figures 5.1f and 5.1g are the calculated (solid lines) and the observed (circles) of the daily mean, and the maximum and minimum ground-surface temperatures, respectively. Ground-surface temperatures are simultaneously obtained in the model. Note that, at the meteorological station in China, the ground-surface temperature is observed at the bare soil ground. The observed surface temperatures are used for checking the calculated results. It can be seen that the calculations are in good agreement with the observed values.

Daily changes were also estimated through model calculation. Figures 5.2 and 5.3 show the daily changes in the heat and water balances for the dry and rainy seasons in Lanzhou, respectively, during 1981. In the dry season (day120–140), the sensible heat flux (Fig.5.2b) responded to the change in shortwave radiation (Fig.5.2a). The values of H increased to maximums of approximately about $200 \mathrm{Wm^{-2}}$ during the daytime, then decreased to around $-30 \mathrm{Wm^{-2}}$ at night. This cycle corresponds to the maximum of ground-surface temperatures (Fig.5.2e) of about 50–60°C during the daytime and minimums of about 0–10°C at night. The maximum values of latent heat flux (Fig.5.2c) appeared in the daytime at about $50 \mathrm{Wm^{-2}}$ and minimum values near $0 \mathrm{Wm^{-2}}$ at night. Soil-water content (Fig.5.2d) exhibited a daily variation in the surface layer (solid line, 0.01m), and a decreasing trend at depths of 0.04m (dotted line) and 0.1m (dashed line). During the rainy season (day 220 – 240), soil-water content (Fig.5.3d) obviously

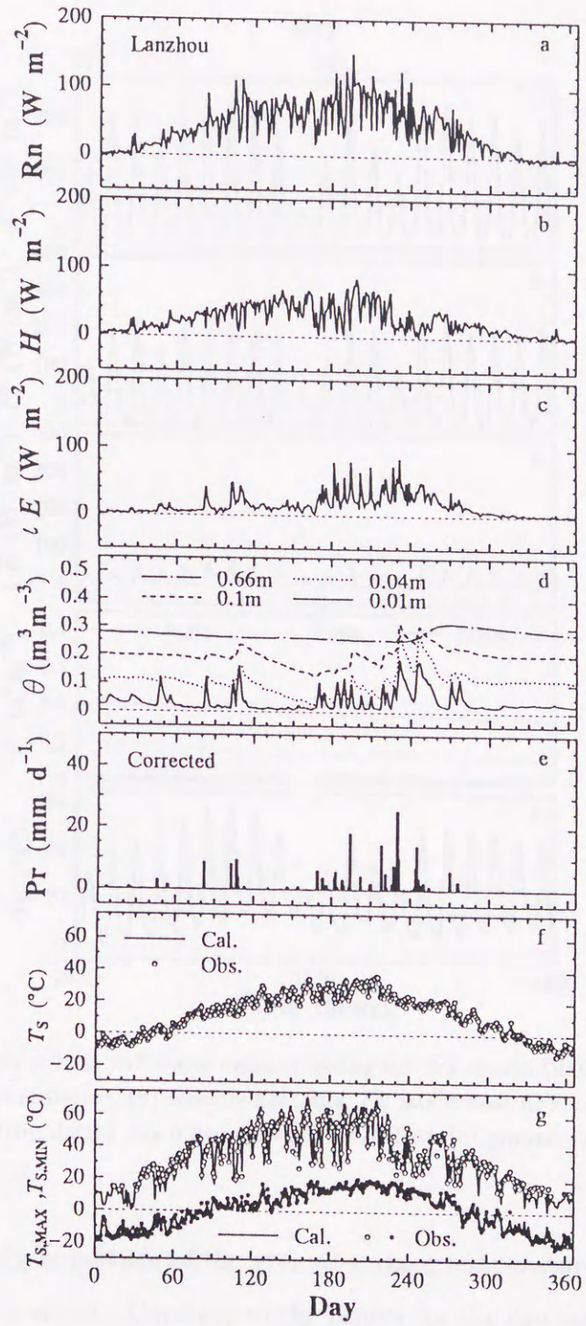

Fig. 5.1: The calculated results of seasonal variation for Lanzhou in 1981. (a) daily mean net radiation (Wm^{-2}), (b) sensible heat flux (Wm^{-2}), (c) latent heat flux (Wm^{-2}), (d) volumetric soil-water content (solid line 0.01m; dotted line 0.04m; dashed line 0.1m; dash-dotted line 0.66m), (e) daily amount of corrected precipitation, (f) daily mean value of ground-surface temperature (plotted points observed, solid line calculated.), (g) maximum and minimum ground-surface temperature (circles observations, solid lines calculated results).

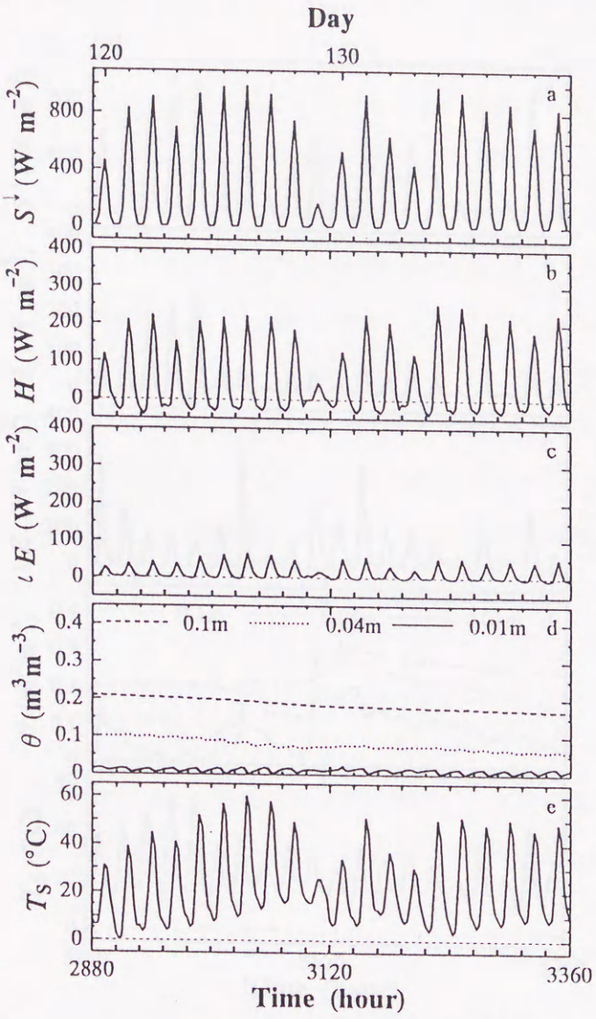

Fig. 5.2: Daily changes of heat and water balance during the dry season (day120 to 140) at Lanzhou in 1981. (a) shortwave radiation, (b) sensible heat flux, (c) latent heat flux, (d) volumetric soil-water content (solid line 0.01m; dotted line 0.04m; dashed line 0.1m), (e) ground-surface temperature.

increased. The daily amplitude of the ground-surface temperature (Fig.5.2e) was less than that in the dry season. Contrary to the results for the dry season, ιE was greater than H after a rainfall event. During day220 to 225 (there was a 14.4mm rainfall on day218), the maximum values of H increased continuously as 80, 120, 170, 220, and 270Wm^{-2}, while the maximum value of ιE decreased as 300, 170, 90, 80, and 70Wm^{-2}.

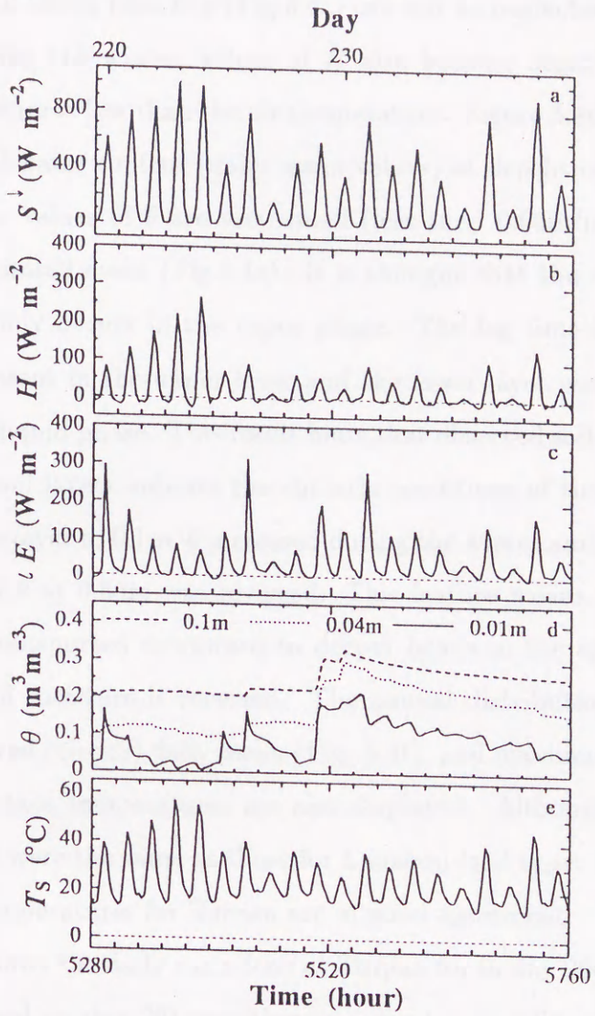

Fig. 5.3: The same as in Fig.5.2, except for the rainy season (day 220 to 240).

5.2 Turpan

Turpan is located in the northern region of the Taklimakan Desert, and the southern portion of the Gurbantunggut Desert. The total annual precipitation at Turpan was 14mm in 1981. The seasonal variations for Turpan are shown in Fig.5.4. Values of net radiation exhibit a sinusoidal curve in Fig.5.4a, with values of Rn being negative during the winter. Sensible heat flux (Fig.5.4b) generally corresponds to changes in Rn,

while the value of latent heat flux (Fig.5.4c) can not be neglected after a rainfall event (Fig.5.4e). During the winter, values of H also become negative when the ground-surface temperature is less than the air temperature. Figure 5.4d displays the seasonal variations of soil-water content (daily mean values) at depths of 0.01m, 0.04m, 0.1m, and 0.66m. The values of θ are very small (less than $0.03\mathrm{m}^3\mathrm{m}^{-3}$) in all soil layers, except after a rainfall event (Fig.5.4e). It is thought that the water exchange in the inner soil is mainly occurs in the vapor phase. The lag time between the variation in soil-water content in the upper layer and the lower layer was longer than that for exchange in the liquid phase. This result hints that observed soil-water content data in relatively deep soil layers indicate the climatic conditions of times past in the desert. From the surface layer to 0.1m, θ increased during the winter and decreased in summer, but the trend of θ at 0.66m was reversed. This feature means that soil-water in the upper layer is transported downward to deeper layers in the spring. In the fall, the movement of soil moisture is reversed. The annual distribution of calculated (solid lines) and observed (circles) daily mean (Fig. 5.4f), and maximum and minimum (Fig. 5.4g) ground-surface temperatures are also displayed. Although the soil parameters (Table 3.1) used were the same as those for Lanzhou (soil type: Soil 2), the calculated and observed temperatures for Turpan are in good agreement.

Figure 5.5 shows the daily variations at Turpan for in day 200–220. A 1.6mm rainfall event occurred on day 201 resulting in a maximum soil-water content (Fig.5.5d) in the surface layer (solid line) of $0.06\mathrm{m}^3\mathrm{m}^{-3}$. The latent heat flux (Fig.5.5c) also reached a maximum on day 201 ($244\mathrm{Wm}^{-2}$). Values of the maximum ground-surface temperature (Fig.5.5e) increased continuously from day201 to day 204, namely, 58°C, 69°C, 72°C, and 75°C. The sensible heat flux (Fig.5.5b) changed in response to the change in the shortwave radiation (Fig.5.5a). Except for the one rainy day, the maximum value of ιE was about $30\mathrm{Wm}^{-2}$ during the day, the minimum about $-10\mathrm{Wm}^{-2}$ at night, and a daily mean near zero. It is thought that the soil-water evaporated from the soil surface during the day and condensed on the soil surface at night. In humid areas, the relative humidity of the air in soil pore is generally in a saturated state, with

liquid water also existing in the soil pores. Therefore, evaporation always takes place from the soil surface. Being as dry as in Turpan, however, the soil-water content is so small that the relative humidity can not reach saturation values in the soil pore. The vapor is then exchanged between atmosphere and soil surface in trying to achieve an equilibrium state. Contrary to air, a soil layer will contain more moisture when the temperature decreases. This phenomenon also appears in the annual variation (Fig. 5.4d).

Curves in Fig. 5.6 show the relationship between ground-surface temperature T_S and volumetric soil-water content θ when the soil is in a state of equilibrium state with the atmosphere (Eqs. 3.2 and 3.1). The plots are obtained from the monthly mean values of calculated surface temperature and soil-water content in Turpan for the year 1981. Monthly mean values of vapor pressure e are used here; namely $e = 11.7$hPa (June, left panel) and $e = 1.8$hPa (December, right panel). The soil-water content in June ($T_S = 40°$C) is less than that in December ($T_S = -10°$C). Although soil-water content is not instantaneously in an equilibrium state with the ground-surface temperature, the monthly values of θ and T_S approximate to an equilibrium state.

5.3 Altay

Altay is situated between the southern slopes of the Altay Mountain Range, and the northern regions of the Gurbantunggut Desert. During 1981, the annual total precipitation was 228mm and the maximum depth of snow cover was 40cm. The yearly net radiation (Fig.5.7a) exhibits negative value from November to the end of March, then increases rapidly during the snow melting period (day73–86). During the same period, the latent-heat flux (Fig.5.7c) increased. This resulted from a decreased albedo (Fig.5.7d). Values of the sensible heat flux also become negative during the winter. Figure 5.8c displays the soil-water content at the four depths. Only a very small change in θ occurs over the winter period, but θ rapidly increased at each depth during the snow melting period. Although the total annual precipitation at Altay

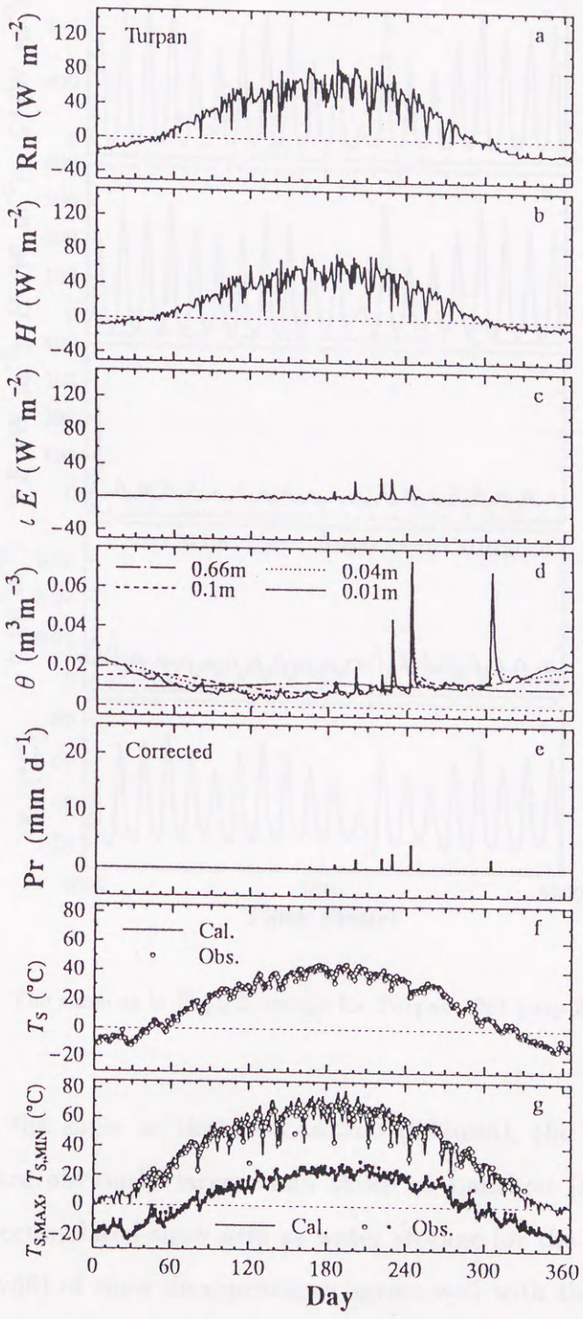

Fig. 5.4: The same as in Fig. 5.1 except for Turpan in 1981.

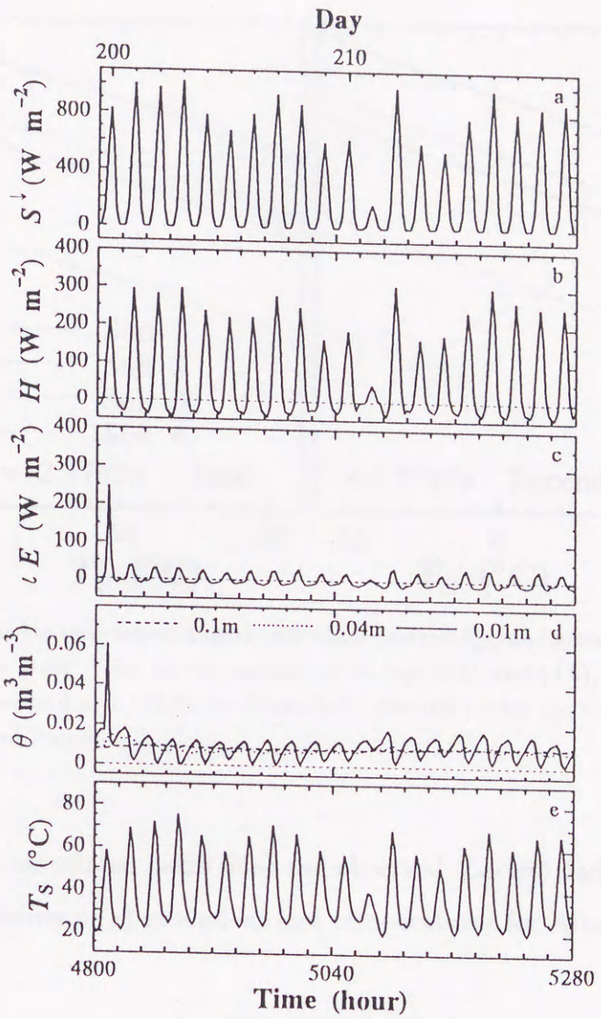

Fig. 5.5: The same as in Fig.5.2, except for Turpan 1981 (day 200 – 220).

(228mm) is about the same as that at Lanzhou (202mm), the values of soil-water content at Altay are obviously larger than those at Lanzhou (see Fig.5.1d). It is thought that the accumulated snow acts as water storage for the water balance. The calculated day (day86) of snow disappearance agrees well with that observed (day88, Figs.5.8a and b). When air temperatures (Fig.5.8e) are below -20°C, the calculated snow density (=snow water equivalent/depth of the observed snow cover) is determined as 200kgm^{-3}, and increases to 400kgm^{-3} during the snow melting period. Figures 5.8f

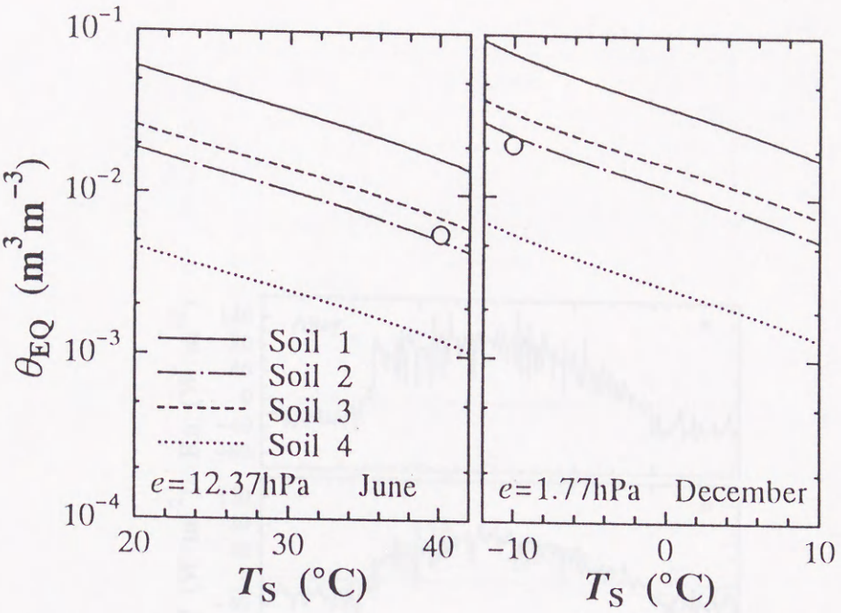

Fig. 5.6: The relationship between volumetric soil-water content θ_{EQ} and ground-surface temperature T_S in an equilibrium state. The curves correspond to Eqs.(3.1) and (3.2), with $T_G(= T_S)$ and e (e = 11.7hPa for June and e = 1.8hPa for December). Plotted circles are the calculated results for June and December of Turpan.

and 5.8g show the calculated (solid line) and observed (circles) daily mean (f), and the maximum and minimum (g) ground-surface temperatures for Altay.

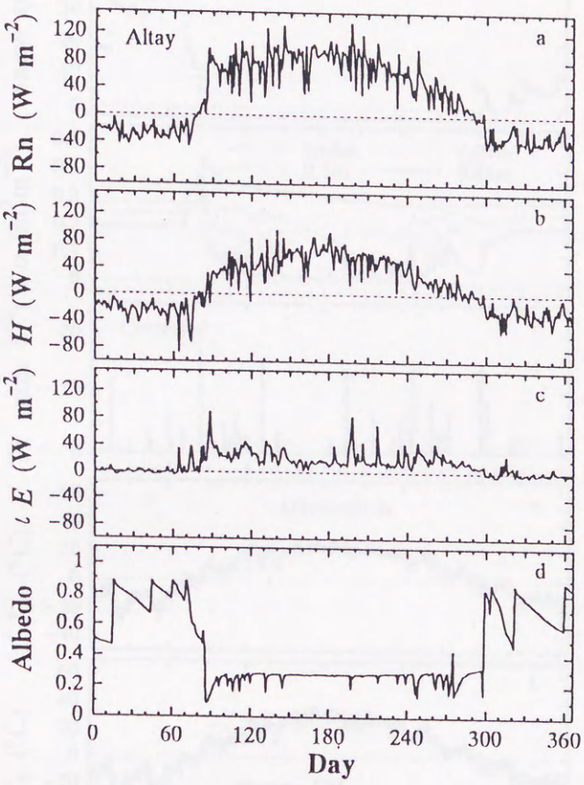

Fig. 5.7: The calculated results of seasonal variation for Altay in 1981. (a) daily mean net radiation, (b) sensible-heat flux, (c) latent- heat flux, and (d) albedo.

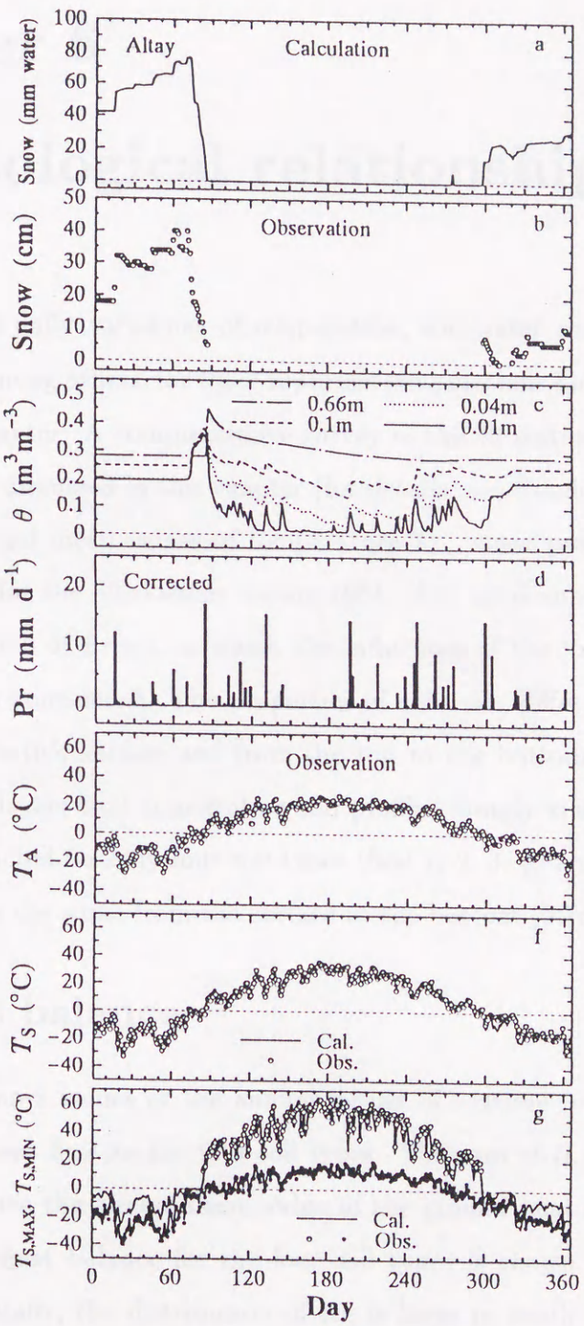

Fig. 5.8: The seasonal variations for Altay in 1981. (a) calculated value of the water equivalent of snow (mm), (b) depth of the observed snow cover (cm), (c) volumetric soil-water content (solid line 0.01m; dotted line 0.04m; dashed line 0.1m; dash-dotted line 0.66m), (d) daily amount of precipitation, (e)daily mean value of observed air temperature, (f) daily mean ground-surface temperature (plotted circles observed; solid line calculated results), (g) maximum and minimum of ground-surface temperature (plotted circles observations; solid lines calculated results).

Chapter 6

Climatological relationship

Seasonal and daily variations of evaporation, soil-water content, air and ground temperatures, among others, for three representative stations having Soil 2 were shown in the former chapter. A comprehensive survey of the 30 stations with four soil types in China will be discussed in this chapter (for details, see Kondo and Xu 1997). Table 6.1 lists the annual mean values of temperature T_A, vapor pressure e, and potential evaporation E_P for the 30 stations during 1981. The total annual precipitation Pr is the corrected value of Pr_{OBS}, in which the influences of the 'capture rate' and wind speed have been considered. The properties of soils can differ greatly from place to place over the earth's surface and from the top to the bottom through a succession of horizontal or layers that constitute a soil profile. Simply stated, these calculations have been conducted for only four soil types (Soil 1, 2, 3, 4) and it was assumed that the soil type was the same from the surface to the bottom (0.7m).

6.1 Heat balance

Figure 6.1 shows values of the annual means of sensible (open areas) and latent (shaded areas) heat flux for the four soil types. The sum of H and ιE equals the net radiation Rn, since the annual mean value of the ground heat flux G can be ignored (Eq.2.22). The heat balance for the four soil types is shown in one block for each station. In generally, the distribution of Rn is large in south and over the Tibetan Plateau region (Tuotuohe, Madoi, Deqen, Lhasa, Baingoin and Xigaze). Due to the elevation of the Tibetan Plateau being higher, precipitable water (Eqs.2.34 and 2.35) is less, and solar radiation is greater than other stations at the same latitude.

Table 6.1: The international index numbers, locations, and elevations of the observatories where the data for the calculations have been collected. Corresponding map is shown in Fig.6.1. T_A: annual mean air temperature, e: annual mean vapor pressure, Pr: annual value of corrected precipitation, E_P: annual potential evaporation in 1981. S, A, C, R, and T in the brackets represent that the locations of the corresponding observatories are in snow, arid, city, rural regions, and the Tibetan Plateau, respectively.

Name of the observatory	International index number	Lat. (N)	Long. (E)	Elev. (m)	T_A °C	e hPa	Pr mm/y	E_P mm/y
[S] Hailar	50527	49°13'	119°45'	612.8	−2.1	5.7	353	835
[S] Bugt	50632	48°46'	121°55'	738.6	−0.8	5.4	564	843
[S] Harbin	50593	45°45'	126°46'	142.3	3.8	8.0	665	1032
[S] Altay	51076	47°44'	88°05'	735.3	4.0	6.1	228	1161
[S] Fuyun	51087	46°59'	89°31'	823.6	3.2	5.1	175	1259
[S] Urumqi	51463	43°47'	87°37'	917.9	6.6	6.1	273	1226
[A] Turpan	51573	42°56'	89°12'	34.5	14.3	7.4	14	1635
[A] Hotan	51828	37°08'	79°56'	1374.6	12.2	6.6	50	1507
[A] Andir	51848	37°56'	83°39'	1262.8	10.5	5.5	39	1652
[A] Dunhuang	52418	40°09'	94°41'	1138.7	9.1	6.0	64	1468
[A] Jiuquan	52533	39°46'	98°29'	1477.2	6.8	6.0	136	1282
[A] Jurh	53276	42°24'	112°54'	1150.5	4.0	5.4	346	1725
[C] Lanzhou	52889	36°03'	103°53'	1517.2	9.7	7.6	202	1024
[C] Shenyang	54342	41°46'	123°26'	41.6	8.2	9.5	614	1158
[C] Beijing	54511	39°56'	116°17'	54.0	12.3	10.0	401	1404
[C] Jinan	54823	36°41'	116°59'	51.6	14.7	10.7	399	1752
[C] Xi'an	57036	34°18'	108°56'	396.9	13.4	12.3	735	977
[C] Changsha	57679	28°12'	113°05'	44.9	17.1	17.5	1458	1011
[C] Guangzhou	59287	23°08'	113°19'	6.6	22.0	22.1	2224	1107
[R] Lushi	57067	34°00'	111°01'	568.8	12.3	11.8	690	933
[R] Boxian	58102	33°52'	115°46'	37.7	14.3	13.4	652	1307
[R] Dongtai	58251	32°52'	120°19'	6.3	14.1	14.8	927	1127
[R] Hefei	58321	31°52'	117°14'	27.9	15.4	15.2	894	1223
[R] Nanping	58834	26°39'	118°10'	125.6	19.3	18.9	1570	1007
[T] Tuotuohe	56004	34°13'	92°26'	4533.1	−3.7	3.2	429	1246
[T] Madio	56033	34°55'	98°13'	4272.3	−3.2	3.5	425	1111
[T] Baingoin	55279	31°22'	90°01'	4700.0	1.3	3.1	470	1476
[T] Xigaze	55578	29°15'	88°53'	3836.0	6.1	4.7	335	1481
[T] Lhasa	55591	29°40'	91°08'	3648.7	7.4	5.4	338	1465
[T] Deqen	56444	28°30'	98°54'	3485.0	5.8	6.9	554	1292

Because of the shortage of water, H dominates the heat balance and the latent heat flux is extremely small in desert regions (Hotan, Andir, Turpan and etc.). The value of evaporation equals precipitation and has no relationship or dependence on the soil type. Due to the fact that the precipitation is so small, the values of precipitation

are less than the limits of evaporation for all soil types in the desert region. Sensible heat flux also exhibits a large value over Tibetan Plateau.

The value of Rn for Soil 1 is the largest among the four soil types, and Rn for Soil 4 is about 60% of that for Soil 1. Since soil-water can be retained in Soil 1 (volcanic ash soil) for a relatively long time, it is difficult for the soil surface to dry. The latent heat flux ιE maintains a large value and the ground-surface a low temperature for Soil 1 among the four soil types. In contrast to Soil 1, the soil-water in Soil 4 (sand) easily drains off, and the ground-surface dries rapidly after rainfall, increasing the surface temperature (σT_S^4) that leads to a small value of Rn. For Soil 1, the value of Rn in northern China and snow regions is about 38–57 W m^{-2}, in the southeast about 72–84 W m^{-2}, and in the Tibetan Plateau about 78–95 W m^{-2}. For Soil 4, the respective values are 22–37 W m^{-2}, 42–47 W m^{-2}, and 52–65 W m^{-2}.

6.2 Water balance

First, the concept of potential evaporation needs to be introduced. Potential evaporation is an important climatological index. Potential evaporation E_P in the present study is defined to be the evaporation expected in the conditions that the ground-surface maintains a continuous saturated state of soil-water content, and the daily mean values of the surface temperature, sensible and latent heat fluxes can be estimated from the daily mean energy balance, neglecting the ground heat flux G. According to this definition, E_P is related to air temperature, solar radiation, wind speed, and air humidity. This index is suitable to judge the degree of an arid climate.

Figure 6.2 displays the relationship between total annual precipitation Pr and evaporation E. The dimensions of Pr and E are normalized each by potential evaporation E_P. Plotted points represent the calculated values of 30 stations for the four soil types. The water resource of a station, which equals the annual drainage ($= \mathrm{Pr} - E$), is the balance between total annual precipitation and evaporation. In an area where the total

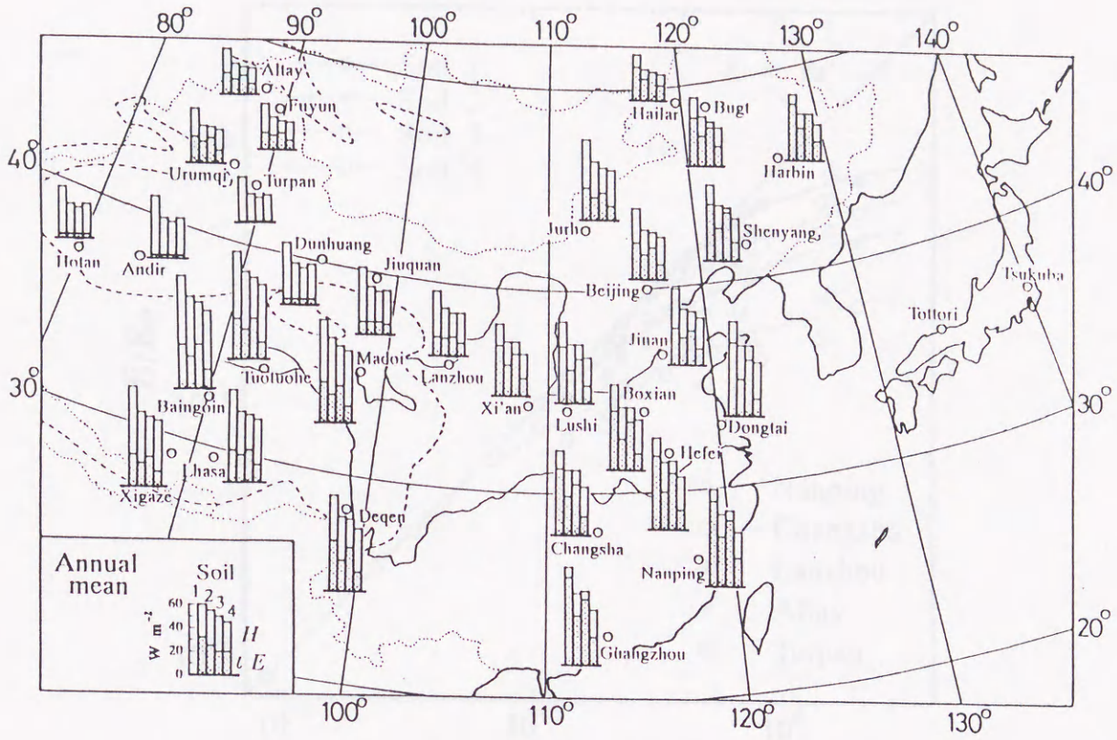

Fig. 6.1: The distribution of the annual means of sensible (H) and latent (ιE) heat flux in China, 1981. For the annual mean, $H + \iota E = \mathrm{Rn}$ and $G = 0$ (Eq.2.22). The heat balances for the four soil types (Soil 1 to 4) are shown in one block for each station.

annual precipitation is less than 100mm ($\mathrm{Pr}/E_\mathrm{P} \leq 0.05$), evaporation equals precipitation and has no relationship to the soil type. Drainage will occur when $\mathrm{Pr}/E_\mathrm{P} > 0.5$ for Soil 1 (volcanic ash soil), and $\mathrm{Pr}/E_\mathrm{P} > 0.05$ for Soil 4 (sand). The scatter in the plot is related to the temporal pattern of rainfall. For example, the total 1981 precipitation at Changsha (Fig.6.2: diamond) was 1458mm and at Nanping (Fig.6.2: triangle) 1574mm. The drainage in Changsha, however, is greater than Nanping for all soil types. This results because the 1981 rainfall in Changsha was concentrated in the spring, autumn, and winter. In Nanping, on the other hand, the precipitation was distributed throughout the year. Any concentration of rainfall advantageous to drain from soil and the value of evaporation during the summer is relatively small.

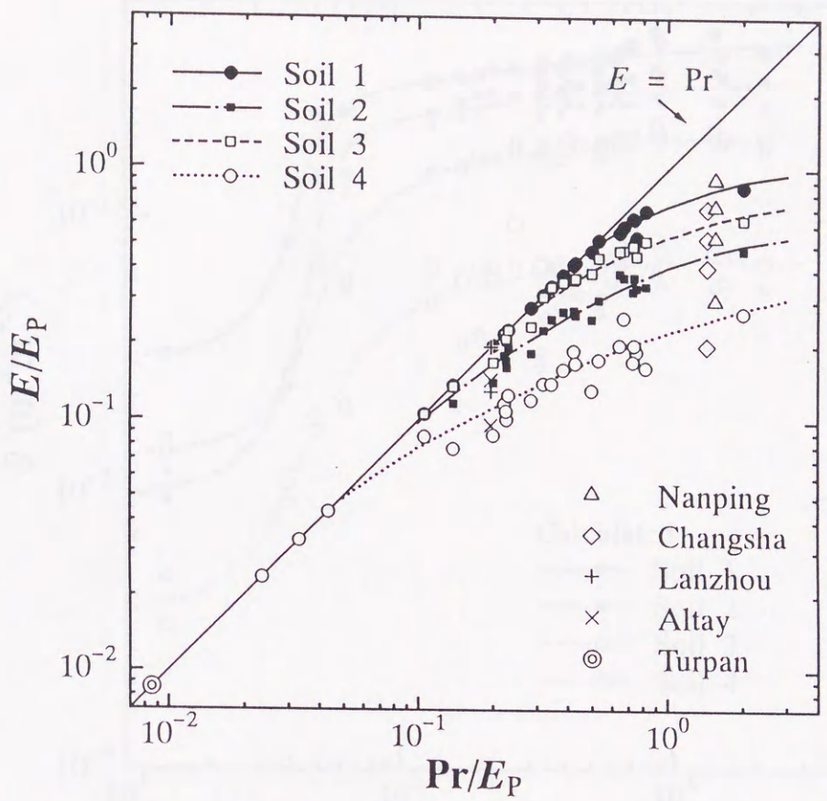

Fig. 6.2: The relationship between the non-dimensional annual precipitation Pr/E_P and the non-dimensional annual evaporation E/E_P. Plotted points represent the calculated values of the 30 stations for the four soil types. Curves are drawn based on the calculated values.

In arid and semi-arid areas, the drainage of a snow region is greater than a non-snow region. The total 1981 precipitation at Lanzhou was almost the same as Altay, but the drainage in Altay (Fig.6.2: cross) is greater than that in Lanzhou (Fig.6.2: plus).

6.3 Soil-water content

The day-to-day variation of θ is relatively small in winter. Figure 6.3 shows the relationship between volumetric soil-water content θ and the annual precipitation Pr for 1981. The plotted θ values are the daily mean on December 31 at each station. The plotted points have two scales, the small scale represents the calculated values at

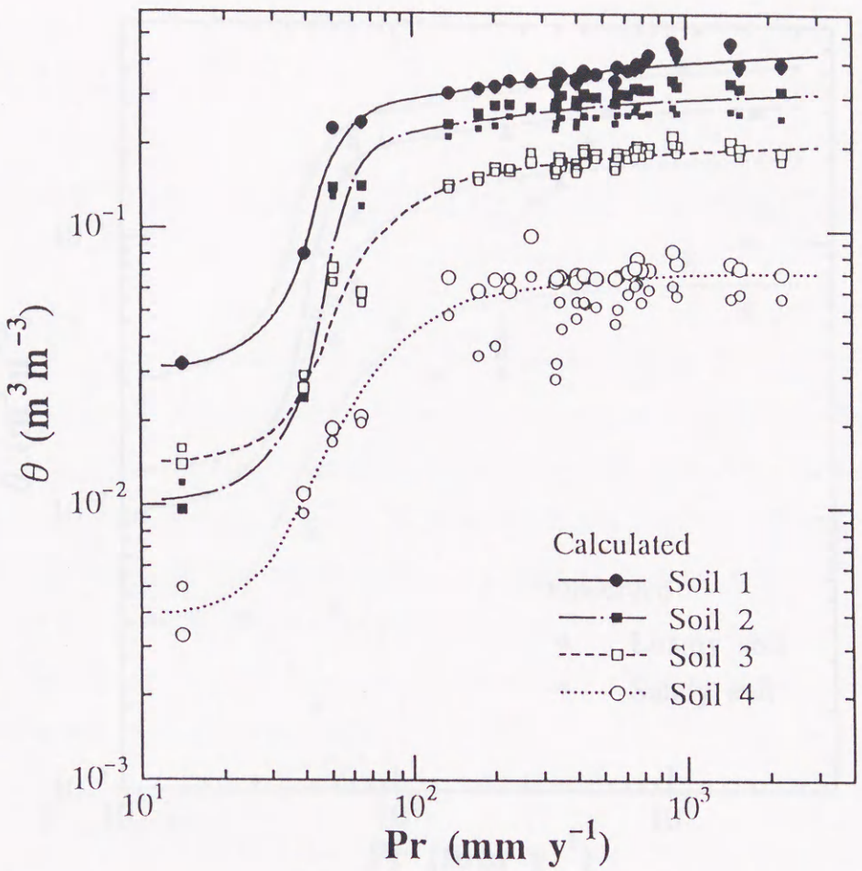

Fig. 6.3: The relationships between volumetric soil-water θ and the annual precipitation Pr in 1981. θ is the daily mean value on December 31 at each station. The small scale plotted points are the calculated values at the depth of 0.26m; large scale plotted points the calculated value at the depth of 0.66m. Each curve is drown along the medial values.

the depth of 0.26m, and the larger scale the calculated values at the depth of 0.66m. Compared to Soil 4 (sand), the plotted values are concentrated in Soil 1 (volcanic ash soil). The four lines (solid, dash-dot, dashed, and dotted) in Fig. 6.3 have the asymptotic values when Pr becomes very large or sufficiently small. When Pr becomes very large, θ tends toward field capacity θ_f values (see Table 3.1) of the four soil types. When Pr becomes very small, θ tends to θ_{EQ} (Eq.3.2) of the soil types.

Fig. 6.4 shows the observed data (plotted points) of soil-water content at depths of 0.2, 0.4, 0.75, 0–0.5, 0.3–0.4, 0.2–0.6m, etc. These data were collected from locations

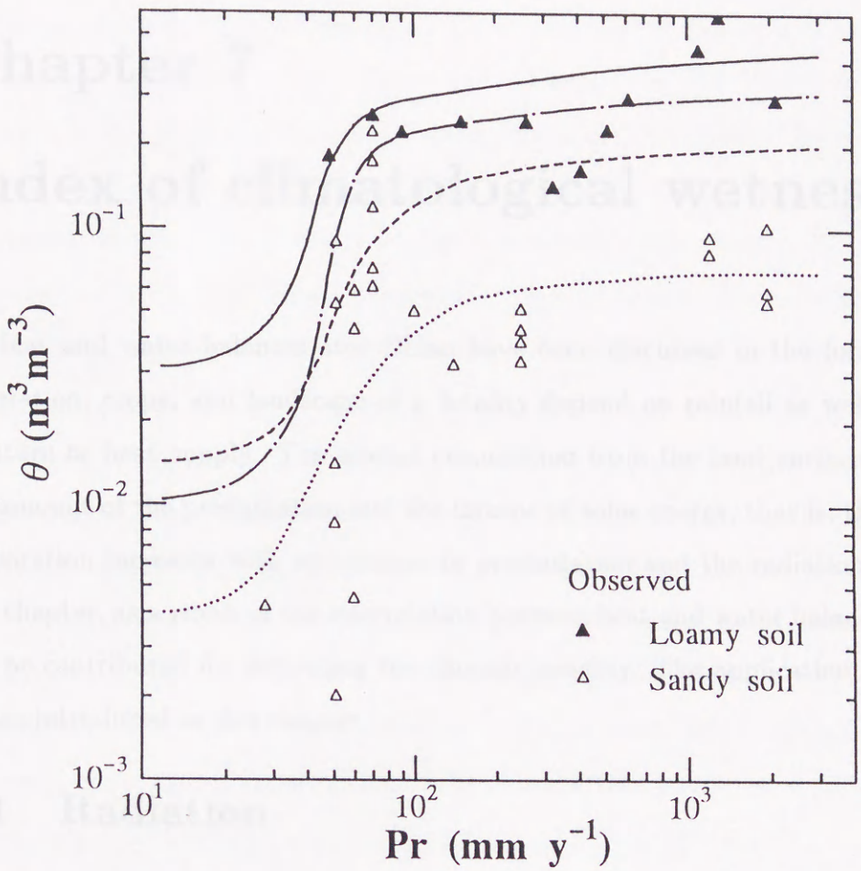

Fig. 6.4: The same as in Fig. 6.3, except for the plotted points are observed data.

in China, Japan, and Sri Lanka. Details concerning the observed data are discussed in Kondo and Xu (1997). Although the soil types, date and depth for the observed data in Fig. 6.4 are not consistent with the calculated conditions, the calculated results do not greatly differ from observations.

Chapter 7

Index of climatological wetness

Heat and water balances over China have been discussed in the former chapter. Vegetation, crops, and landscape of a locality depend on rainfall as well as on temperature or heat supply. The annual evaporation from the land surface depends on the amount of the precipitation and the income of solar energy, that is, the amount of evaporation increases with an increase in precipitation and the radiation balance. In this chapter, as a result of the interrelation between heat and water balances, an index will be contributed for delimiting the climatic zonality. The application of this index is also introduced in this chapter.

7.1 Radiation

The incoming energy arriving to the soil ground surface is the solar radiation and the downward longwave radiation. Using the routine meteorological data and the calculation method described in section2.3, the monthly mean values of the solar radiation and the longwave radiation fluxes were estimated for the 30 stations in China (Kondo and Xu 1997a). The geographic distributions of the solar radiation flux $S^{\downarrow}$ and the effective longwave radiation flux $\sigma T_{\mathrm{A}}^4 - L^{\downarrow}$ have been displayed in Figs.7.1–7.5, with the reference of the radiation data at 66 stations in Japan (Kondo and Kuwagata 1992). Light broken lines show the mountainous areas. Downward longwave radiation is very sensitive to the air temperature, water vapor, the amount of cloud, and the elevation, then the value of $\sigma T_{\mathrm{A}}^4 - L^{\downarrow}$ is suitable to analyze the longwave radiation.

In January (Fig.7.1), solar radiation flux is larger than 100 Wm^{-2} in the areas around and north of the Huanghe River (the Yellow River), the Tibetan Plateau,

northwest of China, the belt region on the Pacific side of Japan, and the subtropical sea area of the Pacific Ocean. There is a maximum as 180 Wm^{-2} in the Tibetan Plateau. In the areas of the Yungui Plateau, north of the Xinjiang Uygur Autonomous Region, and the the Sea of Japan, solar radiation is weaker than 60 Wm^{-2}. The geographic distribution of effective longwave radiation flux roughly corresponds with the solar radiation flux. The minimum of $\sigma T_A^4 - L^{\downarrow}$ located from the middle reaches of the Changjiang River (the Yangzi River) to the East China Sea.

In April (Fig.7.2), solar radiation is generally larger than that in January, but the geographic distribution of solar radiation flux is almost as same as in Fig.7.1. $S^{\downarrow}$ shows a value larger than 240 Wm^{-2} over the Tibetan Plateau to its northeast. The maximum of 300 Wm^{-2} places in west of the Tibetan Plateau. The minimum of $S^{\downarrow}$ is less than 100 Wm^{-2}, and located in the northern China. The difference between the maximum and the minimum of $S^{\downarrow}$ is even larger than 200 Wm^{-2}. $\sigma T_A^4 - L^{\downarrow}$ is larger than 80 Wm^{-2} from the Tibetan Plateau to the northern part of China. The place of the minimum $\sigma T_A^4 - L^{\downarrow}$ corresponds to that of the solar radiation.

In July (Fig.7.3), solar radiation flux is larger than 240 Wm^{-2} over the Tibetan Plateau to Mongolia, but the maximum of $S^{\downarrow}$ maintains its value in the Tibetan Plateau. The minimum area showed in April disappears in this month. The difference between the maximum and the minimum values of $S^{\downarrow}$ is not as large as in April. The value of $\sigma T_A^4 - L^{\downarrow}$ is relatively large in the Tibetan Plateau and Mongolia.

In October (Fig.7.4), the difference between the maximum and the minimum values of $S^{\downarrow}$ enlarges again. Close to the east of the Tibetan Plateau with the maximum of 260 Wm^{-2}, there is the minimum of 60Wm^{-2} in the southeast China, this distribution forms a sharp contrast. The geographic distribution of effective longwave radiation flux shows almost a same pattern with those of the solar radiation flux.

Fig.7.5 shows the geographic distributions of the solar radiation flux $S^{\downarrow}$ and the effective longwave radiation flux $\sigma T_A^4 - L^{\downarrow}$ in annual mean. Generally, The solar radiation and the effective longwave radiation fluxes are large in the arid region and the

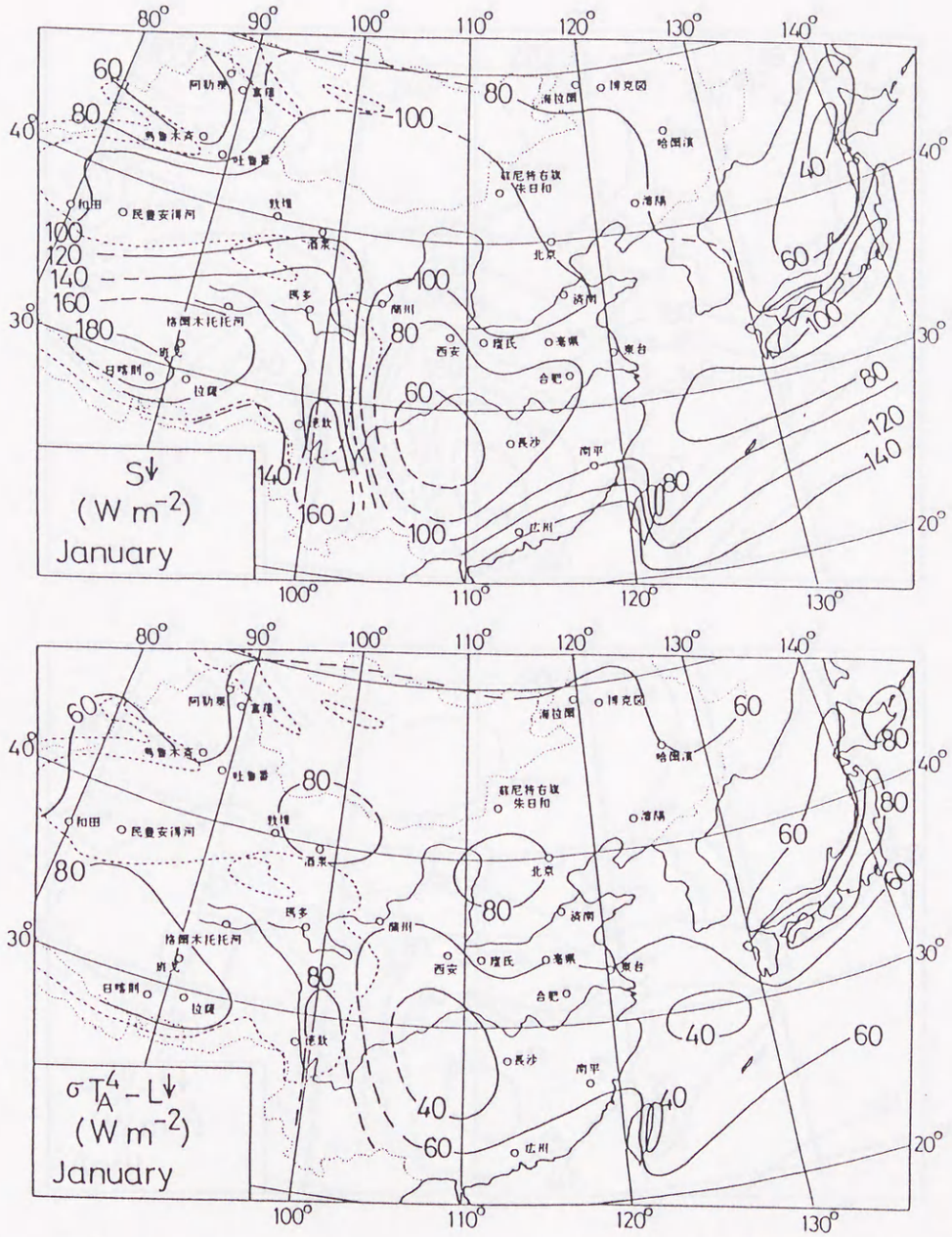

Fig. 7.1: Monthly mean of the radiation fluxes in January. Top: solar radiation flux $S^{\downarrow}$; bottom: longwave effective radiation flux $\sigma T_A^4 - L^{\downarrow}$.

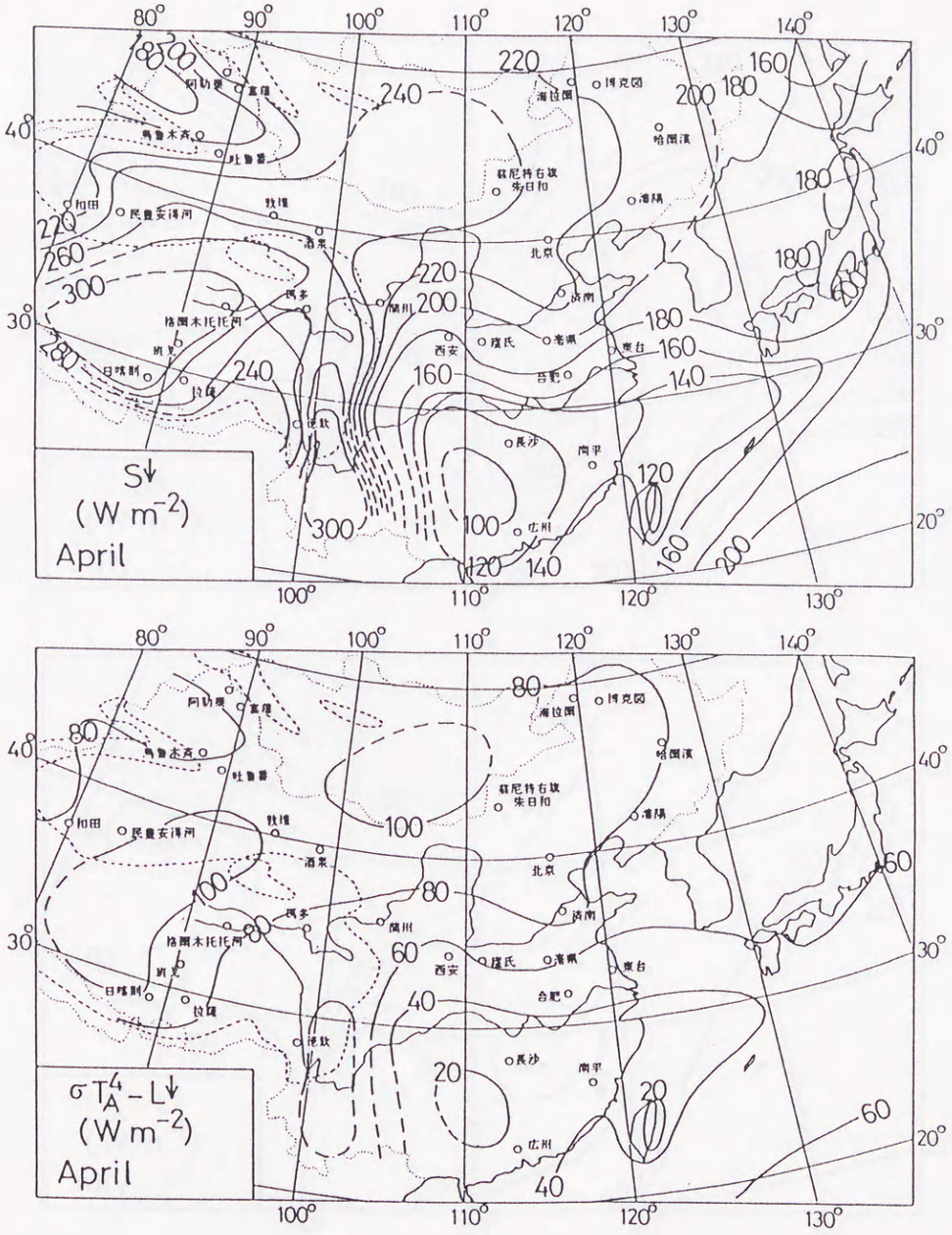

Fig. 7.2: The same as in Fig.7.1, except for April.

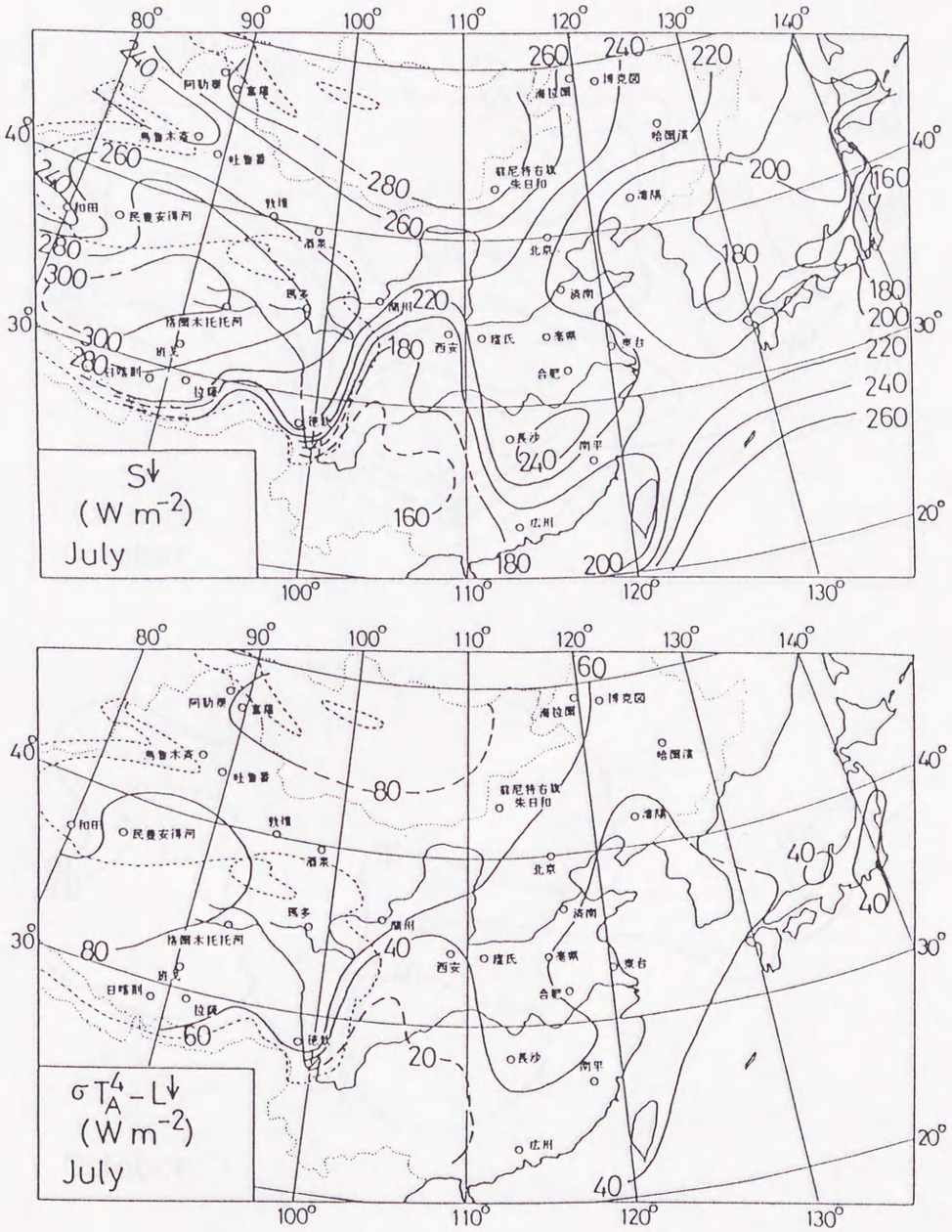

Fig. 7.3: The same as in Fig.7.1, except for July.

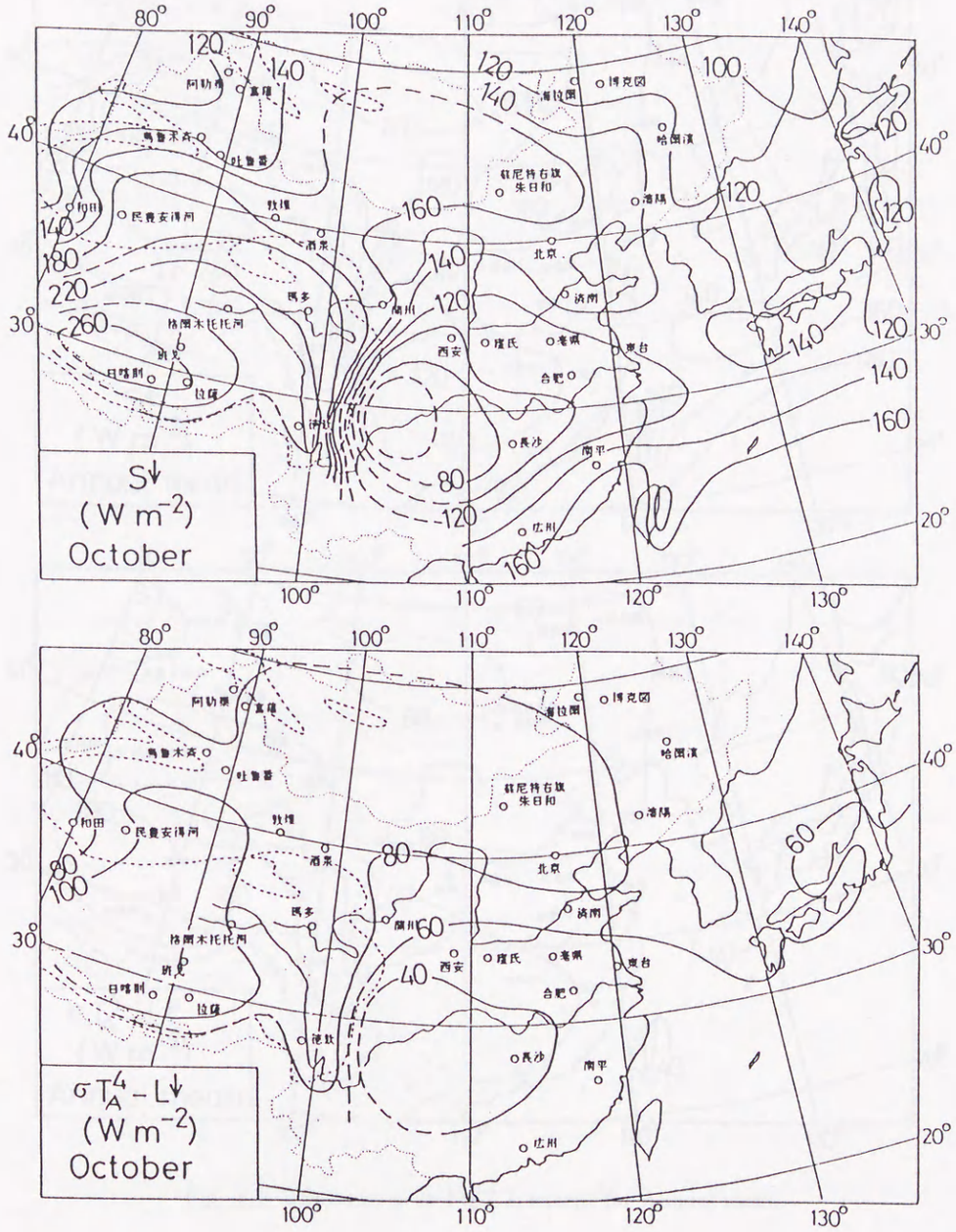

Fig. 7.4: The same as in Fig.7.1, except for October.

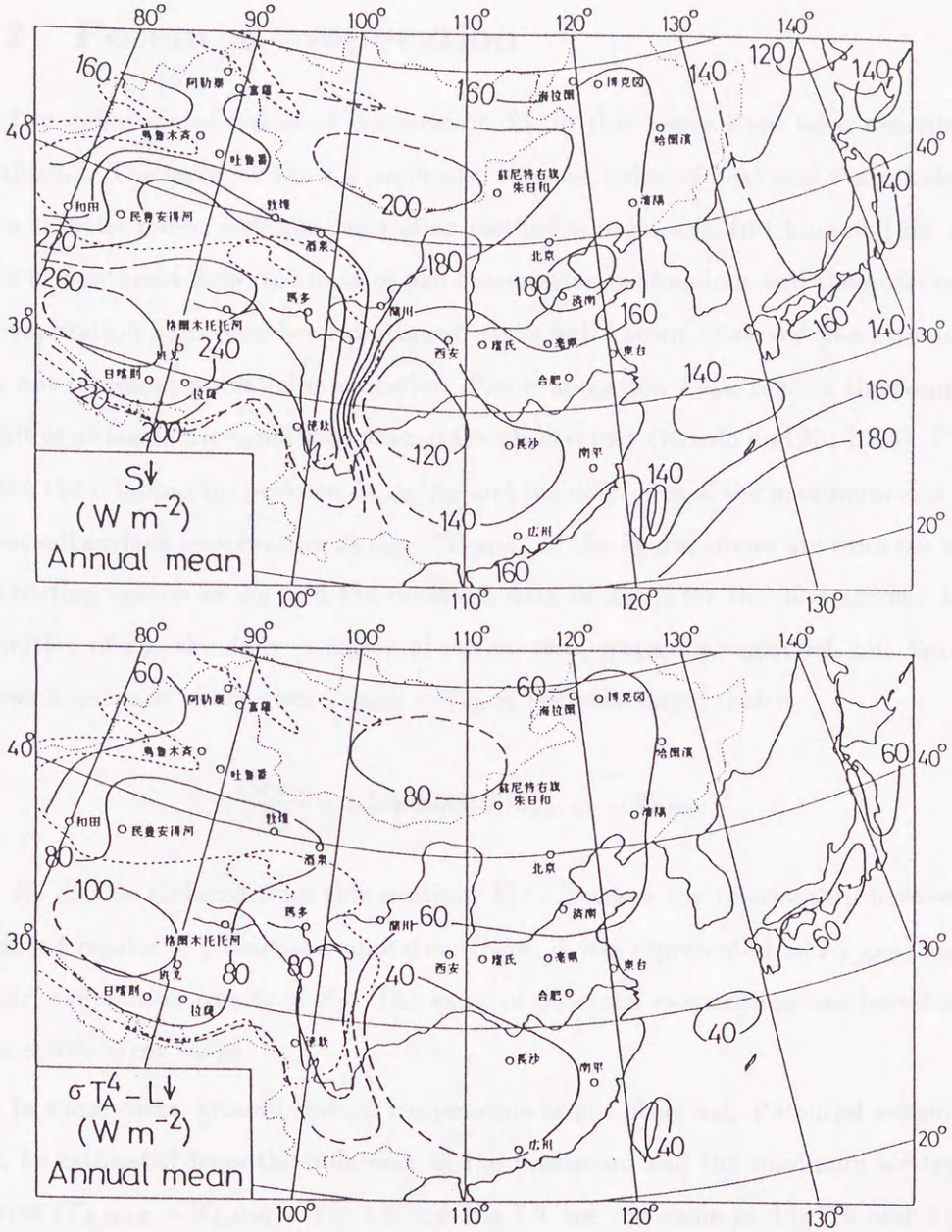

Fig. 7.5: The same as in Fig.7.1, except for Annual mean.

Tibetan Plateau, and small in the moist region. The effective longwave radiation flux shows a similar distribution with the solar radiation.

7.2 Potential evaporation

The definition of potential evaporation E_P in this paper have been described in section6.2. The value of E_P is a composite climatic index of heat and water balances. As a climatic index, a simple calculation method is necessary. In China and the countries in Southeast Asia, the data of pan evaporation is abundant and the observations of evaporation pans have been continued. As is well known, observed pan evaporation can not represent potential evaporation. Pan evaporation E_{PAN} reflects the composite result of atmospheric conditions around the observatory (Kondo and Xu 1996). Fig.7.6 shows the relationship between E_{PAN}/E_P and the difference of the maximum and minimum soil surface temperature $T_{S,MAX} - T_{S,MIN}$. In the figure, circles are from the model calculation results of E_P and the observed data of E_{PAN} for the 30 stations. In the definition of E_P, the daily variation of surface temperature is neglected, but E_{PAN}/E_P shows a increase trend when $T_{S,MAX} - T_{S,MIN}$ becomes large, that is

$$\frac{E_{PAN}}{E_P} = 1.1 + 0.00035(T_{S,MAX} - T_{S,MIN})^2 . \tag{7.1}$$

E_P can be deduced from this relation. Fig.7.7 shows the relationship between the deduced results of potential evaporation (here, it was represented as $E_{P,APP}$) and the model calculation results of E_P. The value of potential evaporation can be estimated in a $\pm 20\%$ error range.

In some cases, ground surface temperature is not observed. Potential evaporation can be estimated from the difference of the maximum and the minimum air temperatures ($T_{A,MAX} - T_{A,MIN}$). Fig.7.8 and Fig.7.9 are the same as Fig.7.6 and Fig.7.7, respectively, except that the ground surface temperature is replaced by the air temperature.

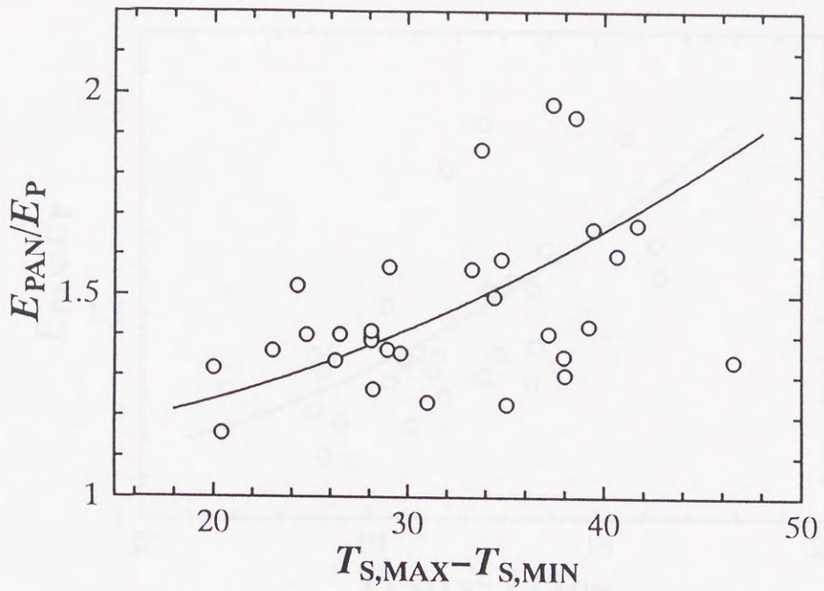

Fig. 7.6: The relationship between E_{PAN}/E_P and $T_{S,MAX} - T_{S,MIN}$, circles are from the model calculation results of E_P and the observed data of E_{PAN} of the 30 stations.

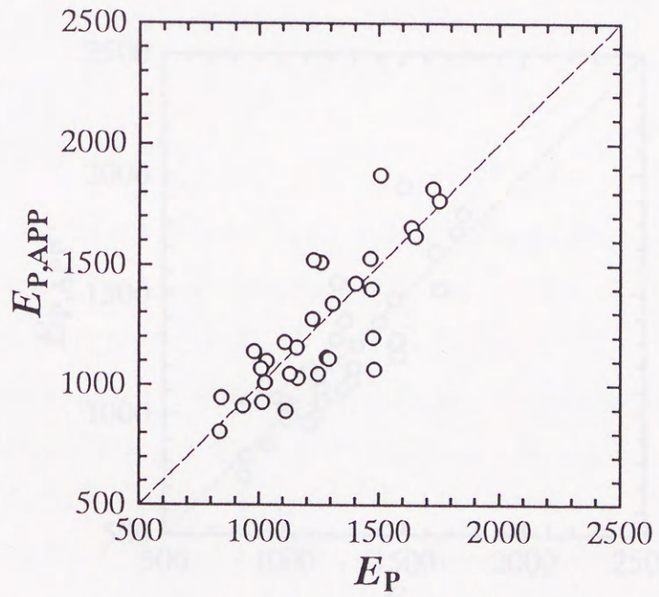

Fig. 7.7: The relationship between the deduced results of potential evaporation ($E_{P,APP}$) and the model calculation results of E_P.

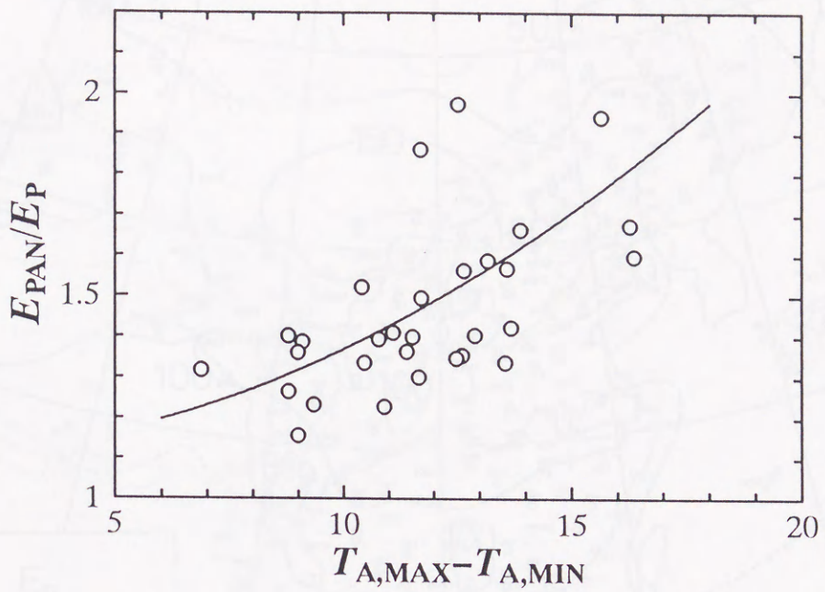

Fig. 7.8: The same as in Fig.7.6, except for air temperature.

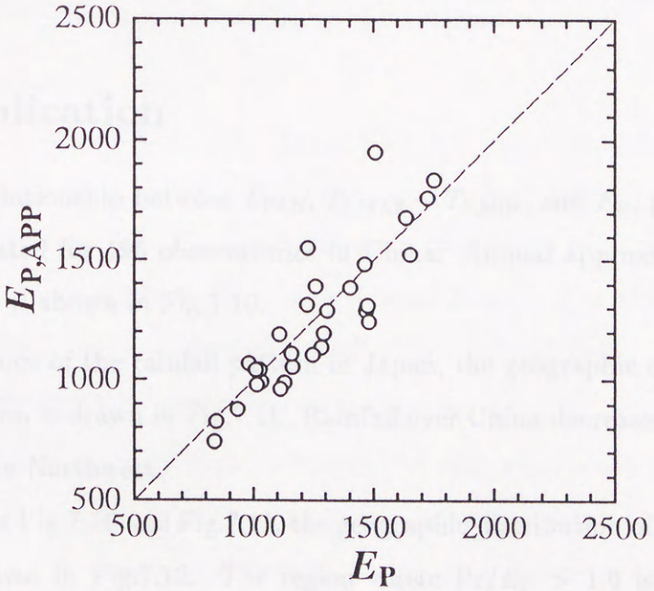

Fig. 7.9: The same as in Fig.7.7, except for estimation from the air temperature difference.

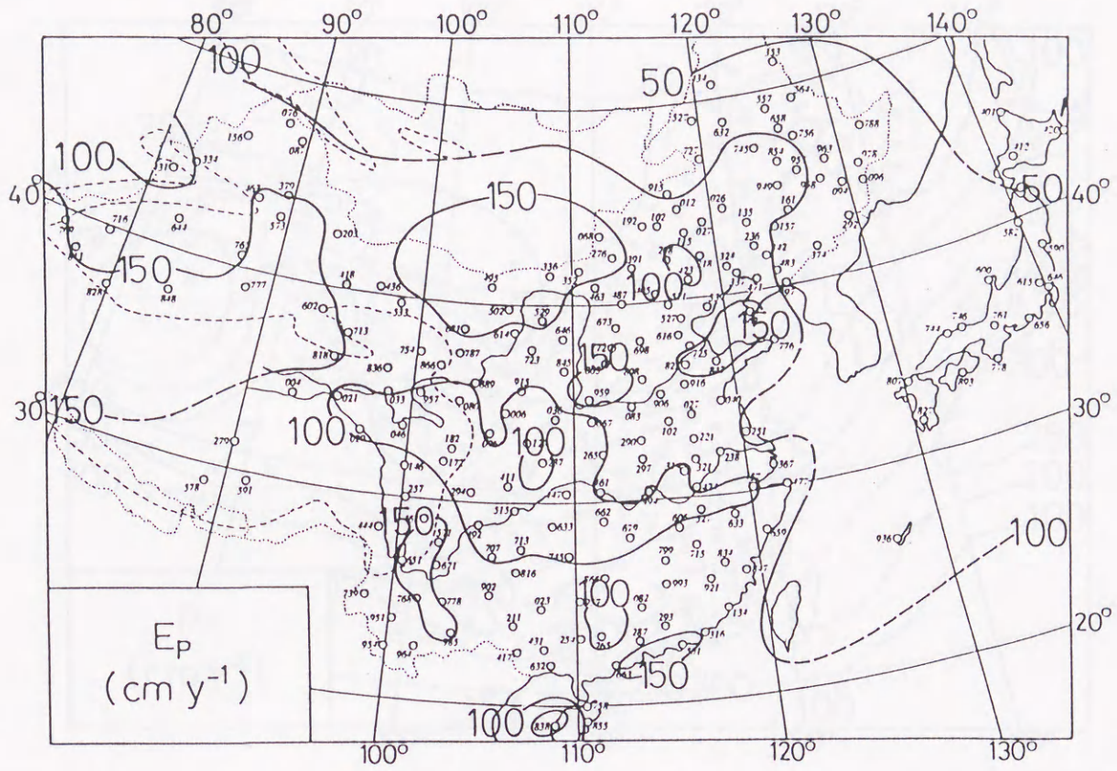

Fig. 7.10: Annual approximation of potential evaporation E_P(cm y^{-1}).

7.3 Application

Using the relationship between E_{PAN}, $T_{S,MAX} - T_{S,MIN}$, and E_P, potential evaporation was estimated for 195 observatories in China. Annual approximate of potential evaporation E_P is shown in Fig.7.10.

With reference of the rainfall pattern in Japan, the geographic distribution of annual precipitation is drawn in Fig.7.11. Rainfall over China decreases rapidly from the Southeast to the Northwest.

Synthesizing Fig.7.10 and Fig.7.11, the geographic distribution of the wetness index Pr/E_P was drawn in Fig.7.12. The region where $Pr/E_P > 1.0$ is defined as moist zone, $0.5 < Pr/E_P \leq 1.0$ is sub-moist zone, $0.2 < Pr/E_P \leq 0.5$ semi-arid zone, and $Pr/E_P \leq 0.2$ arid zone. Arid zone extends from the west of the Tibetan Plateau to

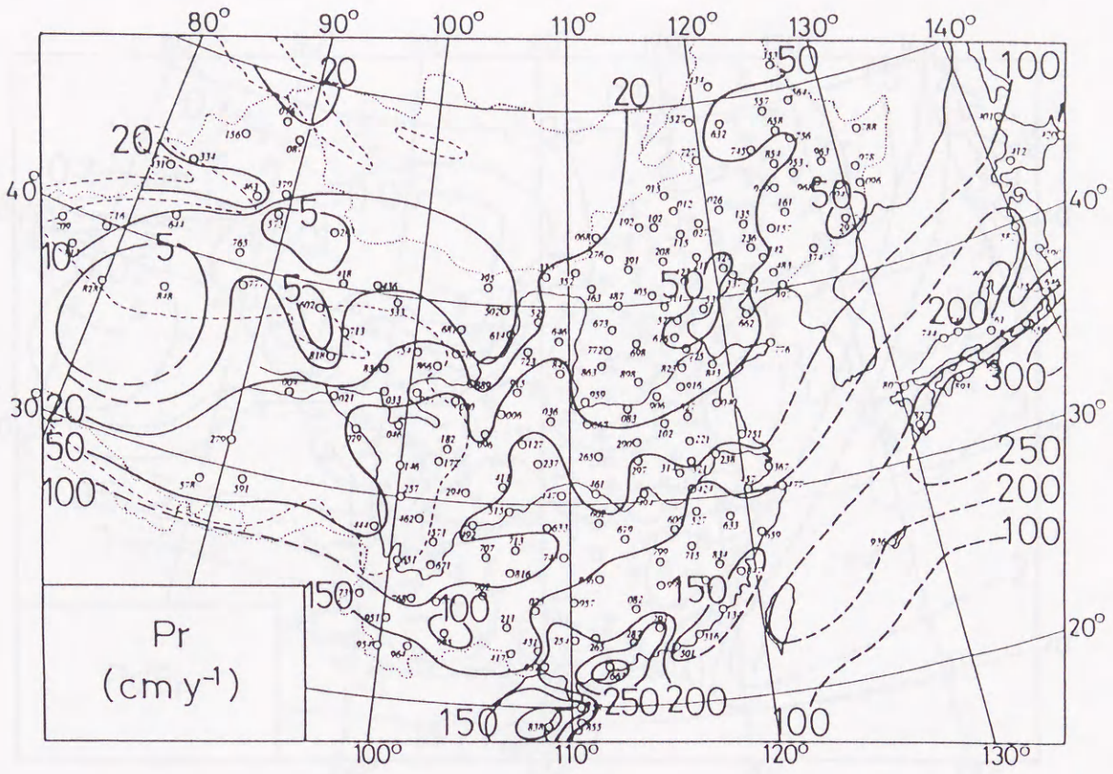

Fig. 7.11: Annual precipitation Pr (cm y^{-1}). Small circles with the numbers on the side represent the locations and the international index numbers of the observatories.

the northwest China and Mongolia. Strong solar and longwave radiation fluxes, short of precipitation, large potential evaporation, result small latent heat flux and large sensible heat flux (see Fig.6.1). Semi-arid zone distributes from northeast China to the middle and upper reaches of Huanghe River and the east of the Tibetan Plateau. Sub-moist zone is situated in the east side of semi-arid zone. Japan, Korean Peninsula and the northern part of China belong to moist zone.

The relationship between annual precipitation and evaporation has been shown in Fig.6.2. Clearly, the run-off will happen in the moist and sub-moist zones no matter what type of the soil. Run-off will decrease in the semi-arid zone, and even stop if the soil ground is composed by Soil 1. In arid zone, the annual evaporation approximately equals the annual precipitation ($E \simeq$Pr).

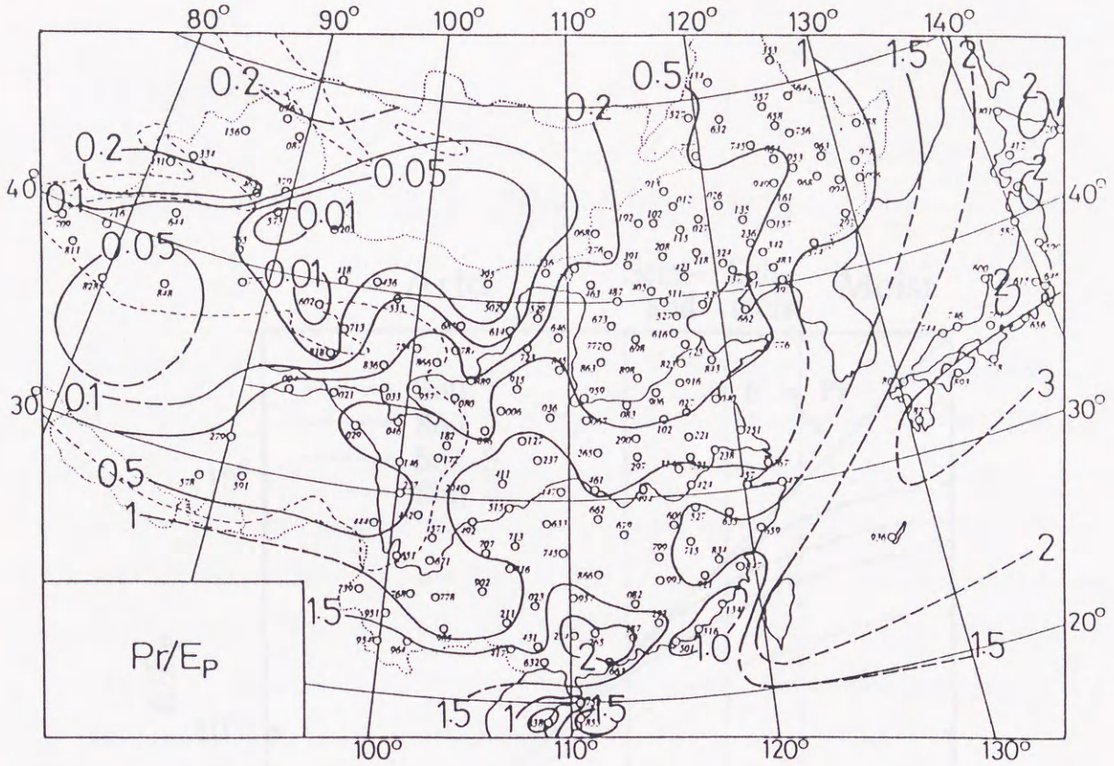

Fig. 7.12: The distribution of the wetness index Pr/E_P in 1981. $Pr/E_P \leq 0.2$: arid zone; $0.2 < Pr/E_P \leq 0.5$: semi-arid zone; $0.5 < Pr/E_P \leq 1.0$: sub-moist zone; $Pr/E_P > 1.0$: moist zone.

An index of wetness has been discussed in this chapter. The data in 1981 was used to plot the geographic distribution of the index in China and Japan. In the future studies, the yearly variations of this index should be investigated. The changes of semi-arid and sub-moist zones for a certain area should relate to the harvest yield. Monthly heat and water balances for 4 soil types in this study are tabulated in Appendix A.

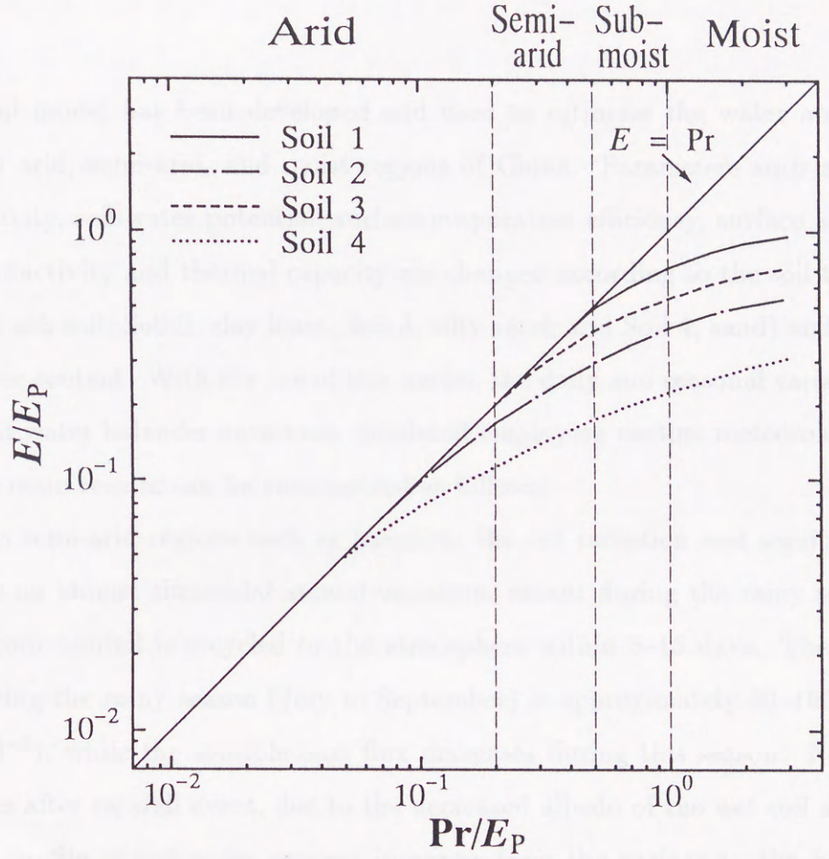

Fig. 7.13: The relationship between the non-dimensional annual precipitation Pr/E_P and the non-dimensional evaporation E/E_P (see Fig.6.2). $\mathrm{Pr}/E_\mathrm{P} \leq 0.2$: arid zone; $0.2 < \mathrm{Pr}/E_\mathrm{P} \leq 0.5$: semi-arid zone; $0.5 < \mathrm{Pr}/E_\mathrm{P} \leq 1.0$: sub-moist zone; $\mathrm{Pr}/E_\mathrm{P} > 1.0$: moist zone.

Chapter 8

Summary and conclusion

A soil model has been developed and used to estimate the water and heat balances in arid, semi-arid, and moist regions of China. Parameters such as hydraulic conductivity, soil-water potential, surface-evaporation efficiency, surface albedo, thermal conductivity and thermal capacity are changed according to the soil type (Soil 1, volcanic ash soil; Soil 2, clay loam; Soil 3, silty sand; and Soil 4, sand) and volumetric soil-water content. With the use of this model, the daily and seasonal variations of the heat and water balances have been simulated employing routine meteorological data.

The main results can be summarized as follows:

1) In semi-arid regions such as Lanzhou, the net radiation and sensible-heat flux undergo an almost sinusoidal annual variation, except during the rainy season. Soil-water from rainfall is recycled to the atmosphere within 5–15 days. The latent-heat flux during the rainy season (July to September) is approximately 30–100 Wm^{-2} (1–3.5mmd^{-1}), while the sensible-heat flux decreases during this season. Net radiation increases after rainfall event, due to the decreased albedo of the wet soil surface. The vertical profile of soil-water content increases from the surface to the bottom most layer.

2) In arid areas such as Turpan, the net radiation, sensible-heat flux, and surface temperature change annually in a sinusoidal manner while the latent-heat flux is very small. The annual mean value of soil-water content does not increase with depth. The monthly value of the soil-water content in the top soil layer is in an approximate equilibrium state with atmospheric water vapor pressure. Since the water exchange within the soil is very slow, it is thought that the desert soil-water content profile is an indication of the past climate.

3) Snow cover plays an important role in the heat and water balances through its high albedo and snow melt process. Net radiation exhibits negative values of about -20 to $-40 \mathrm{Wm}^{-2}$ over the period of snow cover, and then increases rapidly during the snow melt period while the latent-heat flux increases at the same time. The water content in the top soil layer increases for about 10 days due to the snow melt water and then decreases during the later stage. The ground-surface temperature begins to rise just after the disappearance of the snow cover.

4) The precipitable water is small over the Tibetan Plateau, resulting in a relatively large value of net radiation. In the desert, net radiation is relatively small due to the lack of water and the relatively high ground-surface temperatures.

5) The annual amount of evaporation depends on the annual precipitation. In arid regions, annual evaporation is proportional to the annual amount of precipitation. In humid regions, it tends to have an upper limit value, which is determined as functions of the potential evaporation and soil types. The upper limit value for a loamy soil is about 2–3 times that for a sandy soil.

6) As a result of the interrelation between heat and water balances, wetness index was contributed for delimiting the climatic zonality. The application of this index in China shows that from the moist zone to the arid zone, climatic zonality formed a very sharp contrast.

Acknowledgments

The author is most grateful to Professor Junsei Kondo of Tohoku University, for his valuable advice, helpful guidance and continuous encouragement.

The author also wishes to thank Dr. N. Saigusa, National Institute for Resources and Environment, for her assistance in experiments. The author would like to thank Mr. S. Ishida of Tohoku University, for his valuable comments on the thesis style. The author is also grateful to Mr. M. Nakazono of Central Research Institute of Electric Power Industry, for his kindness to provide the thesis style and useful suggestions. Thanks are due to Professor N. Yasuda, Dr. T. Yamazaki, Mr. D. Matsushima and her colleagues at Tohoku University for their helpful comments on this study. The author also wants to thank her husband for his help in experiments and giving up rests on many weekends.

Appendix A. Tables of monthly heat and water balances

Observation values

T_A	air temperature (0.1°C)
e	water vapor pressure (0.1hPa)
U_{OBS}	mean wind speed (0.1m s^{-1})
N	total duration of sunshine (0.1hour)
T_S	ground-surface temperature (0.1°C)
Pr_{OBS}	total amount of precipitation (mm)
E_{PAN}	total pan evaporation (mm)

Corrected values

Pr	total amount of corrected precipitation (mm)

Calculated values

E_P	total amount of potential evaporation (mm)
$S^{\downarrow}$	solar radiation (W m^{-2})
$L^{\downarrow}$	downward longwave radiation (W m^{-2})

Calculated values depending on the soil types

Rn	net radiation flux (W m^{-2})
H	sensible-heat flux (W m^{-2})
ιE	latent heat flux (W m^{-2})
G	heat flux into ground (W m^{-2})
E	total evaporation from the bare soil surface (mm)

(1) Hailar: 49.2°N, 119.8°E, Elevation=613m

	Jan	Feb	Mar	Apr	May	Jun	Jul	Aug	Sep	Oct	Nov	Dec	Annual
T_A	−279	−239	−116	49	96	161	216	154	103	−13	−174	−200	−21
e	5	8	21	49	70	106	165	130	69	37	14	11	57
U_{OBS}	15	17	23	40	38	24	26	26	29	26	20	23	26
N	1970	1924	2069	2747	2345	3297	2927	2394	2580	2069	1882	1731	27935
T_S	−271	−232	−91	56	109	198	243	186	128	4	−152	−205	−2
Pr_{OBS}	2	7	4	39	60	27	70	57	5	11	6	2	289
E_{PAN}	2	5	26	134	174	199	219	136	164	59	9	47	11336
Pr	2	10	8	48	100	27	70	57	5	15	8	4	353
E_P	0	2	20	102	125	160	170	111	103	40	4	−1	835
$S_M^{\downarrow}$	68	101	136	216	213	277	256	202	183	114	76	55	158
$L^{\downarrow}$	143	157	203	258	296	321	361	331	285	237	176	168	245
Soil 1	(volcanic ash soil)												
Rn	−31	−26	−20	82	98	124	120	90	56	14	−26	−31	38
H	−27	−24	−26	15	26	65	58	39	32	7	−22	−26	10
ιE	−2	−2	3	63	67	52	61	51	26	12	0	−2	28
G	−3	0	2	4	5	6	2	0	−1	−5	−4	−3	0
E	−2	−1	3	66	72	55	65	55	26	13	0	−2	350
Soil 2	(clay loam)												
Rn	−27	−24	−20	66	74	95	97	72	38	5	−29	−32	26
H	−23	−22	−26	23	30	55	46	36	22	4	−23	−26	8
ιE	−1	−1	3	39	38	32	47	35	18	8	0	−2	18
G	−4	0	3	5	7	8	5	1	−2	−7	−6	−4	0
E	−1	−1	3	40	41	33	50	38	19	9	0	−1	230
Soil 3	(silty sand)												
Rn	−32	−26	−20	59	75	94	97	68	31	0	−30	−32	24
H	−26	−24	−26	3	12	40	30	21	17	−2	−23	−26	0
ιE	−2	−1	3	52	57	45	62	46	17	10	0	−2	24
G	−4	0	3	5	6	9	5	1	−3	−8	−6	−5	0
E	−2	−1	3	53	61	46	67	50	18	11	0	−2	304
Soil 4	(sand)												
Rn	−20	−19	−20	45	60	89	91	60	31	1	−30	−32	22
H	−16	−19	−26	23	33	57	44	34	24	1	−24	−26	9
ιE	−1	0	3	18	22	25	43	25	10	6	0	−2	13
G	−3	0	3	4	5	6	4	0	−2	−6	−5	−4	0
E	−1	0	3	18	24	26	47	27	10	6	0	−2	159

(2) Bugt: 48.8°N, 121.9°E, Elevation=739m

	Jan	Feb	Mar	Apr	May	Jun	Jul	Aug	Sep	Oct	Nov	Dec	Annual
T_A	−210	−183	−84	54	92	140	189	140	84	−11	−145	−162	−8
e	8	10	20	37	57	101	171	126	62	34	14	13	54
U_{OBS}	39	29	28	40	40	27	23	22	27	31	26	31	30
N	2209	2239	2630	2864	2519	2900	2293	2290	2677	2104	1958	1585	28268
T_S	−231	−201	−83	74	120	185	220	170	105	−8	−151	−192	1
Pr_{OBS}	1	5	8	7	35	64	279	98	5	15	3	2	519
E_{PAN}	12	18	60	190	230	224	182	130	164	81	20	13	1323
Pr	4	10	13	10	48	64	279	98	5	22	6	5	564
E_P	4	8	38	118	135	150	138	101	93	45	9	5	843
S_M^1	76	114	162	217	221	276	242	204	190	116	80	53	163
L^1	155	165	202	256	288	310	354	323	272	236	182	182	244
Soil 1	(volcanic ash soil)												
Rn	−15	17	44	76	85	123	153	117	76	22	−3	−16	57
H	−16	6	24	48	42	72	20	16	14	−2	−4	−17	17
ιE	4	11	17	24	39	47	129	100	63	29	5	5	40
G	−2	0	3	4	5	4	5	2	−1	−5	−4	−3	0
E	4	11	18	25	41	49	138	107	66	31	5	5	501
Soil 2	(clay loam)												
Rn	−20	4	35	57	71	103	122	89	38	10	−7	−19	41
H	−19	−4	20	34	32	54	36	33	24	2	−5	−19	16
ιE	3	8	15	19	33	42	82	55	17	15	4	5	25
G	−3	0	4	5	7	7	4	1	−2	−7	−6	−5	0
E	3	8	16	19	36	43	88	59	18	16	4	5	316
Soil 3	(silty sand)												
Rn	−21	1	29	50	66	99	122	94	37	7	−11	−22	38
H	−20	−7	4	27	18	37	18	12	11	−6	−9	−21	5
ιE	3	7	20	18	42	54	99	80	29	22	4	4	32
G	−4	0	5	5	6	8	6	2	−3	−7	−7	−5	0
E	3	7	21	19	45	56	106	86	30	23	4	4	404
Soil 4	(sand)												
Rn	−17	6	28	51	61	96	92	62	32	4	−10	−21	32
H	−18	−3	13	34	31	49	40	35	26	−1	−8	−21	15
ιE	3	9	12	13	25	41	48	27	9	11	3	4	17
G	−3	0	4	4	5	6	4	0	−2	−6	−5	−4	0
E	4	8	13	14	27	42	52	28	9	12	4	4	218

(3) Harbin: 45.8°N, 126.8°E, Elevation=142m

	Jan	Feb	Mar	Apr	May	Jun	Jul	Aug	Sep	Oct	Nov	Dec	Annual
T_A	−200	−147	−32	90	141	198	240	195	138	48	−91	−129	38
e	11	15	33	54	83	140	235	180	108	60	22	16	80
U_{OBS}	26	24	39	44	44	35	40	31	32	38	37	31	35
N	1678	1832	2407	2596	2345	2727	2638	2220	2355	2042	1747	1386	25973
T_S	−206	−147	−23	109	163	238	274	217	159	51	−86	−137	51
Pr_{OBS}	1	6	18	8	56	107	152	198	32	36	7	2	623
E_{PAN}	6	14	64	224	264	249	193	142	146	86	32	25	1445
Pr	3	9	37	11	56	108	152	198	32	42	14	3	665
E_P	1	8	48	137	171	177	174	124	102	62	18	9	1032
$S_M^{\downarrow}$	70	106	155	208	215	244	236	198	174	122	79	55	155
$L^{\downarrow}$	173	187	228	279	318	353	395	362	315	267	208	200	274
Soil 1	(volcanic ash soil)												
Rn	−19	−5	21	83	99	117	153	127	82	31	−18	−9	55
H	−17	−11	−16	39	47	63	28	8	8	−8	−25	−13	8
ιE	0	6	34	40	49	49	121	117	76	44	12	7	47
G	−2	0	3	4	3	5	3	1	−2	−5	−5	−3	0
E	0	6	37	41	52	51	129	126	79	47	12	8	583
Soil 2	(clay loam)												
Rn	−24	−10	12	65	82	97	123	93	52	18	−26	−17	39
H	−18	−13	−15	33	40	50	49	34	24	1	−28	−15	12
ιE	0	5	24	24	35	40	68	58	29	21	10	7	27
G	−6	−2	4	7	6	7	5	1	0	−5	−8	−9	0
E	−1	5	25	25	37	42	73	63	30	23	11	8	400
Soil 3	(silty sand)												
Rn	−17	−2	13	58	77	94	124	101	50	15	−27	−19	39
H	−13	−9	−20	17	23	37	18	7	8	−14	−30	−21	0
ιE	1	7	29	36	49	50	101	94	45	36	10	7	39
G	−4	0	4	5	5	8	5	0	−3	−8	−7	−6	0
E	1	7	31	37	53	52	108	101	47	39	10	8	493
Soil 4	(sand)												
Rn	−16	−2	4	53	68	88	95	69	38	7	−27	−19	30
H	−14	−9	−13	38	42	49	58	36	28	−1	−31	−22	14
ιE	1	7	14	11	22	33	32	33	13	14	9	7	16
G	−3	0	3	4	4	6	4	0	−3	−6	−5	−4	0
E	1	7	15	11	24	34	35	35	13	15	9	8	207

(4) Altay: 47.7°N, 88.1°E, Elevation=735m

	Jan	Feb	Mar	Apr	May	Jun	Jul	Aug	Sep	Oct	Nov	Dec	Annual
T_A	−144	−215	−30	97	167	221	215	200	135	28	−64	−133	40
e	17	15	37	57	75	120	125	112	87	42	30	16	61
U_{OBS}	8	9	27	41	36	27	23	28	22	27	15	11	23
N	1509	1944	2039	2760	3289	3393	3357	3254	2476	2178	1812	1698	29709
T_S	−160	−170	−37	111	212	294	281	255	146	30	−61	−164	61
Pr_{OBS}	15	6	16	23	21	0	27	16	44	19	9	3	199
E_{PAN}	11	17	64	176	274	299	280	247	140	85	22	12	1626
Pr	16	6	28	23	21	0	27	16	44	31	12	4	228
E_P	4	7	43	142	206	209	196	184	100	56	11	3	1161
$S_M^{\downarrow}$	62	107	142	223	266	287	276	248	178	122	78	59	171
$L^{\downarrow}$	194	182	236	277	312	349	349	336	306	250	217	190	267
Soil 1	(volcanic ash soil)												
Rn	−29	−28	7	94	107	111	107	88	54	10	−31	−33	38
H	−25	−27	−18	35	66	87	78	67	29	2	−27	−28	20
ιE	−1	0	23	57	36	17	25	18	27	12	1	−1	18
G	−3	0	3	2	5	6	4	1	−3	−4	−4	−3	0
E	−1	0	25	59	38	18	27	19	28	13	1	−1	226
Soil 2	(clay loam)												
Rn	−26	−28	4	69	81	85	83	67	41	1	−32	−34	26
H	−22	−27	−17	36	50	64	56	47	20	−2	−27	−28	13
ιE	0	0	17	29	25	14	23	18	24	9	1	−1	13
G	−4	0	4	4	6	7	5	1	−3	−6	−6	−5	0
E	0	0	18	30	27	14	25	20	25	10	1	−1	169
Soil 3	(silty sand)												
Rn	−30	−28	3	68	76	80	80	61	37	−4	−32	−34	23
H	−24	−27	−21	11	40	61	48	43	9	−7	−27	−28	7
ιE	−1	0	20	54	30	10	26	17	32	9	1	−1	16
G	−4	0	4	3	7	8	6	1	−4	−7	−6	−5	0
E	−1	0	21	56	32	11	28	19	33	10	1	−1	208
Soil 4	(sand)												
Rn	−30	−28	−3	55	75	81	80	63	34	−4	−32	−33	22
H	−25	−27	−17	36	52	69	57	48	18	−3	−28	−28	13
ιE	−1	0	10	17	18	6	19	14	19	5	1	−1	9
G	−3	0	3	3	5	6	4	0	−3	−5	−5	−4	0
E	−1	0	10	18	19	6	20	15	19	5	1	−1	112

(5) Fuyun: 47.0°N, 89.5°E, Elevation=824m

	Jan	Feb	Mar	Apr	May	Jun	Jul	Aug	Sep	Oct	Nov	Dec	Annual
T_A	−180	−195	−33	95	161	229	222	201	134	24	−94	−181	32
e	13	11	35	54	61	91	104	98	71	36	25	12	51
U_{OBS}	4	2	20	33	32	40	33	30	24	23	6	2	21
N	1750	2124	2303	2457	3169	3423	3274	2963	2614	2064	1758	1795	29694
T_S	−187	−197	−27	120	209	291	271	246	160	33	−112	−202	50
Pr_{OBS}	8	7	12	21	12	9	23	21	7	20	8	3	151
E_{PAN}	10	12	65	202	369	528	475	422	227	108	19	8	2446
Pr	9	7	17	22	12	9	23	21	7	33	10	5	175
E_P	4	4	45	120	189	280	241	199	112	56	8	1	1259
$S_M^{\downarrow}$	70	117	153	205	260	294	282	242	188	124	80	63	174
$L^{\downarrow}$	179	165	230	281	306	343	344	334	298	247	206	174	259
Soil 1	(volcanic ash soil)												
Rn	−28	−25	16	74	96	114	109	84	51	13	−24	−22	38
H	−24	−23	−13	37	66	91	78	64	39	10	−19	−18	24
ιE	−1	−1	26	35	24	18	27	18	13	7	0	−1	14
G	−3	0	3	2	5	5	4	1	−2	−4	−4	−3	0
E	−1	−1	28	37	26	19	28	19	14	8	0	−1	174
Soil 2	(clay loam)												
Rn	−27	−25	12	58	72	88	86	63	33	3	−24	−23	27
H	−22	−23	−10	28	46	65	55	45	24	3	−18	−17	15
ιE	−1	−1	17	27	19	17	26	17	12	6	0	−1	12
G	−4	0	5	4	6	7	5	1	−3	−6	−6	−5	0
E	−1	−1	18	28	21	17	28	18	12	7	0	−1	147
Soil 3	(silty sand)												
Rn	−29	−25	10	56	68	82	81	59	28	−1	−25	−23	24
H	−23	−23	−15	10	38	60	47	39	20	−1	−18	−17	10
ιE	−1	−1	21	42	23	15	28	19	12	7	0	−1	14
G	−4	0	4	4	7	8	6	1	−3	−7	−6	−5	0
E	−1	−1	23	43	24	15	30	20	12	7	0	−1	172
Soil 4	(sand)												
Rn	−28	−25	3	47	67	83	83	59	31	0	−24	−23	23
H	−23	−23	−8	29	49	69	55	46	24	1	−18	−18	15
ιE	−1	−1	8	15	13	9	24	13	10	5	0	−1	8
G	−3	0	4	3	5	6	4	1	−3	−5	−5	−4	0
E	−1	−1	9	15	14	9	25	14	10	5	0	−1	98

(6) Urumqi: 43.8°N, 87.6°E, Elevation=918m

	Jan	Feb	Mar	Apr	May	Jun	Jul	Aug	Sep	Oct	Nov	Dec	Annual
T_A	−129	−111	9	110	177	227	232	220	163	54	−49	−110	66
e	20	22	49	61	67	105	123	111	77	45	34	19	61
U_{OBS}	9	12	20	33	30	26	22	22	23	19	13	16	20
N	981	1411	1940	1977	2709	2863	2410	2863	2449	2249	1409	1641	24902
T_S	−146	−105	19	126	214	279	275	266	184	54	−55	−141	81
Pr_{OBS}	3	7	25	45	21	21	25	14	18	36	16	10	243
E_{PAN}	10	13	61	221	373	401	386	374	282	120	24	17	2281
Pr	4	9	36	46	22	22	26	15	18	41	20	14	273
E_P	4	9	45	145	205	216	193	186	136	64	14	10	1226
$S_M^{\downarrow}$	58	99	148	184	254	265	233	240	196	140	79	70	164
$L^{\downarrow}$	211	210	255	299	318	355	368	350	313	260	233	202	282
Soil 1	(volcanic ash soil)												
Rn	−11	14	48	76	97	103	91	85	54	25	−9	−32	45
H	−10	4	7	23	57	69	56	57	40	14	−12	−30	23
ιE	1	9	37	50	35	28	30	26	16	16	8	2	22
G	−3	1	4	3	5	6	4	2	−2	−4	−4	−3	0
E	1	9	40	52	38	30	32	27	17	17	8	2	272
Soil 2	(clay loam)												
Rn	−20	−6	35	64	76	81	72	66	38	14	−13	−34	31
H	−13	−6	8	20	38	50	39	38	24	6	−11	−28	14
ιE	0	5	25	38	30	24	28	25	15	13	6	2	18
G	−6	−2	5	6	8	7	6	3	0	−4	−8	−8	0
E	0	4	26	40	32	25	30	26	16	14	7	3	223
Soil 3	(silty sand)												
Rn	−15	4	36	63	73	78	69	60	34	10	−14	−33	30
H	−11	−2	0	0	27	44	33	34	20	1	−14	−30	9
ιE	0	6	30	58	40	27	31	25	17	15	6	2	21
G	−4	0	6	4	7	7	6	2	−3	−7	−6	−5	0
E	1	5	33	60	43	28	33	26	18	16	6	2	271
Soil 4	(sand)												
Rn	−10	7	23	46	69	76	67	60	34	9	−16	−32	28
H	−8	2	11	25	44	53	42	42	26	6	−14	−30	17
ιE	2	6	8	19	21	17	22	18	11	8	3	2	11
G	−3	0	4	3	4	6	4	1	−3	−6	−5	−4	0
E	2	6	9	19	22	18	24	19	11	9	3	2	143

(7) Turpan: 42.9°N, 89.2°E, Elevation=35m

	Jan	Feb	Mar	Apr	May	Jun	Jul	Aug	Sep	Oct	Nov	Dec	Annual
T_A	−75	−10	116	213	268	327	323	292	233	109	8	−89	143
e	18	21	42	69	76	126	155	155	120	55	31	15	74
U_{OBS}	5	10	15	22	20	22	20	19	14	13	10	7	15
N	1689	1795	2739	2687	2631	2754	2829	2861	2473	2099	1879	1706	28142
T_S	−88	−10	131	258	326	401	399	355	279	129	5	−103	174
Pr_{OBS}	0	0	0	0	0	0	3	9	0	2	0	0	14
E_{PAN}	21	50	180	317	434	507	428	349	232	137	51	18	2723
Pr	0	0	0	0	0	0	3	9	0	2	0	0	14
E_P	13	32	99	189	243	300	277	225	140	76	31	10	1635
$S_M^{\downarrow}$	78	111	179	217	237	254	242	226	182	138	94	72	170
$L^{\downarrow}$	214	235	280	335	367	415	421	401	364	287	242	207	314
Soil 1	(volcanic ash soil)												
Rn	−4	9	35	60	70	82	82	73	47	18	−2	−9	39
H	0	10	33	55	64	76	75	67	45	21	3	−2	37
ιE	0	0	1	1	1	1	2	4	2	0	1	0	1
G	−4	−1	2	4	5	5	4	2	0	−3	−6	−6	0
E	0	0	1	1	1	1	2	4	2	0	1	0	14
Soil 2	(clay loam)												
Rn	−12	−1	19	41	51	62	62	55	32	5	−11	−17	24
H	−6	0	16	35	42	54	53	47	29	8	−4	−8	22
ιE	0	0	1	1	1	1	2	4	2	0	1	0	1
G	−6	−2	3	6	7	6	5	3	0	−4	−8	−9	0
E	0	0	1	1	1	1	2	4	2	0	1	0	14
Soil 3	(silty sand)												
Rn	−14	−3	17	38	47	59	59	51	28	2	−13	−18	21
H	−7	−2	13	31	39	50	50	44	26	7	−6	−9	20
ιE	0	0	1	1	1	1	2	4	2	0	1	0	1
G	−7	−1	4	7	8	7	6	3	−1	−5	−9	−9	0
E	0	0	1	1	1	1	3	4	2	0	1	0	14
Soil 4	(sand)												
Rn	−12	−1	19	40	49	61	61	53	31	4	−11	−17	23
H	−7	−1	16	35	43	55	54	47	28	8	−5	−9	22
ιE	0	0	0	0	1	1	2	4	3	0	1	0	1
G	−5	−1	3	5	6	5	4	2	−1	−4	−8	−8	0
E	0	0	0	0	1	1	3	5	3	0	1	0	14

(8) Hotan: 37.1N, 79.9E, Elevation=1375m

	Jan	Feb	Mar	Apr	May	Jun	Jul	Aug	Sep	Oct	Nov	Dec	Annual
T_A	−41	6	108	174	226	237	256	224	191	106	28	−47	122
e	22	32	33	55	76	111	128	144	90	44	32	20	66
U_{OBS}	17	18	24	26	28	27	22	24	21	17	19	18	22
N	1405	1476	2031	2044	1044	1717	1459	1666	2067	1334	1816	1699	19758
T_S	−5	21	135	221	287	308	325	286	236	124	16	−70	153
Pr_{OBS}	3	0	0	1	0	14	11	17	0	0	0	0	45
E_{PAN}	43	78	248	348	440	432	430	328	282	187	106	51	2974
Pr	4	0	0	1	1	15	11	18	0	0	0	0	50
E_P	30	44	130	170	209	216	215	173	147	89	54	31	1507
$S_M^{\downarrow}$	91	124	175	207	161	241	235	225	199	121	119	96	166
$L^{\downarrow}$	234	251	286	323	377	368	382	367	335	302	251	224	309
Soil 1	(volcanic ash soil)												
Rn	7	24	42	60	52	86	80	79	54	20	11	3	43
H	9	22	38	52	44	72	68	67	50	21	16	9	39
ιE	2	3	2	3	3	10	7	10	5	2	1	0	4
G	−4	−1	2	4	5	5	4	3	0	−3	−6	−6	0
E	2	3	3	4	3	10	8	11	5	2	1	0	50
Soil 2	(clay loam)												
Rn	−2	13	26	43	40	69	62	62	37	9	−1	−7	29
H	3	12	22	34	30	52	50	48	34	11	6	1	25
ιE	2	3	2	3	3	10	7	11	4	2	1	0	4
G	−6	−2	3	6	7	7	6	3	−1	−4	−8	−8	0
E	2	3	2	3	3	11	7	11	4	2	1	0	50
Soil 3	(silty sand)												
Rn	−4	10	24	40	37	66	59	59	34	7	−4	−10	27
H	1	9	19	31	28	46	46	43	31	10	4	0	22
ιE	2	3	2	2	2	12	7	13	4	1	0	0	4
G	−7	−2	3	7	7	7	6	4	−1	−5	−9	−9	0
E	2	2	2	2	2	12	7	14	4	2	0	0	50
Soil 4	(sand)												
Rn	−2	12	26	42	38	67	60	61	37	9	−2	−7	28
H	1	10	22	35	31	51	50	46	33	11	5	0	25
ιE	2	2	1	2	2	11	6	13	5	2	1	0	4
G	−5	−1	3	5	6	6	4	2	−1	−4	−7	−7	0
E	2	2	2	2	2	12	6	14	6	2	1	0	50

(9) Andir: 37.9°N, 83.7°E, Elevation=1263m

	Jan	Feb	Mar	Apr	May	Jun	Jul	Aug	Sep	Oct	Nov	Dec	Annual
T_A	−81	−23	86	163	223	245	250	230	177	79	−5	−89	105
e	17	18	23	49	58	103	123	126	75	33	24	15	55
U_{OBS}	14	20	24	27	29	26	25	23	23	25	17	14	22
N	2055	1890	2336	2672	2547	2615	2867	3026	3023	2688	2344	2235	30298
T_S	−76	−9	107	202	270	313	318	294	220	97	−1	−92	137
Pr_{OBS}	1	0	0	1	0	4	25	6	0	0	0	0	37
E_{PAN}	37	71	217	338	452	390	377	323	268	185	70	40	2767
Pr	1	0	0	1	0	5	25	6	0	0	0	0	39
E_P	22	48	128	182	258	232	236	205	162	110	47	21	1652
$S_M^{\downarrow}$	113	141	188	248	257	264	272	265	241	182	136	111	202
$L^{\downarrow}$	203	226	266	301	338	363	367	354	307	256	223	195	284
Soil 1	(volcanic ash soil)												
Rn	10	25	44	74	80	90	95	90	64	34	12	4	52
H	14	25	41	67	73	80	81	77	62	36	17	10	49
ιE	1	1	1	2	2	5	10	10	3	1	0	0	3
G	−4	−1	2	4	5	5	4	3	0	−3	−6	−6	0
E	1	1	1	2	2	6	11	11	3	1	0	0	39
Soil 2	(clay loam)												
Rn	−1	11	27	53	59	69	74	69	43	17	−2	−8	34
H	4	12	24	45	51	57	59	55	41	20	5	0	31
ιE	1	1	1	2	2	5	10	11	3	1	0	0	3
G	−6	2	3	6	7	6	5	3	−1	−4	−8	−8	0
E	1	1	1	2	2	5	11	12	3	1	0	0	39
Soil 3	(silty sand)												
Rn	−3	8	24	50	55	66	71	66	39	13	−5	−10	31
H	2	9	20	41	47	53	55	49	38	17	4	−1	28
ιE	1	0	1	2	1	5	11	12	2	1	0	0	3
G	−6	−2	3	7	7	7	6	4	−1	−5	−9	−9	0
E	1	0	1	2	1	5	12	13	2	1	0	0	39
Soil 4	(sand)												
Rn	−1	11	27	52	58	68	72	69	42	16	−2	−8	34
H	3	11	23	45	51	58	59	52	41	19	5	−1	31
ιE	1	0	1	2	1	5	10	13	2	1	0	0	3
G	−5	−1	3	6	6	5	4	3	−1	−4	−8	−7	0
E	1	0	1	2	1	5	11	14	2	1	0	0	39

(10) Dunhuang: 40.2°N, 94.7°E, Elevation=1139m

	Jan	Feb	Mar	Apr	May	Jun	Jul	Aug	Sep	Oct	Nov	Dec	Annual
T_A	−83	−37	59	142	183	231	248	219	168	63	−12	−90	91
e	14	19	29	45	65	116	136	131	86	36	27	17	60
U_{OBS}	16	22	27	36	30	26	23	22	18	22	19	17	23
N	2116	2203	2980	2902	3186	2796	2773	2558	2851	2723	2361	2157	31306
T_S	−87	−40	72	179	245	302	312	274	203	77	−15	−106	118
Pr_{OBS}	1	4	0	0	0	9	7	29	7	0	2	0	60
E_{PAN}	40	63	211	345	382	247	321	255	233	162	64	29	2348
Pr	1	7	1	0	0	9	7	29	7	0	3	0	64
E_P	24	42	112	192	221	215	210	168	136	89	41	19	1468
S_M^1	107	148	211	250	280	274	260	235	225	175	127	100	200
L^1	200	213	245	288	315	358	372	355	310	250	221	196	277
Soil 1	(volcanic ash soil)												
Rn	6	23	54	78	93	100	93	80	62	31	9	1	53
H	7	18	48	72	85	85	79	66	56	34	12	3	47
ιE	1	5	4	3	4	10	9	13	8	2	1	1	5
G	−3	0	2	3	4	5	4	1	−2	−4	−4	−3	0
E	1	5	4	3	4	10	10	14	9	2	1	1	64
Soil 2	(clay loam)												
Rn	−6	11	34	55	69	78	72	64	44	14	−5	−10	35
H	−1	7	28	47	60	62	57	45	36	17	2	−3	30
ιE	1	5	3	2	3	9	9	15	9	2	1	2	5
G	−6	−2	3	6	7	7	6	3	0	−4	−8	−8	0
E	2	5	3	2	3	9	9	16	9	2	2	2	64
Soil 3	(silty sand)												
Rn	−9	6	30	51	66	73	68	60	40	10	−8	−13	31
H	−3	2	24	43	55	57	53	38	31	14	0	−6	26
ιE	1	5	3	2	2	9	8	18	9	1	1	1	5
G	−7	−1	4	7	8	8	7	4	0	−5	−9	−9	0
E	1	5	3	2	2	9	9	19	9	1	1	2	64
Soil 4	(sand)												
Rn	−6	8	33	54	68	75	70	62	43	14	−5	−11	34
H	−3	4	27	47	60	63	57	42	34	16	0	−5	29
ιE	1	5	4	2	2	7	8	18	9	2	2	1	5
G	−5	−1	3	5	6	5	5	3	−1	−4	−7	−7	0
E	1	5	4	2	2	7	8	20	10	2	2	1	64

(11) Jiuquan: 39.8°N, 98.5°E, Elevation=1477m

	Jan	Feb	Mar	Apr	May	Jun	Jul	Aug	Sep	Oct	Nov	Dec	Annual
T_A	−99	−51	38	112	152	205	221	200	149	45	−35	−114	68
e	14	17	25	45	54	113	148	135	89	40	26	17	60
U_{OBS}	19	24	30	29	28	25	19	20	19	21	21	20	23
N	2264	2357	3030	2735	3253	2891	2616	2405	2605	2365	2048	2055	30624
T_S	−98	−41	53	149	201	260	268	241	169	47	−39	−119	91
Pr_{OBS}	1	3	0	3	0	30	29	28	20	8	3	2	126
E_{PAN}	35	64	189	264	310	241	213	187	161	100	40	19	1825
Pr	2	4	1	3	1	30	30	28	21	9	5	3	136
E_P	24	44	109	152	193	196	173	147	121	75	35	13	1282
$S_M^{\downarrow}$	118	159	220	257	283	285	254	230	217	163	119	99	200
$L^{\downarrow}$	189	204	233	274	297	342	363	349	306	252	220	192	269
Soil 1	(volcanic ash soil)												
Rn	10	30	60	83	96	107	98	84	66	31	10	0	57
H	10	24	51	70	84	36	71	58	49	27	12	−3	45
ιE	3	5	6	9	8	16	22	24	18	8	3	6	11
G	−2	1	3	3	4	5	4	2	−2	−4	−5	−3	0
E	3	5	6	10	8	17	24	26	19	9	3	6	136
Soil 2	(clay loam)												
Rn	−1	15	39	61	73	86	79	68	50	19	−2	−6	40
H	2	12	31	46	60	62	50	40	31	14	4	−3	29
ιE	3	5	5	9	6	18	23	25	19	9	3	6	11
G	−6	−1	3	6	7	7	6	4	0	−4	−8	−8	0
E	3	5	5	9	6	18	24	26	20	9	3	6	135
Soil 3	(silty sand)												
Rn	−5	10	35	56	68	83	74	66	45	14	−5	−10	36
H	−1	7	27	42	56	54	45	34	25	10	2	−7	25
ιE	2	4	4	6	4	22	22	28	21	8	2	6	11
G	−6	−1	4	7	8	8	7	4	−1	−4	−9	−8	0
E	3	4	4	7	4	22	23	30	22	9	2	6	136
Soil 4	(sand)												
Rn	−3	12	38	58	70	83	75	63	45	16	−2	−9	37
H	0	9	31	48	61	61	51	41	31	12	2	−7	28
ιE	3	4	4	5	3	16	19	19	16	7	3	5	9
G	−5	−1	3	6	6	6	5	3	−1	−4	−7	−7	0
E	3	4	4	5	3	17	21	21	16	8	3	6	111

(12) Lanzhou: 36.1°N, 103.9°E, Elevation=1517m

	Jan	Feb	Mar	Apr	May	Jun	Jul	Aug	Sep	Oct	Nov	Dec	Annual
T_A	−56	−10	73	126	172	210	239	216	161	78	10	−57	97
e	25	25	38	68	63	125	168	159	118	58	39	21	76
U_{OBS}	3	7	11	12	13	12	14	10	4	7	4	1	8
N	1418	2016	2557	2273	2612	1839	2581	1812	1840	223	1802	1984	23301
T_S	−69	−6	99	161	230	265	289	251	188	100	9	−74	120
Pr_{OBS}	2	3	9	22	1	13	43	68	37	3	0	0	201
E_{PAN}	17	44	132	167	261	219	249	174	113	95	40	22	1532
Pr	2	4	9	22	1	13	43	68	37	3	0	0	202
E_P	18	40	84	104	153	130	169	125	82	65	34	21	1024
$S_M^{\downarrow}$	96	156	208	223	257	217	256	201	169	167	121	111	182
$L^{\downarrow}$	230	230	262	302	317	363	375	371	337	275	247	214	294
Soil 1	(volcanic ash soil)												
Rn	11	33	57	76	86	80	102	82	61	40	15	8	54
H	11	26	44	53	68	58	65	40	29	30	17	11	38
ιE	3	8	10	18	13	16	31	40	32	12	4	3	16
G	−4	−1	3	5	6	5	5	2	0	−3	−6	−6	0
E	3	7	10	18	14	17	33	43	33	13	4	3	201
Soil 2	(clay loam)												
Rn	2	19	39	60	65	63	85	68	48	24	3	−3	40
H	5	14	27	36	46	40	46	30	21	17	8	3	25
ιE	3	7	9	18	12	16	32	36	28	11	3	2	15
G	−6	−1	3	7	7	7	6	2	0	−4	−8	−8	0
E	3	6	10	18	13	17	35	38	29	12	4	2	186
Soil 3	(silty sand)												
Rn	0	15	36	57	60	60	82	67	46	21	0	−5	37
H	3	10	22	29	43	37	39	21	15	14	6	2	20
ιE	2	6	10	20	9	14	36	43	32	12	3	2	16
G	−6	−1	4	7	8	8	7	2	−1	−4	−9	−9	0
E	3	6	11	21	9	15	39	46	33	13	3	2	201
Soil 4	(sand)												
Rn	1	16	36	56	61	60	80	59	39	21	2	−4	36
H	4	13	27	36	49	42	46	32	23	18	7	2	25
ιE	2	4	6	14	6	12	30	26	16	7	2	1	11
G	−5	−1	3	6	6	6	5	1	−1	−4	−7	−7	0
E	2	4	7	15	7	13	32	28	17	8	2	1	134

(13) Jurh: 42.4°N, 112.9°E, Elevation=1151m

	Jan	Feb	Mar	Apr	May	Jun	Jul	Aug	Sep	Oct	Nov	Dec	Annual
T_A	−191	−120	−3	83	137	212	236	184	136	27	−89	−130	40
e	10	16	23	36	43	74	163	136	81	31	20	14	54
U_{OBS}	46	55	59	60	67	55	49	40	45	62	53	64	55
N	2291	2196	2779	2974	3113	3080	3158	2831	2674	2615	2062	2337	32110
T_S	−192	−108	23	124	187	269	270	219	159	39	−80	−128	65
Pr_{OBS}	2	2	3	8	3	16	150	76	46	6	6	0	319
E_{PAN}	14	39	179	323	475	541	397	236	233	190	42	31	2701
Pr	5	6	5	9	6	17	151	76	47	10	13	1	346
E_P	9	28	116	199	288	321	258	172	161	120	32	22	1725
$S_M^{\downarrow}$	104	140	198	247	273	290	284	242	207	162	107	97	196
$L^{\downarrow}$	163	186	223	260	289	331	366	337	298	237	201	178	256
Soil 1	(volcanic ash soil)												
Rn	12	34	64	92	110	115	135	129	83	38	3	−8	67
H	10	28	50	70	90	94	78	27	25	16	−1	−11	40
ιE	5	8	12	17	14	16	53	99	58	24	10	8	27
G	−4	−1	3	5	5	5	4	2	−1	−3	−6	−6	0
E	6	7	12	18	15	17	57	106	60	26	10	9	344
Soil 2	(clay loam)												
Rn	5	22	45	69	85	88	113	99	59	21	−5	−15	49
H	5	17	33	48	65	67	60	38	27	9	−5	−15	29
ιE	5	7	9	14	13	15	47	57	32	16	8	8	19
G	−5	−2	3	7	7	7	6	3	−1	−4	−8	−8	0
E	6	7	9	14	14	16	51	61	34	17	8	8	244
Soil 3	(silty sand)												
Rn	1	17	39	62	78	83	107	99	56	15	−10	−19	44
H	2	12	27	41	60	60	48	12	9	2	−9	−17	21
ιE	5	7	9	13	10	15	53	84	49	19	8	7	23
G	−6	−2	4	8	8	7	5	2	−2	−5	−9	−9	0
E	5	7	9	14	11	15	57	90	51	20	9	8	294
Soil 4	(sand)												
Rn	3	19	41	65	81	85	102	77	46	16	−9	−18	42
H	2	14	33	49	67	71	64	49	31	9	−8	−19	30
ιE	5	6	6	10	8	9	34	26	17	11	6	7	12
G	−5	−1	3	6	6	5	5	2	−1	−4	−7	−7	0
E	5	6	6	10	8	9	36	28	17	12	6	8	152

(14) Shenyang: 41.8°N, 123.4°E, Elevation=42m

	Jan	Feb	Mar	Apr	May	Jun	Jul	Aug	Sep	Oct	Nov	Dec	Annual
T_A	−143	−72	22	124	167	230	259	230	174	92	−31	−66	82
e	14	21	43	68	101	168	262	207	134	70	30	20	95
U_{OBS}	21	29	31	35	34	33	30	25	27	30	24	22	28
N	1829	1595	2102	2535	2452	2903	1829	2376	2363	2207	1693	1402	25286
T_S	−153	−70	25	128	192	283	283	254	185	92	−28	−79	93
Pr_{OBS}	5	9	70	15	47	34	162	108	107	20	6	1	583
E_{PAN}	23	45	88	199	209	262	175	176	168	116	49	39	1548
Pr	7	14	87	16	47	36	162	108	108	21	8	1	614
E_P	9	27	64	145	166	200	143	145	123	83	31	21	1158
$S_M^{\downarrow}$	85	105	151	217	222	263	194	213	206	142	90	65	163
$L^{\downarrow}$	189	219	256	297	332	373	416	384	332	284	233	224	295
Soil 1	(volcanic ash soil)												
Rn	−4	3	45	94	100	124	126	127	106	47	7	−6	64
H	−3	−9	11	32	46	75	19	18	13	−1	−6	−6	16
ιE	3	13	31	57	49	43	102	108	93	52	19	6	48
G	−4	−1	3	5	4	6	4	2	0	−4	−6	−6	0
E	3	12	33	59	53	44	110	116	96	55	19	7	608
Soil 2	(clay loam)												
Rn	−11	−1	35	71	81	100	102	94	77	26	−4	−13	47
H	−7	−10	10	32	40	61	33	36	29	10	−5	−9	18
ιE	2	12	20	32	34	31	63	56	50	21	9	4	28
G	−6	−2	4	7	7	7	5	1	−1	−5	−8	−8	0
E	2	11	22	33	37	32	68	60	51	23	10	4	353
Soil 3	(silty sand)												
Rn	−14	−5	28	71	78	95	106	104	80	25	−8	−16	46
H	−9	−16	0	10	22	52	11	9	5	−10	−12	−11	4
ιE	2	13	25	53	49	35	89	93	75	41	13	4	41
G	−6	−2	3	7	6	8	6	2	−1	−6	−9	−9	0
E	2	13	27	55	52	36	95	99	78	44	13	4	518
Soil 4	(sand)												
Rn	−12	−4	22	57	71	92	80	75	56	16	−9	−15	36
H	−9	−14	9	38	42	67	41	41	34	8	−9	−10	20
ιE	2	11	11	13	24	19	35	34	23	13	7	2	16
G	−5	−2	3	6	5	6	4	1	−1	−5	−7	−7	0
E	2	11	11	14	25	20	38	36	24	14	7	2	204

(15) Beijing: 39.9°N, 116.3°E, Elevation=54m

	Jan	Feb	Mar	Apr	May	Jun	Jul	Aug	Sep	Oct	Nov	Dec	Annual
T_A	−48	−14	72	160	205	254	278	248	203	113	23	−14	123
e	15	20	42	70	100	168	267	223	164	68	35	23	100
U_{OBS}	24	31	26	30	30	25	20	19	18	26	24	24	25
N	2040	1947	2489	2716	2896	2770	2543	2364	2068	2493	1929	1784	28039
T_S	−65	−22	81	191	248	307	313	277	227	121	16	−36	138
Pr_{OBS}	1	2	3	11	14	19	171	103	48	15	5	1	393
E_{PAN}	47	65	140	248	310	291	222	185	155	161	77	59	1959
Pr	1	3	3	11	15	20	171	103	49	15	7	2	401
E_P	39	58	100	168	210	204	169	142	115	102	52	45	1404
$S_M^{\downarrow}$	98	126	177	221	252	248	231	205	189	158	104	82	174
$L^{\downarrow}$	214	229	266	312	342	386	420	397	359	286	248	234	308
Soil 1	(volcanic ash soil)												
Rn	1	20	47	75	97	102	136	115	33	40	9	−5	60
H	0	14	37	56	73	76	32	25	27	15	−1	−8	29
ιE	5	8	8	14	18	21	100	89	57	28	16	9	31
G	−4	−1	2	6	5	5	4	2	−1	−3	−6	−6	0
E	5	7	9	15	20	22	107	95	59	30	16	10	396
Soil 2	(clay loam)												
Rn	−10	6	30	57	76	83	106	86	59	22	−1	−15	42
H	−7	3	21	36	51	56	39	32	28	10	−3	−12	21
ιE	3	6	6	14	18	20	62	51	33	18	10	6	21
G	−6	−2	3	7	7	7	6	2	−1	−5	−8	−8	0
E	3	5	7	14	19	21	67	55	34	19	10	6	261
Soil 3	(silty sand)												
Rn	−13	3	26	52	71	79	113	91	62	19	−6	−18	40
H	−9	0	17	31	45	51	19	15	14	1	−9	−14	13
ιE	3	5	6	13	18	20	88	73	50	23	11	5	27
G	−6	−2	3	8	8	8	6	2	−2	−5	−9	−9	0
E	3	5	6	13	19	21	94	79	52	24	12	6	334
Soil 4	(sand)												
Rn	−11	5	28	53	73	79	87	70	51	17	−6	−16	36
H	−8	2	22	37	52	57	49	38	29	10	−5	−13	23
ιE	2	4	4	10	15	16	34	30	24	11	6	4	13
G	−5	−2	2	6	5	6	4	2	−2	−4	−7	−7	0
E	2	4	4	10	16	17	37	32	25	11	6	4	170

(16) Jinan: 36.7N, 117.0E, Elevation=52m

	Jan	Feb	Mar	Apr	May	Jun	Jul	Aug	Sep	Oct	Nov	Dec	Annual
T_A	−25	22	105	174	226	265	285	264	229	145	62	16	147
e	24	36	53	74	98	163	280	247	145	83	46	32	107
U_{OBS}	24	33	34	33	41	36	26	22	33	33	28	28	31
N	1978	1769	2572	2678	3175	2593	2211	2025	2604	2158	1879	2107	27758
T_S	−33	25	122	216	273	304	319	290	275	164	62	−1	168
Pr_{OBS}	13	7	11	4	22	102	108	95	1	16	3	4	386
E_{PAN}	47	91	210	300	432	361	179	243	179	105	72	2431	
Pr	18	11	11	4	22	103	108	95	2	16	5	5	399
E_P	40	63	135	193	288	270	174	152	188	125	70	54	1752
$S_M^{\downarrow}$	105	128	200	230	279	249	216	199	207	149	116	106	182
$L^{\downarrow}$	229	252	277	319	345	389	428	412	365	312	268	240	320
Soil 1	(volcanic ash soil)												
Rn	−2	27	59	83	114	120	126	114	79	40	14	2	65
H	−4	10	41	63	88	56	41	26	51	21	8	−3	33
ιE	6	19	16	15	21	58	81	88	28	22	11	11	31
G	−4	−1	3	5	5	5	4	1	0	−3	−6	−6	0
E	7	18	17	16	23	60	87	94	29	23	12	12	397
Soil 2	(clay loam)												
Rn	−11	17	43	61	88	98	102	90	55	23	1	−8	47
H	−10	6	25	42	61	47	37	32	41	14	2	−8	24
ιE	4	14	14	13	20	44	60	56	14	13	7	8	23
G	−6	−2	3	6	7	6	5	2	−1	−5	−8	−8	0
E	5	13	15	14	22	56	64	60	15	14	8	9	285
Soil 3	(silty sand)												
Rn	−14	13	37	56	83	94	105	97	54	21	−2	−13	45
H	−12	−4	20	38	54	35	18	11	32	6	−1	−12	16
ιE	4	20	14	10	22	51	82	84	23	20	8	9	29
G	−6	−2	4	7	7	7	5	2	−1	−5	−9	−9	0
E	5	19	15	11	23	53	88	90	24	21	8	9	365
Soil 4	(sand)												
Rn	−12	11	38	58	84	86	84	73	51	19	0	−11	40
H	−11	3	27	43	62	55	45	38	46	15	2	−10	26
ιE	4	10	9	9	17	26	35	33	7	9	5	6	14
G	−5	−2	3	6	5	5	4	2	−1	−4	−7	−7	0
E	4	10	9	10	18	26	37	35	7	10	5	6	178

(17) Xi'an: 34.3°N, 108.9°E, Elevation=397m

	Jan	Feb	Mar	Apr	May	Jun	Jul	Aug	Sep	Oct	Nov	Dec	Annual
T_A	−8	28	102	148	207	264	264	243	190	113	56	2	134
e	38	46	71	117	127	185	254	242	184	96	70	42	123
U_{OBS}	14	16	19	16	14	18	18	18	9	15	11	15	15
N	1112	1143	1957	1793	2409	1912	1315	1235	592	970	969	1455	16862
T_S	−7	35	117	172	249	311	292	268	203	116	58	1	151
Pr_{OBS}	9	18	25	44	35	30	125	204	180	24	27	5	726
E_{PAN}	37	57	133	127	250	287	207	146	82	79	44	39	1488
Pr	13	18	25	44	36	30	125	204	180	24	27	7	735
E_P	24	36	84	90	149	177	141	111	57	51	28	29	977
$S_M^{\downarrow}$	77	102	171	179	234	223	191	153	107	95	77	87	141
$L^{\downarrow}$	260	274	296	335	356	401	419	410	380	326	296	256	334
Soil 1	(volcanic ash soil)												
Rn	13	35	60	80	97	90	108	87	58	44	24	20	60
H	−4	2	28	32	53	53	26	20	4	−3	2	−2	18
ιE	21	35	30	44	39	31	78	65	54	50	28	27	42
G	−4	−1	2	5	7	5	4	2	0	−3	−5	−6	0
E	23	33	32	45	41	32	84	70	56	53	29	29	529
Soil 2	(clay loam)												
Rn	1	21	44	68	77	78	90	73	41	26	16	5	45
H	−1	9	23	28	40	42	29	24	13	6	6	4	19
ιE	8	15	18	33	30	29	56	48	28	24	18	9	26
G	−6	−2	3	7	7	7	5	2	0	−4	−8	−8	0
E	8	14	19	34	32	30	60	51	30	26	18	10	332
Soil 3	(silty sand)												
Rn	−1	18	40	64	76	77	95	73	44	31	17	5	45
H	−5	−1	14	16	32	35	13	14	5	−5	0	−5	10
ιE	10	21	23	41	36	34	76	57	40	40	25	20	35
G	−7	−2	3	7	8	8	6	2	−1	−5	−8	−9	0
E	11	20	25	42	38	35	82	61	42	43	26	21	445
Soil 4	(sand)												
Rn	−2	11	36	54	68	72	73	57	30	15	4	−2	35
H	−2	7	24	29	46	45	36	28	16	8	4	0	20
ιE	5	6	10	19	17	22	33	27	14	10	6	5	15
G	−5	−2	2	6	6	5	4	1	−1	−4	−7	−7	0
E	5	6	11	20	18	23	36	29	15	11	6	5	185

(18) Lushi: 34.0°N, 111.0°E, Elevation=569m

	Jan	Feb	Mar	Apr	May	Jun	Jul	Aug	Sep	Oct	Nov	Dec	Annual
T_A	−20	22	90	139	191	237	255	232	181	104	43	−4	123
e	33	46	69	104	114	183	258	242	174	93	63	36	118
U_{OBS}	9	9	13	15	14	15	11	8	4	10	15	8	11
N	1540	1473	1672	1922	2844	2356	2343	1231	1209	1290	1381	1869	21130
T_S	−13	36	115	173	248	282	300	264	208	115	54	−3	148
Pr_{OBS}	10	14	42	43	6	88	223	110	90	21	31	2	679
E_{PAN}	40	54	116	122	217	213	172	106	77	73	47	39	1273
Pr	13	15	42	44	7	89	224	111	90	21	33	2	690
E_P	25	33	67	92	153	154	145	89	66	49	33	28	933
S_M^I	98	122	161	190	258	238	229	151	138	114	97	106	159
L^I	245	263	293	325	340	383	408	404	365	314	280	241	322
Soil 1	(volcanic ash soil)												
Rn	7	36	56	87	100	111	143	95	77	50	31	23	68
H	−1	10	26	31	71	53	25	12	11	3	2	2	21
ιE	13	27	27	50	23	54	114	81	65	50	34	27	47
G	−5	−1	3	6	6	4	5	2	0	−2	−5	−6	0
E	14	26	29	52	24	56	122	86	68	54	35	29	595
Soil 2	(clay loam)												
Rn	−2	23	42	72	78	92	112	71	51	29	19	3	49
H	−2	11	18	27	52	42	35	22	20	12	9	4	21
ιE	6	13	21	37	19	44	70	46	31	21	18	7	28
G	−6	−2	3	8	8	6	6	2	0	−4	−7	−8	0
E	6	13	22	38	20	46	74	49	32	23	19	8	350
Soil 3	(silty sand)												
Rn	−4	21	39	70	75	94	117	76	53	31	21	1	50
H	−5	3	12	15	44	31	19	11	11	0	1	−3	12
ιE	8	20	23	47	23	55	92	62	43	36	28	13	37
G	−7	−2	4	8	9	7	6	3	−1	−5	−8	−9	0
E	8	19	24	48	24	57	99	66	44	39	29	14	473
Soil 4	(sand)												
Rn	−4	14	34	55	73	82	88	53	37	19	5	−3	38
H	−2	9	20	32	56	45	45	28	24	11	6	2	23
ιE	3	6	12	18	11	32	39	24	14	12	6	3	15
G	−5	−2	2	6	6	5	5	1	−1	−4	−7	−7	0
E	4	6	13	19	12	33	42	25	14	13	6	3	188

(19) Changsha: 28.2°N, 113.1°E, Elevation=45m

	Jan	Feb	Mar	Apr	May	Jun	Jul	Aug	Sep	Oct	Nov	Dec	Annual
T_A	33	72	130	173	210	265	296	302	236	159	110	63	171
e	64	86	128	171	196	273	312	315	227	151	114	68	175
U_{OBS}	25	23	21	21	23	24	27	23	26	23	23	19	23
N	880	413	691	468	1428	1791	2542	2744	1228	697	199	1392	14473
T_S	42	82	139	187	235	313	354	371	276	177	119	65	197
Pr_{OBS}	77	57	189	260	183	157	41	9	95	174	190	2	1432
E_{PAN}	32	38	73	82	132	165	221	234	146	66	36	55	1279
Pr	99	57	190	260	183	157	42	9	95	174	190	2	1458
E_P	27	28	51	58	103	137	186	187	117	50	26	42	1011
S_M^1	73	67	114	111	163	192	236	244	168	86	44	97	134
L^1	290	318	342	373	385	422	435	436	398	361	344	290	366
Soil 1	(volcanic ash soil)												
Rn	19	29	62	68	107	127	150	117	85	45	17	34	72
H	1	2	9	8	8	17	31	72	37	−1	−1	−1	15
ιE	23	29	49	56	94	104	115	41	48	49	24	41	56
G	−5	−2	3	4	5	5	4	3	−1	−2	−6	−6	0
E	24	28	52	58	101	108	123	44	50	52	25	43	709
Soil 2	(clay loam)												
Rn	12	25	56	59	84	91	107	91	65	35	15	15	55
H	6	4	11	13	22	36	52	63	37	4	0	9	22
ιE	13	23	41	41	56	47	49	24	29	35	23	14	33
G	−7	−2	4	6	7	7	6	3	−1	−4	−9	−8	0
E	14	22	44	42	60	49	52	26	30	37	24	15	416
Soil 3	(silty sand)												
Rn	11	23	52	58	85	96	113	88	65	37	12	21	55
H	1	0	6	4	7	18	31	57	27	−2	−1	−3	12
ιE	18	25	42	48	71	70	75	26	40	43	22	33	43
G	−7	−3	4	6	7	7	6	4	−2	−4	−9	−9	0
E	19	24	45	49	76	73	80	28	42	46	23	36	541
Soil 4	(sand)												
Rn	3	12	36	41	62	73	93	85	55	20	5	5	41
H	5	5	13	16	29	45	61	68	41	8	2	9	25
ιE	3	9	20	20	28	22	28	15	16	16	11	4	16
G	−6	−2	3	5	5	5	5	2	−2	−4	−7	−7	0
E	4	9	21	21	30	23	30	16	17	17	11	4	202

(20) Boxian: 33.9°N, 115.8°E, Elevation=38m

	Jan	Feb	Mar	Apr	May	Jun	Jul	Aug	Sep	Oct	Nov	Dec	Annual
T_A	−12	29	100	153	214	253	287	265	212	133	68	17	143
e	34	56	81	113	124	201	304	283	184	113	71	39	134
U_{OBS}	29	32	33	31	39	30	31	25	25	27	27	28	30
N	1426	1385	1967	2183	2944	2337	2376	1877	1731	1488	1370	2062	23146
T_S	−12	38	117	182	268	288	332	305	249	136	67	13	165
Pr_{OBS}	16	38	39	15	2	140	57	139	40	64	34	8	592
E_{PAN}	55	59	145	175	368	274	232	164	153	95	65	60	1845
Pr	26	79	40	15	2	140	57	140	40	64	35	13	652
E_P	38	41	93	123	230	188	184	133	110	71	46	49	1307
$S^{\downarrow}_M$	89	114	166	200	261	226	228	187	158	117	95	111	163
$L^{\downarrow}$	250	271	298	331	352	396	431	420	378	328	292	246	333
Soil 1	(volcanic ash soil)												
Rn	3	30	72	94	111	118	135	110	79	57	33	16	72
H	−4	1	16	39	84	48	46	32	19	−6	−5	−4	22
ιE	12	30	53	51	21	65	83	76	61	66	43	26	49
G	−5	−1	2	5	6	4	4	2	−1	−3	−6	−6	0
E	13	29	57	52	23	68	89	82	63	70	45	28	619
Soil 2	(clay loam)												
Rn	−3	23	50	75	86	96	104	87	52	39	19	3	52
H	−5	6	26	38	65	45	53	37	30	11	7	0	26
ιE	8	19	21	30	14	45	45	47	23	33	20	12	26
G	−6	−2	3	7	7	6	6	2	−1	−4	−8	−8	0
E	8	18	23	31	15	47	49	50	24	35	20	12	332
Soil 3	(silty sand)												
Rn	−7	19	50	73	81	98	110	90	55	42	19	−1	53
H	−10	−3	5	22	59	28	30	23	15	−8	−7	−11	12
ιE	10	23	42	43	14	63	73	64	42	54	35	19	40
G	−6	−2	3	7	8	7	6	3	−2	−4	−9	−9	0
E	10	23	45	45	15	65	79	69	43	53	36	20	509
Soil 4	(sand)												
Rn	−7	9	39	62	82	84	91	70	45	22	6	−4	42
H	−7	6	26	41	69	47	61	44	33	13	5	−3	28
ιE	5	5	11	16	7	31	25	23	13	13	8	7	14
G	−5	−2	2	6	6	5	5	2	−2	−4	−7	−7	0
E	5	5	11	16	8	32	27	25	14	14	8	7	174

(21) Dongtai: 32.9°N, 120.3°E, Elevation=4m

	Jan	Feb	Mar	Apr	May	Jun	Jul	Aug	Sep	Oct	Nov	Dec	Annual
T_A	−1	29	87	134	197	232	278	266	211	148	83	31	141
e	42	61	90	121	149	219	320	293	205	137	88	56	148
U_{OBS}	34	34	38	35	36	36	34	28	33	33	35	33	34
N	1483	1254	1668	1612	2704	1843	2381	2200	1859	1381	1403	1798	21586
T_S	9	43	97	153	241	262	303	289	226	153	86	32	158
Pr_{OBS}	41	49	33	54	47	153	153	111	75	118	75	2	910
E_{PAN}	42	37	83	109	208	181	171	151	122	84	56	59	1304
Pr	51	51	34	54	47	153	154	111	75	118	76	3	927
E_P	38	36	67	88	177	143	164	145	108	70	46	44	1127
$S_M^{\downarrow}$	94	109	143	163	247	193	229	208	176	119	98	104	157
$L^{\downarrow}$	255	274	303	333	353	395	428	419	377	339	302	263	337
Soil 1	(volcanic ash soil)												
Rn	20	38	73	89	120	100	163	121	102	62	38	31	80
H	−5	3	9	21	65	55	21	41	16	−3	−2	−5	18
ιE	29	36	61	63	50	40	138	77	86	67	46	42	61
G	−4	−1	3	5	4	5	4	2	0	−3	−5	−6	0
E	31	34	66	65	54	41	148	83	89	72	48	45	776
Soil 2	(clay loam)												
Rn	6	31	53	72	95	83	121	91	71	44	26	11	59
H	2	8	26	30	58	45	49	47	33	14	8	9	28
ιE	11	25	23	35	31	30	65	40	39	34	26	11	31
G	−6	−2	3	7	7	7	6	3	−1	−5	−8	−9	0
E	11	25	25	36	33	32	69	43	40	37	27	11	389
Soil 3	(silty sand)												
Rn	2	27	53	71	93	80	126	92	75	47	28	11	59
H	−5	0	4	13	40	36	24	33	13	−4	−4	−5	12
ιE	14	29	45	51	46	37	95	56	63	56	41	26	47
G	−7	−2	3	7	7	7	6	3	−1	−5	−8	−9	0
E	15	28	49	53	49	38	102	60	65	60	42	28	589
Soil 4	(sand)												
Rn	0	15	37	53	87	75	98	79	55	26	10	2	45
H	1	8	25	35	60	50	60	54	39	16	7	6	30
ιE	4	9	10	13	21	20	33	22	17	14	10	3	15
G	−5	−2	2	5	5	5	5	3	−1	−4	−7	−8	0
E	4	8	10	13	23	20	35	23	17	15	10	4	185

(22) Hefei: 31.9N, 117.2E, Elevation=28m

	Jan	Feb	Mar	Apr	May	Jun	Jul	Aug	Sep	Oct	Nov	Dec	Annual
T_A	11	44	107	156	217	225	287	277	220	145	88	38	154
e	46	67	97	132	155	230	319	303	200	133	90	55	152
U_{OBS}	34	33	36	32	39	35	36	32	29	34	34	26	33
N	1035	745	1197	1504	2448	2187	2229	1758	1664	1123	984	1739	18613
T_S	14	50	119	178	257	301	330	317	256	161	95	36	176
Pr_{OBS}	37	71	53	76	50	46	189	45	48	138	104	13	871
E_{PAN}	54	51	111	142	296	247	238	182	168	97	61	67	1715
Pr	55	72	54	77	50	47	190	46	48	138	105	13	894
E_P	38	34	74	103	200	173	182	144	118	69	43	44	1223
S_M^1	74	80	127	175	235	217	232	186	173	110	81	104	150
L^1	272	294	319	343	367	405	432	430	382	341	313	267	348
Soil 1	(volcanic ash soil)												
Rn	17	30	70	104	120	109	154	115	84	57	32	32	77
H	−11	−2	−2	10	50	59	34	27	33	−6	−5	−5	15
ιE	32	34	69	89	66	46	116	88	52	66	42	43	62
G	−4	−2	3	5	4	5	4	1	−1	−3	−6	−6	0
E	35	33	74	92	71	47	124	94	54	71	44	46	784
Soil 2	(clay loam)												
Rn	6	25	47	79	92	89	123	83	63	39	22	16	57
H	−1	4	19	28	53	51	47	43	34	12	4	7	25
ιE	13	24	25	45	33	31	69	73	30	32	26	18	32
G	−6	−3	3	7	6	6	6	3	−1	−5	−9	−8	0
E	14	23	26	47	35	32	74	40	31	35	27	19	405
Soil 3	(silty sand)												
Rn	3	22	48	81	93	87	125	89	63	42	23	21	58
H	−10	−4	−1	8	33	41	26	23	23	−7	−6	−7	10
ιE	20	29	46	67	54	39	91	64	41	53	37	36	48
G	−7	−3	3	7	6	7	6	3	−1	−4	−9	−9	0
E	22	28	50	69	58	40	98	68	42	57	39	39	610
Soil 4	(sand)												
Rn	−1	11	33	58	84	81	100	72	53	25	8	2	44
H	−3	5	19	33	55	54	61	49	38	11	4	4	28
ιE	8	8	12	21	24	22	35	21	16	18	11	5	17
G	−5	−2	3	5	5	5	5	2	−1	−4	−7	−7	0
E	8	8	12	21	26	23	37	23	17	20	11	6	212

(23) Nanping: 26.7°N, 118.2°E, Elevation=126m

	Jan	Feb	Mar	Apr	May	Jun	Jul	Aug	Sep	Oct	Nov	Dec	Annual
T_A	94	118	155	198	214	254	279	293	257	210	152	93	193
e	89	113	146	191	200	254	287	311	257	192	140	83	189
U_{OBS}	13	13	11	11	11	10	14	11	12	11	14	10	12
N	1217	701	879	857	1537	1500	1978	2640	1242	1618	1023	1838	17030
T_S	104	128	166	212	241	288	319	336	287	240	163	106	216
Pr_{OBS}	38	85	230	324	208	147	203	152	72	34	66	7	1565
E_{PAN}	66	55	83	92	129	150	181	218	133	124	67	75	1372
Pr	39	85	230	324	208	148	204	152	73	35	69	7	1570
E_P	39	41	57	69	97	108	138	167	101	91	49	50	1007
$S_M^{\downarrow}$	100	98	124	132	173	177	203	248	156	158	99	127	150
$L^{\downarrow}$	310	333	354	383	386	416	428	431	416	375	348	295	373
Soil 1	(volcanic ash soil)												
Rn	31	43	69	81	110	119	124	170	101	81	45	36	84
H	8	7	10	9	11	10	25	15	6	12	3	9	10
ιE	27	39	55	69	94	103	94	152	94	66	47	33	73
G	−4	−2	3	4	5	5	4	3	0	−2	−6	−6	0
E	29	38	59	71	100	107	100	163	98	71	49	35	920
Soil 2	(clay loam)												
Rn	19	35	64	70	89	85	96	119	67	50	30	16	62
H	9	11	10	14	21	26	34	39	22	23	9	12	19
ιE	16	28	50	52	61	51	58	79	46	31	29	12	43
G	−6	−3	4	4	7	7	4	3	−1	−4	−8	−8	0
E	17	27	54	54	66	53	62	84	48	33	30	13	541
Soil 3	(silty sand)												
Rn	17	34	59	70	91	91	99	132	78	55	34	17	65
H	2	2	7	5	8	11	21	16	6	9	1	2	8
ιE	22	35	47	58	75	72	72	112	73	50	42	24	57
G	−6	−3	5	6	7	8	6	4	−1	−4	−9	−9	0
E	23	34	51	61	81	75	77	120	76	54	43	26	720
Soil 4	(sand)												
Rn	11	22	42	52	63	66	83	98	53	40	17	11	47
H	9	10	12	14	29	35	35	47	27	27	10	12	22
ιE	7	15	27	34	30	26	44	49	28	18	15	6	25
G	−5	−3	2	4	5	6	4	3	−1	−4	−7	−7	0
E	8	14	29	36	32	27	47	52	29	19	15	7	315

(24) Guangzhou: 23.1°N, 113.3°E, Elevation=7m

	Jan	Feb	Mar	Apr	May	Jun	Jul	Aug	Sep	Oct	Nov	Dec	Annual
T_A	145	155	195	238	241	270	276	293	272	233	187	140	220
e	106	141	194	258	255	289	314	327	290	226	163	89	221
U_{OBS}	16	21	18	19	15	18	20	16	16	19	19	20	18
N	1629	494	545	555	1057	1642	1605	2274	1534	1518	1271	2063	16187
T_S	174	181	210	257	265	312	302	346	306	259	213	170	250
Pr_{OBS}	1	2	16	21	15	37	65	15	27	15	7	0	222
E_{PAN}	128	77	84	94	109	174	144	191	149	138	118	155	1460
Pr	15	23	164	211	150	365	654	152	273	146	68	4	2224
E_P	74	49	52	65	81	125	125	152	115	99	78	93	1107
$S_M^{\downarrow}$	139	81	88	108	133	190	187	217	167	149	120	145	144
$L^{\downarrow}$	324	362	389	416	414	426	432	437	426	395	363	312	392
Soil 1	(volcanic ash soil)												
Rn	41	30	51	71	89	130	132	150	114	94	64	41	84
H	19	12	4	6	8	12	12	14	5	0	−4	14	9
ιE	26	19	44	61	77	105	116	134	109	96	73	33	75
G	−4	−2	3	4	5	5	5	2	0	−2	−6	−6	0
E	28	19	47	64	82	109	124	143	113	102	75	35	942
Soil 2	(clay loam)												
Rn	25	21	45	63	75	89	111	104	81	62	33	19	61
H	17	12	7	10	15	35	23	36	23	17	14	16	19
ιE	14	12	35	47	53	48	82	66	59	49	27	10	42
G	−6	−3	4	5	6	6	6	3	−1	−4	−8	−8	0
E	15	11	38	49	57	50	88	71	61	53	28	11	531
Soil 3	(silty sand)												
Rn	23	20	43	62	76	95	108	116	88	68	37	17	63
H	11	7	1	3	5	17	12	14	7	1	0	10	7
ιE	18	17	38	53	65	71	91	100	83	71	46	16	56
G	−6	−3	4	6	7	7	7	3	−1	−4	−9	−9	0
E	19	16	40	55	69	74	97	107	86	76	48	17	704
Soil 4	(sand)												
Rn	21	18	31	44	53	76	85	87	62	45	23	16	47
H	17	11	9	15	22	40	32	42	31	23	19	18	23
ιE	9	9	18	25	27	31	48	44	33	26	11	5	24
G	−5	−3	3	4	5	5	5	1	−2	−4	−7	−7	0
E	9	9	20	26	29	31	52	47	34	28	11	5	301

(25) Baingoin: 31.4°N, 90.0°E, Elevation=4700m

	Jan	Feb	Mar	Apr	May	Jun	Jul	Aug	Sep	Oct	Nov	Dec	Annual
T_A	−132	−75	−62	−18	20	78	87	89	58	−4	−85	−115	13
e	9	7	12	18	39	57	76	75	51	17	11	5	31
U_{OBS}	43	62	54	50	39	48	39	39	47	39	35	44	45
N	2253	2208	2267	2731	2721	2567	2182	2265	2506	3012	2525	2600	29837
T_S	−112	−64	−26	32	69	124	114	118	86	13	−62	−111	15
Pr_{OBS}	5	2	4	6	33	42	142	97	42	5	2	0	380
E_{PAN}	70	131	138	183	179	235	178	209	194	199	112	96	1922
Pr	10	4	13	15	63	50	142	97	63	8	4	1	470
E_P	51	98	113	148	152	183	156	165	153	126	69	62	1476
S_M^1	172	212	240	302	312	313	281	293	281	256	198	178	253
L^1	178	193	208	217	240	268	284	276	251	207	185	171	223
Soil 1	(volcanic ash soil)												
Rn	48	70	90	116	116	134	146	140	114	72	51	37	95
H	41	62	71	90	74	84	40	51	47	48	41	38	57
ιE	10	8	16	20	37	45	103	88	67	26	14	6	37
G	−3	−1	3	6	6	6	4	1	0	−2	−5	−6	0
E	11	8	17	21	40	47	111	95	69	28	15	7	468
Soil 2	(clay loam)												
Rn	37	51	78	100	107	114	124	115	93	48	34	18	77
H	32	47	50	75	66	65	52	54	48	35	32	23	49
ιE	10	6	14	17	33	41	68	59	44	17	9	3	27
G	−5	−2	3	7	9	9	4	2	1	−4	−7	−8	0
E	11	6	15	18	35	42	73	63	46	18	10	3	339
Soil 3	(silty sand)												
Rn	30	45	69	90	101	107	132	122	88	43	28	14	73
H	25	41	51	64	52	50	18	23	27	24	25	19	35
ιE	10	6	14	17	40	49	106	95	61	23	11	3	37
G	−5	−2	4	8	9	9	7	4	0	−4	−8	−9	0
E	11	6	15	18	43	50	114	102	63	25	11	4	462
Soil 4	(sand)												
Rn	32	47	70	91	93	100	97	91	73	42	29	17	65
H	28	44	56	71	66	72	50	58	54	36	30	22	49
ιE	8	4	11	13	21	23	43	34	21	10	5	2	16
G	−4	−2	3	7	6	6	3	−1	−1	−3	−7	−7	0
E	9	4	12	14	23	23	46	36	22	10	6	2	208

(26) Xigaze: 29.3°N, 88.9°E, Elevation=3836m

	Jan	Feb	Mar	Apr	May	Jun	Jul	Aug	Sep	Oct	Nov	Dec	Annual
T_A	−55	10	19	65	100	147	140	146	120	80	5	−47	61
e	14	11	19	31	53	79	112	108	78	32	18	12	47
U_{OBS}	13	28	25	26	23	19	12	12	11	13	15	10	17
N	2486	2502	2470	2843	2969	2968	2260	2549	2526	3191	2819	2831	32414
T_S	−46	17	63	134	178	234	192	204	170	92	−5	−50	99
Pr_{OBS}	0	0	3	4	21	52	168	62	18	0	0	0	328
E_{PAN}	64	130	148	233	245	270	173	179	173	191	109	70	1983
Pr	1	0	4	5	22	53	169	63	19	0	0	0	47
E_P	55	104	121	155	171	185	148	151	131	122	83	57	1481
S_M^1	181	226	246	303	319	333	279	283	272	260	211	186	258
L^1	201	216	234	248	270	294	313	309	284	239	210	193	251
Soil 1	(volcanic ash soil)												
Rn	38	55	78	103	112	121	142	122	93	63	40	30	83
H	37	50	67	86	89	85	34	46	56	51	38	31	56
ιE	4	7	8	12	17	30	103	74	35	14	7	4	27
G	−3	−1	2	5	6	5	5	2	2	−2	−5	−6	0
E	5	6	9	12	18	31	111	79	36	15	7	5	334
Soil 2	(clay loam)												
Rn	22	34	60	81	88	98	120	98	68	38	20	11	62
H	24	32	49	64	65	61	36	40	42	33	23	16	41
ιE	3	4	8	10	16	30	77	53	25	9	4	3	20
G	−5	−2	3	6	7	7	7	5	1	−4	−8	−8	0
E	3	4	8	11	17	31	83	56	26	9	4	3	256
Soil 3	(silty sand)												
Rn	18	30	54	75	84	96	124	106	66	34	15	7	59
H	20	28	44	59	58	53	19	22	33	29	20	14	33
ιE	3	3	6	9	16	34	98	80	32	9	4	2	25
G	−5	−2	3	8	9	9	8	5	1	−4	−9	−9	0
E	3	3	7	9	17	36	105	85	33	9	4	3	314
Soil 4	(sand)												
Rn	20	33	56	76	84	92	90	80	61	36	18	10	55
H	23	32	49	65	66	62	41	46	45	34	23	16	42
ιE	2	2	4	6	13	24	46	32	16	5	2	1	13
G	−4	−1	2	6	6	5	3	2	−1	−4	−7	−7	0
E	2	2	4	6	13	25	49	34	17	5	2	1	162

(27) Lhasa: 29.7°N, 91.1°E, Elevation=3649m

	Jan	Feb	Mar	Apr	May	Jun	Jul	Aug	Sep	Oct	Nov	Dec	Annual
T_A	−26	20	37	74	111	156	151	160	131	92	28	−52	74
e	17	15	24	37	57	91	117	115	86	41	23	20	54
U_{OBS}	18	23	26	23	28	21	19	17	19	17	21	20	21
N	2473	2440	2249	2349	2712	2629	2219	2495	2461	3270	2791	2580	30668
T_S	−5	40	84	138	180	200	195	196	156	111	39	−73	105
P_{OBS}	0	0	1	4	41	60	103	72	36	0	0	13	330
E_{PAN}	89	157	196	240	288	291	215	234	197	211	143	69	2329
Pr	1	0	2	6	42	61	104	73	37	0	0	13	338
E_P	62	90	118	137	169	178	153	159	136	126	87	49	1465
S_M^I	178	219	232	273	299	313	279	285	264	261	205	172	249
L^I	211	223	247	262	281	307	319	316	293	245	222	201	261
Soil 1	(volcanic ash soil)												
Rn	36	51	72	92	108	121	129	119	95	64	38	7	78
H	30	45	62	76	81	74	46	52	51	51	36	2	50
ιE	9	7	7	11	21	41	80	65	43	16	8	10	27
G	−3	−1	3	5	5	5	3	2	1	−2	−5	−5	0
E	9	7	8	11	23	43	86	70	45	17	8	11	337
Soil 2	(clay loam)												
Rn	21	32	55	73	88	100	111	100	73	40	18	−11	59
H	20	28	46	56	59	54	41	39	38	34	21	−3	36
ιE	6	5	6	11	22	39	66	56	35	10	5	10	23
G	−5	−2	3	7	7	7	6	4	1	−4	−8	−8	0
E	7	5	7	11	23	41	71	60	36	11	5	10	286
Soil 3	(silty sand)												
Rn	17	28	50	67	84	99	113	99	71	35	14	−5	56
H	16	25	42	51	51	44	22	25	28	30	18	−6	29
ιE	7	4	5	9	25	47	84	71	43	10	4	10	27
G	−6	−1	4	8	8	9	7	4	1	−4	−8	−8	0
E	7	4	5	9	27	49	90	76	44	10	4	11	336
Soil 4	(sand)												
Rn	19	30	52	68	83	90	89	82	63	37	17	−5	52
H	19	29	46	57	60	57	45	47	41	35	21	−6	37
ιE	5	3	3	5	18	29	40	34	23	6	2	8	15
G	−5	−1	3	6	6	4	3	1	−1	−4	−7	−7	0
E	5	3	3	5	19	30	43	37	23	6	2	9	186

(28) Tuotuohe: 34.2°N, 92.4°E, Elevation=4533m

	Jan	Feb	Mar	Apr	May	Jun	Jul	Aug	Sep	Oct	Nov	Dec	Annual
T_A	−167	−123	−92	−41	15	63	86	83	38	−23	−117	−161	37
e	8	8	12	22	36	60	77	75	53	19	8	6	32
U_{OBS}	36	56	41	48	42	35	31	30	34	49	44	43	41
N	2261	1992	2195	2928	2768	2658	2408	2636	2458	2905	2510	2552	30271
T_S	−157	−107	−60	15	74	130	146	130	78	1	−103	−156	−1
Pr_{OBS}	4	1	3	15	27	38	100	106	36	0	1	0	330
E_{PAN}	52	87	102	136	182	211	211	209	154	177	90	68	1680
Pr	7	2	6	75	46	41	101	106	41	1	2	1	429
E_P	33	61	80	126	150	160	158	153	120	114	55	37	1246
$S_M^{\downarrow}$	155	185	224	304	309	316	300	296	265	233	178	156	244
$L^{\downarrow}$	170	187	201	208	238	263	279	271	247	206	177	163	218
Soil 1	(volcanic ash soil)												
Rn	39	63	86	93	132	132	134	138	108	73	44	32	90
H	38	58	74	52	70	81	63	50	48	58	42	34	56
ιE	5	5	9	35	55	45	71	89	60	19	8	3	34
G	−4	−1	3	6	6	7	3	2	0	−3	−5	−6	0
E	6	5	9	37	59	46	76	96	62	20	8	4	428
Soil 2	(clay loam)												
Rn	28	48	72	83	117	111	118	116	91	50	25	15	73
H	28	44	61	49	67	64	52	52	51	43	29	21	47
ιE	5	5	7	26	42	39	58	61	40	11	4	2	25
G	−5	−1	3	8	8	8	8	3	1	−4	−8	−8	0
E	5	5	8	27	45	41	62	65	41	12	5	2	317
Soil 3	(silty sand)												
Rn	23	41	65	75	114	107	117	119	88	44	21	11	69
H	23	38	54	38	44	48	30	25	29	38	25	18	34
ιE	5	5	7	30	61	50	79	89	59	11	5	2	34
G	−5	−1	4	8	2	9	7	5	1	−5	−9	−9	0
E	6	5	8	31	66	52	85	95	61	12	5	2	426
Soil 4	(sand)												
Rn	25	44	67	72	99	97	93	89	70	46	23	14	62
H	25	41	58	48	72	71	60	55	53	44	28	20	48
ιE	4	3	5	17	22	21	32	34	18	6	3	1	14
G	−5	−1	3	6	6	5	1	0	−1	−4	−7	−7	0
E	4	3	6	18	23	21	34	36	19	6	3	1	176

(29) Madoi: 34.9°N, 98.2°E, Elevation=4272m

	Jan	Feb	Mar	Apr	May	Jun	Jul	Aug	Sep	Oct	Nov	Dec	Annual
T_A	−154	−115	−85	−35	19	64	93	88	31	−22	−112	−155	−32
e	11	13	17	29	35	61	77	71	55	27	13	8	35
U_{OBS}	25	35	35	39	41	39	41	41	30	36	31	28	35
N	2265	2063	2628	2256	2633	2482	2294	2187	1883	2632	2443	2440	28206
T_S	−131	−86	−38	5	72	122	148	136	63	−1	−92	−148	4
Pr_{OBS}	2	3	6	23	20	92	48	49	123	3	1	1	369
E_{PAN}	42	67	92	104	178	180	191	184	105	117	59	48	1366
Pr	4	5	12	44	29	94	48	49	129	5	3	2	425
E_P	27	47	78	99	147	153	158	150	96	87	42	28	1111
$S^{\downarrow}_M$	151	184	242	260	297	300	280	263	231	214	171	148	229
$L^{\downarrow}$	174	189	196	225	242	267	286	282	253	216	183	168	224
Soil 1	(volcanic ash soil)												
Rn	35	59	91	89	126	145	123	109	110	76	43	28	86
H	34	52	74	47	85	63	70	64	26	39	37	28	52
ιE	5	7	14	36	35	77	48	43	82	38	11	5	34
G	−3	0	3	6	7	5	5	2	1	−2	−5	−5	0
E	5	7	15	38	38	79	51	46	85	41	12	5	423
Soil 2	(clay loam)												
Rn	26	48	78	80	112	124	105	90	90	56	29	13	71
H	27	42	63	44	72	64	56	52	37	40	30	19	46
ιE	4	6	12	28	22	52	40	34	52	19	7	3	24
G	−5	−1	3	8	8	8	8	4	1	−3	−8	−8	0
E	5	6	12	29	34	54	43	36	54	20	7	3	304
Soil 3	(silty sand)												
Rn	21	42	71	73	104	119	100	85	89	52	24	9	66
H	22	36	54	27	60	40	38	38	19	25	24	15	33
ιE	4	7	13	37	35	72	54	44	69	31	8	3	31
G	−5	−1	4	9	9	8	8	3	1	−4	−9	−9	0
E	5	7	14	38	37	75	57	48	72	33	9	3	396
Soil 4	(sand)												
Rn	22	42	71	67	100	101	88	77	68	45	25	12	60
H	23	40	60	41	74	67	62	56	40	40	28	17	46
ιE	3	4	9	19	20	30	21	20	29	8	4	2	14
G	−4	−1	3	7	7	5	5	1	−1	−3	−7	−7	0
E	4	4	9	20	21	31	23	22	30	9	4	2	178

(30) Deqen: 28.5°N, 98.9°E, Elevation=3485m

	Jan	Feb	Mar	Apr	May	Jun	Jul	Aug	Sep	Oct	Nov	Dec	Annual
T_A	−24	−9	2	43	89	125	126	131	113	77	31	−4	58
e	31	41	46	57	76	107	119	120	98	65	39	31	69
U_{OBS}	41	39	36	39	41	39	30	32	39	41	45	36	38
N	1760	1615	1596	2014	2017	1921	1581	1886	2067	2337	2324	2047	23165
T_S	−13	−5	12	85	150	191	179	190	174	125	58	5	96
Pr_{OBS}	21	32	51	25	26	72	106	67	28	4	2	10	444
E_{PAN}	74	66	84	132	163	195	158	171	169	167	127	88	1594
Pr	36	56	97	38	27	73	106	68	29	5	4	13	554
E_P	62	62	79	116	142	145	130	135	127	123	101	71	1292
$S_M^{\downarrow}$	157	181	198	252	256	259	243	248	239	227	198	166	219
$L^{\downarrow}$	229	240	252	262	288	311	316	314	297	265	235	225	270
Soil 1	(volcanic ash soil)												
Rn	27	43	46	118	114	119	135	123	100	74	54	38	83
H	7	12	2	39	68	68	34	43	55	57	45	29	38
ιE	23	32	42	72	40	46	99	78	44	19	14	14	44
G	−4	−1	3	7	6	6	6	2	0	−2	−5	−5	0
E	25	31	45	75	43	47	106	83	46	21	15	15	551
Soil 2	(clay loam)												
Rn	21	37	37	91	90	97	110	98	78	52	37	25	64
H	8	17	9	50	58	57	45	48	47	43	35	22	37
ιE	18	22	25	33	24	33	59	47	30	13	9	11	27
G	−5	−2	3	8	8	8	6	4	1	−4	−7	−8	0
E	19	21	27	34	26	34	64	50	31	13	10	11	341
Soil 3	(silty sand)												
Rn	15	32	37	92	87	94	113	105	75	47	31	20	62
H	−2	7	−1	27	45	46	23	24	33	37	30	16	24
ιE	23	27	35	56	34	40	83	78	42	14	10	13	38
G	−6	−2	3	8	8	8	8	4	0	−4	−8	−9	0
E	25	26	37	58	36	41	88	83	44	15	10	14	478
Soil 4	(sand)												
Rn	13	27	28	75	83	89	87	81	68	48	33	20	55
H	2	18	12	55	59	57	43	48	50	45	33	20	37
ιE	16	11	13	14	18	26	40	31	18	7	6	8	17
G	−5	−2	2	6	6	6	5	3	0	−4	−7	−7	0
E	17	11	14	14	19	27	43	33	19	7	7	8	220

Appendix B. Notation

a	soil parameter defined in Eq.(2.7) (Table 3.1)
A_n	coefficient for daily variation of $S^{\downarrow}$ (n =1–4)
a_λ (W m^{-1}K^{-1})	soil paramemter defined in Eq.(3.14) (Table 3.1)
b	soil parameter defined in Eq.(2.10) (Table 3.1)
B_n (K or °C)	daily amplitude of T_a (n =1, 2)
b_λ (W m^{-1}K^{-1})	soil paramemter defined in Eq.(3.14) (Table 3.1)
c	soil parameter defined in Eq.(2.5) (Table 3.1)
c_g (J kg^{-1}K^{-1})	specific heat of soil ground
C_HU (m s^{-1})	exchange speed
cor	capture rate of rain gauge
c_p (J kg^{-1}K^{-1})	specific heat of air
$c_s\rho_s$ (J m^{-3}K^{-1})	soil paramemter defined in Eq.(3.14) (Table 3.1)
$c_w\rho_w$ (J m^{-3}K^{-1})	thermal capacity of water (4.2×10^6)
$c\rho_{\mathrm{snow}}$ (J m^{-3}K^{-1})	thermal capacity of snow (0.4×10^6)
D (m^{2}s^{-1})	molecular diffusivity of water vapor
e (hPa)	observed daily mean vapor pressure
e_{SAT}	vapor pressure at saturation
E (kg m^{-2}s^{-1})	evaporation rate
E_{P} (kg m^{-2}s^{-1})	potential evaporation
E_{PAN} (mm)	pan evaporation
E_{soil} (kg m^{-2}s^{-1})	E within soil ($z \geq 0.02$ m)

F (m)	resistance to vaporization and vapor transport in the surface layer ($0 \leq z < 0.02$ m)
f_A, f_B, f_C	soil paramemters defined in Eq.(2.19) (Table 3.1)
F_n (m)	passing route (resistance) of vapor transport within soil ($z \geq 0.02$ m)
g (m s^{-2})	acceleration of gravity
G (W m^{-2})	heat flux into ground
h	relative humidity
H (W m^{-2})	sensible-heat flux
k	attenuation coefficient
K (m s^{-1})	hydraulic conductivity
K_{SAT} (m s^{-1})	K at saturation (Table 3.1)
ι (J kg^{-1})	latent heat of vaporization
$L^{\downarrow}$ (W m^{-2})	downward longwave radiation
N (hour)	observed sunshine duration
N_0 (hour)	duration of possible sunshine
Pr (mm)	corrected precipitation
$\mathrm{Pr}_{\mathrm{OBS}}$ (mm)	observed daily amount of precipitation
p_s (hPa)	observed surface pressure
p_0 (hPa)	standard atmosphere pressure (=1013hPa)
q	specific humidity of air
Q_h (J m^{-2}K^{-1})	heat flux in soil
Q_{liq} (kg m^{-2}K^{-1})	liquid-water flux in soil
q_{SAT}	saturated specific humidity
Q_{vap} (kg m^{-2}K^{-1})	water-vapor flux in soil
q^*	specific humidity in soil pore
Rn (W m^{-2})	net radiation flux
R_w (J kg^{-1}K^{-1})	gas constant of water vapor (461.5 J kg^{-1}K^{-1})
ref	albedo of ground-surface

ref_{DRY}	ref of the dry ground-surface (Eq. 3.4)
ref_m	ref on number m–day after snow
ref_{MAX}	ref_m when $m = 0$
ref_{WET}	ref of the wet-ground-surface (Table 3.1)
ref_0	ref of the ground-surface when $\theta \simeq 0$ and $\delta = 0$ (Table 3.1)
ref^*	ref of snow surface
$S^{\downarrow}$ (W m^{-2})	downward shortwave radiation
$S^{\downarrow}_{\mathrm{M}}$ (W m^{-2})	daily mean $S^{\downarrow}$
$S^{\downarrow}_{\mathrm{Mf}}$ (W m^{-2})	$S^{\downarrow}_M$ under clear sky
$S^{\downarrow}_0$ (W m^{-2})	$S^{\downarrow}_M$ at the top of the atmosphere
S_{00} (W m^{-2})	solar constant (1365Wm^{-2})
t (s)	time
T_{A} (K or °C)	air temperature
T_{AM} (K or °C)	observed daily mean air temperature
T_c (°C)	criterion for distiguishing rain and snow
T_{G} (K or °C)	temperature under the ground-surface
$T_{\mathrm{A,MAX}}$ (K or °C)	observed daily maximun air temperature
$T_{\mathrm{A,MIN}}$ (K or °C)	observed daily minimun air temperature
T_{S} (K or °C)	ground-surface temperature
U_{OBS} (m s^{-1})	observed daily mean wind speed
U (m s^{-1})	wind speed at the height of 1m
W_{snow} (kg m^{-2} = mm)	snow-water equivalent
w (cm)	precipitable water
z (m)	depth, positive in the downward direction
z_B (m)	depth at the bottom (z_B =0.7m)
β_{DUST}	Robinson's atmospheric turbidity
β^*	surface evaporation efficiency defined in Eq.(2.17)

γ (kg m^{-2}s^{-1} =mm s^{-1})	precipitation intensity
$\gamma_{\max}$ (kg m^{-2}s^{-1} =mm s^{-1})	maximum of γ
δ (rad)	solar declination
δ_{ref}	soil paramemter defined in Eq.(3.5) (Table 3.1)
Δ_K	soil parameter defined in Eq.(2.6) (Table 3.1)
ϵ	emissivity of ground-surface
ϵ_K	soil parameter defined in Eq.(2.6) (Table 3.1)
ζ (rad)	half-day angle
θ (m^{3}m^{-3})	volumetric soil-water content
$\theta_{\rm EQ}$ (m^{3}m^{-3})	θ in equilibrium state
θ_f (m^{3}m^{-3})	field capacity of soil-water content
θ_K (m^{3}m^{-3})	soil parameter defined in Eq.(2.6) (Table 3.1)
θ_{ref} (m^{3}m^{-3})	soil paramemter defined in Eq.(3.5) (Table 3.1)
$\theta_{\rm SAT}$ (m^{3}m^{-3})	θ at saturation (Table 3.1)
ιE (W m^{-2})	latent heat flux
λ_g (W m^{-1}K^{-1})	thermal conductivity of soil ground
λ_g^* (W m^{-1}K^{-1})	λ_g with snow cover
$\lambda_{\rm snow}$ (W m^{-1}K^{-1})	thermal conductivity of snow
ρ (kg m^{-3})	density of air
ρ_g (kg m^{-3})	density of soil
ρ_w (kg m^{-3})	density of water
σ (W m^{-2}K^{-4})	Stefan-Boltzmann constant (5.670×10^{-8} W m^{-2}K^{-4})
τ (s)	duration time of rainfall
ϕ (rad)	latitude of the observatory
Ψ (m)	soil-water potential
$\Psi_{\rm SAT}$ (m)	Ψ at saturation (Table 3.1)
ω (s^{-1})	angular velocity of diurnal cycle

References

Budyko, M.I., 1974: *Climate and life.* Academic Press, Inc., 508pp.

Jackson, R. D., R. J. Reginato, B. A. Kimball and F. S. Nakayama, 1974: Diurnal soil-water evaporation: Comparison of measured and calculated soil water fluxes. *Soil Sci. Soc. Am. Proc.*, **38**, 861–866.

Kobayashi, T., A. Matsuda, M. Kamichika, and Y. Yamamura, 1991: Why the thickness of the dry surface layer in sand dune fields exhibits a diurnal variation?. *J. Agric. Meteorol.*, **47**, 3–9.

Kondo, J., T. Kuwagata, 1992: Hydrological climate in Japan (1): Radiation and evaporation from shallow lakes. *J. Japanese Soc. Hydro. and Water Resour.*, **5**, 13–27, (in Japanese with English summary).

Kondo, J., 1993a: A guide to study on the surface heat balance of arid regions (2): simulation results. *J. Japanese Soc. Hydro. and Water Resour.*, **6**, 230–237, (in Japanese with English summary).

Kondo, J., 1993b: Time variation in soil water content of the surface soil layer after a rainfall. *J. Japanese Soc. Hydro. and Water Resour.*, **6**, 336–343, (in Japanese with English summary).

Kondo, J., 1994: *Meteorology of the Water Environment — Water and Heat Balance of the Earth's Surface.* Asakura Shoten Press, Japan, 348pp., (in Japanese).

Kondo, J., S. Ishida, 1997: Sensible heat flux from the earth's surface under natural convective conditions. *J. Atmos. Sci.*, **54**, (in press).

Kondo, J., and N. Saigusa, 1994: Modeling the evaporation with a formula for vaporization in the soil pores. *J. Meteor. Soc. Japan*, **72**, 413–421.

Kondo, J., N. Saigusa and T. Sato, 1990: A parameterization of evaporation from bare soil surfaces. *J. Appl. Meteor.*, **29**, 385–389.

Kondo, J., N. Saigusa and T. Sato, 1992: A model and eaperimental study of evaporation from bare-soil surface. *J. Appl. Meteor.*, **31**, 304–312.

Kondo, J., and J. Xu, 1995: Estimations of evaporation from an ando-soil field and a sand dune field. *J. Agric. Meteorol. (Japan)*, **51**, 219–228, (in Japanese with English summary).

Kondo, J., and J. Xu, 1996a: An estimation of heat balance for arid and semi-arid regions in China (1): climatological conditions, soil parameters and calculation method. *J. Japanese Soc. Hydro. and Water Resour.*, **9**, 162–174, (in Japanese with English summary).

Kondo, J., and J. Xu, 1996b: An estimation of heat balance for arid and semi-arid regions in China (2): results. *J. Japanese Soc. Hydro. and Water Resour.*, **9**, 175–187, (in Japanese with English summary).

Kondo, J., and J. Xu, 1996c: Empirical formula for estimating the precipitable water from the dew-point temperature at the ground level. *J. Japanese Soc. Hydro. and Water Resour.*, **9**, 463–467, (in Japanese with English summary).

Kondo, J., and J. Xu, 1996d: Effect of snow cover on heat balance of the bare soil surface over north-western China. *Seppyo. J. Japanese Soc. Snow and Ice*, **52**, 265–275, (in Japanese with English summary).

Kondo, J., and J. Xu, 1996f: Estimating radiation fluxes from pan-evaporation and sun-shine duration measurements. *Tenki. J. Meteoro. Soc. of Japan*, **43**, 613–622.

Kondo, J., and J. Xu, 1997: *Heat and Water Balance of the Ground Surface in China, Tabulated and Graphed Data for Non-Plant-Covered Surfaces.* Geophysical Institute, Tohoku University, Japan, 120pp., (in Japanese with English explanation).

Kondo, J., and J. Xu, 1997a: Heat and water balances of the ground surface in China (1) Geographic and seasonal distribution of radiation fluxes in China and Japan. *J. Japanese Soc. Hydro. and Water Resour.*, **10**, ***–***, (in Japanese with English summary).

Kondo, J., J. Xu and M. Fukumoto, 1995: Evaporation from a bare field of Ando-soil. *J. Japanese Soc. Hydro. and Water Resour.*, **8**, 174–183, (in Japanese with English summary).

Kondo, J., J. Xu and S. Haginoya, 1996: Empirical formula for estimating the solar radiation at an upland from the sunshine duration data. *J. Japanese Soc. Hydro. and Water Resour.*, **9**, 468–472, (in Japanese with English summary).

Kondo, J., and T. Yamazaki, 1990: A prediction model for snowmelt, snow surface temperature and freezing depth using a heat balance method. *J. Appl. Meteor.*, **29**, 375–384.

Okuyama, T., 1988: Annual variation in soil moisture balance and its dependence on climatic condition. *J. Agric. Meteorol. (Japan)*, **44**, 27–31, (in Japanese with English summary).

Philip, J. R., 1957: Evaporation, and moisture and heat fields in the soil. *J. Meteor.*, **14**, 354–366.

Robinson, N., Ed., 1966: *Solar Radiation.* Elsevier, 347pp.

Zhang, J., and Z. Lin, 1992: *Climate of China.* John Wiley & Sons, Inc., 376pp.

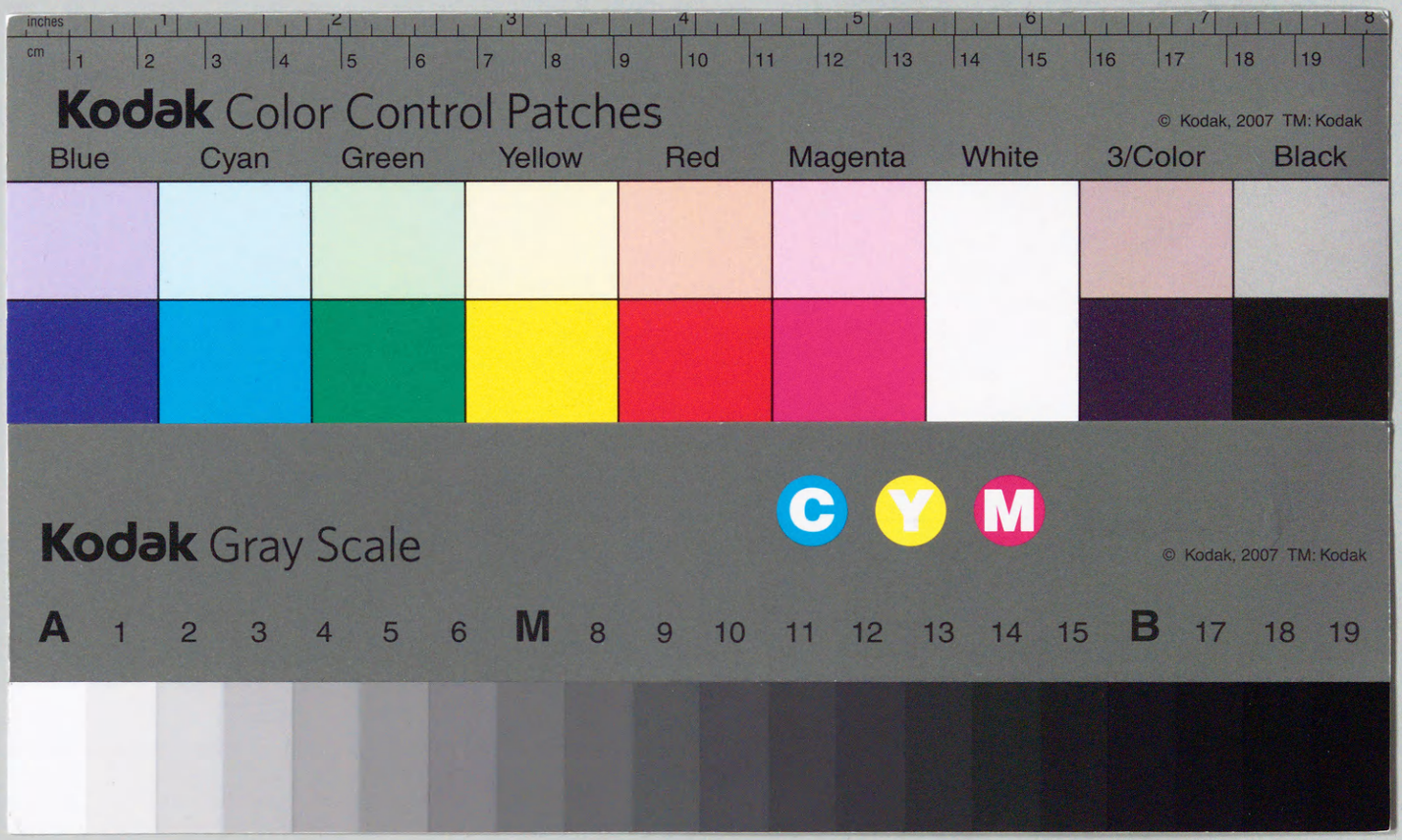
inches
cm
Kodak Color Control Patches
© Kodak, 2007 TM: Kodak
Blue
Cyan
Green
Yellow
Red
Magenta
White
3/Color
Black
Kodak Gray Scale
C
Y
M
© Kodak, 2007 TM: Kodak
A 1 2 3 4 5 6 M 8 9 10 11 12 13 14 15 B 17 18 19